A Coupled Wellbore-Reservoir Simulator utilizing Measured Wellhead Conditions

Halldóra Guðmundsdóttir

Faculty of Industrial Engineering,
Mechanical Engineering and Computer Science
University of Iceland
2012

A COUPLED WELLBORE-RESERVOIR SIMULATOR UTILIZING MEASURED WELLHEAD CONDITIONS

Halldóra Guðmundsdóttir

60 ECTS thesis submitted in partial fulfillment of a
Magister Scientiarum degree in Mechanical Engineering

Advisors
Magnús Þór Jónsson
Halldór Pálsson

Faculty Representative
Guðni Axelsson

Faculty of Industrial Engineering,
Mechanical Engineering and Computer Science
School of Engineering and Natural Sciences
University of Iceland
Reykjavik, October 2012

A Coupled Wellbore-Reservoir Simulator utilizing Measured Wellhead Conditions
A Coupled Wellbore-Reservoir Simulator
60 ECTS thesis submitted in partial fulfillment of a M.Sc. degree in
Mechanical Engineering

Faculty of Industrial Engineering,
Mechanical Engineering and Computer Science
School of Engineering and Natural Sciences
University of Iceland
VRII,Hjarðarhagi 2-6
107, Reykjavik
Iceland

Telephone: 525 4000

Bibliographic information:
Halldóra Guðmundsdóttir, 2012, A Coupled Wellbore-Reservoir Simulator utilizing Measured Wellhead Conditions, M.Sc. thesis, Faculty of Industrial Engineering,
Mechanical Engineering and Computer Science, University of Iceland.

Printing: Háskólaprent, Fálkagata 2, 107 Reykjavík
Reykjavik, Iceland, October 2012

Abstract

Modeling a geothermal system requires simulating the behavior of a reservoir and the flow in production wells, which is usually done individually. The main objective in this study is to develop a coupled wellbore-reservoir simulator to allow for more integrated modeling and to use wellhead conditions to a greater extent than has been done so far by defining them as main inputs to the coupled model. The program TOUGH2 is used to simulate the behavior of a reservoir while a new model, FloWell, is designed to simulate two phase flow in a wellbore. Finally, a detailed numerical model of the Reykjanes geothermal field in Iceland including the coupled FloWell-TOUGH2 model is constructed.

FloWell produced simulations in good agreement with pressure logs from wells at Reykjanes and Svartsengi geothermal fields. An inverse estimation with iTOUGH2 was effective in estimating new permeabilities for the Reykjanes reservoir, providing a reasonable match for the natural state of the reservoir as well as the observed pressure drawdown. Predicting the response of Reykjanes reservoir in 2012-2027, for a production to maintain 150 MW_e power generation with 77.8 kg/s injection, caused the mass being removed at a higher rate than physically possible. Increasing the injection to 220 kg/s resulted in a semi-stable pressure and after 15 years of simulation a total of 18 bar drawdown in pressure was detected in the center of the reservoir and 12 bar at the boundaries.

The coupling procedure suggested in this study, with measured wellhead conditions as main inputs, yielded reasonable results for the Reykjanes geothermal field. Therefore, after further validation, the simulator might prove to be a useful tool in future assessments of geothermal resources, both in Iceland and worldwide.

Útdráttur

Þegar líkan af jarðhitageymi er útbúið er reynt að herma bæði flæði í jarðhitageymi og borholum, venjulega hvort í sínu lagi. Meginmarkmið þessa verkefnis er að þróa líkan þar sem flæði í jarðhitageymi og borholum er hermt í samfelldri keyrslu. Með því að tengja saman jarðhitalíkan og borholulíkan má ná fram nákvæmari niðurstöðum þar sem gert er ráð fyrir að breytingar á flæði í jarðhitageymi hafi áhrif á flæði í borholum og öfugt. Þar að auki er áhersla lögð á að nota mælingar sem framkvæmdar eru á borholutoppum í meira mæli en áður hefur verið gert. Þetta er gert með því að nota þær sem megininntök í líkanið. Forritið TOUGH2 er notað til að herma flæðið í jarðhitageymi en nýtt líkan, FloWell, er hannað til að herma flæðið í borholum. Að lokum er greint frá reiknilíkani af jarðhitakerfinu á Reykjanesi sem nýtir samtengda FloWell-TOUGH2 líkanið.

Samanburður við mæld gildi sýnir að FloWell hermir þrýsting í borholum á Reykjanesi og í Svartsengi nokkuð vel. Ágætlega tókst að herma náttúrulegt ástand jarðhitakerfisins á Reykjanesi sem og að samræma sögu niðurdráttar í kerfinu. Þegar spáð var fyrir um viðbrögð jarðhitakerfisins við 150 MW_e rafmagnsframleiðslu og 77,8 kg/s niðurdælingu kom í ljós að þrýstingur hafi fallið of mikið og reynt var að fjarlægja meiri vökva úr kerfinu en var til staðar. Hins vegar leiddi aukning niðurdælingar í 220 kg/s til stöðugs niðurdráttar í jarðhitakerfinu þar sem niðurdrátturinn var orðinn 18 bar í miðju kerfisins og 12 bar við jaðarinn eftir 15 ár.

Aðferðin sem kynnt var í þessu verkefni til að tengja saman FloWell og TOUGH2, með mældar stærðir á borholutoppum sem megininntök, skilaði ágætum niðurstöðum fyrir jarðhitakerfið á Reykjanesi. Eftir frekari sannprófanir á aðferðinni gæti hún því reynst gagnlegt verkfæri við mat á jarðhitaauðlindum, bæði á Íslandi og um allan heim.

Contents

List of Figures

List of Tables

Nomenclature

A	Cross sectional area	$[m^2]$
C	Specific heat	$[J/kg°C]$
c	Overall contribution of a data set	
B	Concentration of tracer	
b	Relative measure of parameter sensitivity	
D	Distance	$[m]$
d	Well inner diameter	$[m]$
E	Dimensionless number, simplicity factor	
F	Dimensionless number, simplicity factor	
F_1	Dimensionless number, simplicity factor	
F_2	Dimensionless number, simplicity factor	
f	Friction factor	
Fr	Friedel number	
G	Mass velocity	$[kg/m^2s]$
g	Acceleration due to gravity	$[m/s^2]$
H	Model parameter	
h	Enthalpy	$[J/kg]$
K	Dimensionless number, simplicity factor	
k	Absolute permeability	$[m^2]$
k_r	Relative permeability	
M	Mass per volume	$[kg/m^3]$
$\dot{m}$	Mass flow rate	$[kg/s]$
$\dot{m}_T$	Tracer injection mass flow rate	
NK	Number of mass components	
p	Pressure	$[Pa]$

P_c	Critical pressure	$[Pa]$
P_e	Element pressure, reservoir pressure	$[Pa]$
P_t	Wellhead pressure	$[Pa]$
P_b	Wellbore bottomhole pressure	$[Pa]$
PI	Productivity index	$[m^3]$
$\dot{Q}$	Heat loss from pipe	$[W/m]$
q	Mass generation rate	$[kg/s]$
R	Residual	
Re	Reynolds number	
S	Slip ratio, fluid saturation or objective function	
s_0^2	Measure of goodness-of-fit	
T	Temperature	$[K]$
T_c	Critical temperature	$[K]$
t	Time	$[s]$
u	Velocity	$[m/s]$
V	Volume	$[m^3]$
v	Specific internal energy	$[J/kg]$
We	Weber number	
X	Mass fraction	
x	Steam quality	
y	Dimensionless number, simplicity factor	
z	Axial coordinate, depth	$[m]$

Vectors

$\mathbf{C_{pp}}$	Covariance matrix of estimated parameters	
$\mathbf{C_{zz}}$	Covariance matrix of measurement errors	
$\mathbf{F}$	Mass or heat flux	$[kg/m^2s]$ or $[J/m^2s]$
$\mathbf{g}$	Vector of gravitational acceleration	$[m/s^2]$
$\mathbf{H}$	Hessian matrix	
$\mathbf{J}$	Jacobian matrix	
$\mathbf{n}$	Normal vector	

$\mathbf{p}$	Parameter set	
$\mathbf{r}$	Residual vector	
$\mathbf{u}$	Darcy velocity	$[m/s]$
$\mathbf{z}$	Model output vector (e.g. pressure temperature, etc)	
$\mathbf{z}^*$	Observation vector (e.g. pressure temperature, etc)	

Greek letters

α	Void fraction	
Γ	Surface area	$[m^2]$
γ	Dimensionless number, simplicity factor	
ϵ	Well roughness	$[m]$
ε	Convergence tolerance	
η	Dimensionless number, simplicity factor	
λ	Thermal conductivity or Levenberg parameter	$[W/m°C]$ or $[-]$
μ	Dynamic viscosity	$[Pa \cdot s]$
ν	Kinematic viscosity	$[m^2/s]$
ρ	Density	$[kg/m^3]$
ρ_x	Homogenous density based on steam quality	$[kg/m^3]$
ρ_α	Homogenous density based on void fraction	$[kg/m^3]$
σ	Surface tension or standard deviation	$[N/m]$ or $[-]$
Φ^2	Friction correction factor	
ϕ	Rock porosity	

Subscripts

l	Liquid phase
g	Gas or vapor phase
β	Either liquid or gas phase (l,g)
R	Both liquid and gas phase (l,g)

Acknowledgements

I would like to thank my supervisors for their wise guidance and helpful suggestions during this study, Magnús Þór Jónsson and Halldór Pálsson, professor and associate professor at the Department of Industrial Engineering, Mechanical Engineering and Computer Science at the University of Iceland. Sincere thanks are extended to my primary supervisor, Magnús, for his time, patience end endless encouragement throughout this work.

Furthermore, I would like to express gratitude to the HS Orka Power Company for providing data used in this study. Geir Þórólfsson at HS Orka receives special thanks for his helpfulness in the data collecting process.

Lilja Magnúsdóttir, PhD candidate at Stanford University, helped familiarize me with the reservoir simulator TOUGH2 used in this study. Her help and contribution to my work is gratefully acknowledged. Moreover, I would like to thank the geothermal reservoir specialists, Sigríður Sif Gylfadóttir at Iceland GeoSurvey and Andri Arnaldsson at Vatnaskil Consulting Engineers, for their advice regarding TOUGH2.

Lastly, acknowledgements are given to the the GEOthermal Research Group (GEORG) which funded the research behind the development of the models discussed in this paper.

1. Introduction

With growing world population and increasing environmental concerns, the demand for renewable energy and sustainable use of resources is steadily rising. Geothermal energy is classified as a renewable resource and has the potential of contributing greatly to sustainable energy use in many parts of the world. The energy is generated and stored in the Earth. The main source of the heat is the radioactive decay of unstable isotopes within the mantle and the crust but some of the heat stored in the Earth is also from the formation of the planet. Heat flows continuously from Earth's core to the surface, heating rocks and groundwater, and from the surface it is lost to the atmosphere. In terms of a human life time, the geothermal energy is virtually inexhaustible, if used in a sensible manner [19].

Geothermal energy production can be sustained for decades and even centuries. However, excessive production sometimes occurs, resulting in cooling of rocks, reduced production capacity and finally depletion of geothermal reservoirs. Overexploitation is caused by poor resource management, involving inadequate monitoring and data collection, insufficient understanding of geothermal systems and unreliable modeling. Monitoring the behavior of a geothermal reservoir and wells over time leads to greater understanding of the resource's nature and allows extensive databases of geophysical parameters to be created. Mathematical models are developed on the basis of these databases. These numerical models are one of the most important tools in geothermal resource management. They can be used to extract information on conditions of geothermal systems, predict reservoir's behavior and estimate production potential [8].

With the growth of the geothermal industry, computer models of geothermal systems have become more sophisticated. The geothermal industry began accepting the concept of geothermal simulations in the 1980s. During that time, a great deal of pioneering work was published, but lack of computer power forced the pioneers to simplify the geometry in their models so computational meshes could be created. As the computer power available increased more complex simulators emerged, producing more accurate results than their predecessors. Although modern computers have allowed scientists to model geothermal systems in more detail, most of the models are based on modeling techniques developed in the 1980s [70].

Modeling a geothermal power production requires simulating the behavior of a reservoir, the flow in production and injection wells and the flow in a fluid gathering pipe system. These three components are usually simulated individually with suitable models, where output of one model is used as an input to the next. Few simulators model a complete geothermal system but attempts have been made to link reservoir simulators and wellbore simulators together. Coupling these simulators allows for more accurate modeling of a geothermal system and produces more credible simulation responses to production.

Most reservoirs are monitored by using logging tools to measure pressures and temperatures in wells. From these measurements the drawdown in pressure in a reservoir can be estimated. This is a time consuming and expensive process which usually involves a production stop in producing geothermal wells. On the other hand, well conditions are observed constantly by measuring instruments accessible at the top of wells. From the information gathered at the wellheads much can be learned about the behavior of wells and consequently the reservoir behavior. Therefore, a method for simulating the response of geothermal systems to exploitation, such as the drawdown in pressure, by easily obtained wellhead parameters is very desirable.

The main objective in this study is to create a practical tool to evaluate the state of geothermal reservoirs and well performances using measured wellhead conditions and inverse analysis. This is to be done by coupling a wellbore simulator to a reservoir simulator with the measured conditions as main inputs. For this purpose the program TOUGH2 is used to simulate the multi phase flow in a reservoir while a new wellbore simulator, FloWell, is designed to simulate the behavior of wells. The inverse analysis enables continuous evaluation of chosen parameters in both FloWell and TOUGH2 and the measured wellhead conditions provide up to date data to model the current situation in the geothermal system. The inverse analysis is performed by employing the parameter estimation program iTOUGH2. Emphasis is put on adjusting the permeability distribution in a reservoir, productivity indices of wells and parameters in void fraction correlations for there are some great uncertainties involved in the assessment of these parameters, which have led to disagreement among investigators. The void fraction is for example one of the critical unknown parameter involved in geothermal management. It is an empirical correlation created under specific conditions and has several restrictions attached to it. The permeability is one of the primary factors that control the movement and storage of fluids in the reservoir while the productivity index is a mathematical means of expressing the ability of a reservoir to deliver fluids to a well.

In addition to coupling FloWell to TOUGH2 the wellbore simulator FloWell is validated with pressure logs from Reykjanes and Svartsengi geothermal fields. Finally, a detailed numerical model of the Reykjanes geothermal field in Iceland including the coupled FloWell-TOUGH2 model is constructed and used in several forecasting scenarios where different reservoir management options are examined.

The thesis is organized as follows. Chapter 2 serves as a literature review of earlier findings and published work. In Chapter 3 the theory behind the wellbore simulator FloWell, the reservoir simulator TOUGH2 and the parameter estimation program iTOUGH2 is discussed. In Chapter 4, the basic architecture of FloWell is introduced along with a validation of the model. Chapter 5 presents the methodology behind the coupled wellbore-reservoir simulator and Chapter 6 serves as a case study for the Reykjanes geothermal field where FloWell and the coupled FloWell-TOUGH2 model are put in use. Lastly, Chapter 7 contains discussion and conclusions and final comments about possible improvements and future work.

2. Historical Review

As the numerical solution of differential equations became a possibility, the oil and gas industry were quick to adopt the solution methods and use them to simulate the underground behavior in oil and gas reservoirs. However, due to the complexity involved in coupling between mass and energy transport in geothermal reservoirs, the application of these methods in the geothermal industry lagged behind their application in oil and gas industry. As a result, most well-known correlations used in geothermal simulations are originated from the oil and gas industry. These correlations have been modified to suit the conditions found in geothermal areas [70].

Since the geothermal industry began developing numerous geothermal models have been published. The most used models are those which simulate underground flow in geothermal reservoirs and models that simulate the internal flow processes in geothermal wells. Over the years attempts have been made to couple wellbore simulators with reservoir simulators to predict the behavior of geothermal systems with time. Some have been successful while others not. Following is a short historical review of wellbore simulators, reservoir simulators and coupled wellbore-reservoir models. It is worth noting that the following review is not complete, only what is considered to be the most important published work in the field is mentioned.

2.1. Wellbore Simulators

Two phase flow models fall into two categories; homogenous flow models and separate flow models. In homogenous flow models it is assumed that the liquid and the vapor phases travel at equal velocities and therefore the interaction between the phases is ignored. In separate flow models the restriction on equal velocities is relaxed and instead assumed that the phases flow concurrently. Separate equations are written for each phase, generally in the form of empirical correlations, and the slippage between the phases is taken into account. Separate flow models are considered to be more reliable than homogenous flow models and to provide better predictions of flow behavior [14, 40].

The separated flow model originates from the work of Lockhart and Martinelli (1949). The Lockhart-Martinelli model is one of the simplest models available for predicting pressure drop in two phase flow. The model's main advantage is that it can be used for all flow regimes, but lack of accuracy must be expected due to its wide range of application. Martinelli and Nelson (1948) later extended the correlation of Lockhart and Martinelli to better suit annular and turbulent flow [6].

Poettmann and Carpenter (1952) were the first ones to develop a practical calculation model for vertical two phase flow. It ignored effects of flow patterns and slippage between phases was disregarded. Until the early 1960s, their model was the only one available to calculate pressure drop in oil wells. Due to its low accuracy it is now outdated. The first ones to consider flow regimes and to develop different correlations for each regime were Duns and Ros (1963). By processing extensive experimental data they showed that flow conditions in different flow patterns were different from each other. Their approach is still accepted by scientist studying two phase flow. Hagedorn-Brown (1965) constructed one of the more successful pressure drop calculation model. It was widely used by many investigators for several decades. Their model included the effects of slippage but no flow patterns were distinguished. Orkiszewski (1967) approached the two phase flow in a different manner than foregoing scientists. He put several previous models together with modifications based on 148 pressure drop measurements. As a result, his correlation offered increased accuracy in pressure drop computations. The Orkiszewski correlation is frequently used in two phase flow calculations [88].

Gould (1974) developed the first numerical program capable of modeling two phase flow in geothermal wellbores. Gould used a combination of correlations from the petroleum industry and coupled them with heat transfer equations to model the two phase flow. He compared the predicted pressure drop to measured field data and concluded that Hagedorn-Brown and Turner-Ros correlations were the most consistent [14, 73].

Upadhyay et al. (1977) compared calculated and observed pressure drops in geothermal two phase flow wells. They used several different correlations to predict pressure drop in two phase flow. The Orkiszewski (1976) correlations produced the most accurate predictions while the Hagedorn-Brown correlations came in second [14, 73].

Goyal et al. (1980) used data from the Cerro Prieto geothermal field in Mexico to study the effect of measured wellhead parameters on downhole pressures in wellbores. They used the steady state program WELFLOW to calculate the bottomhole conditions. They concluded that calculated downhole pressures are rather sensitive to changes in wellhead conditions as well as wellbore inside diameters. With this study the effects caused by scale deposits in wellbores became evident to scientists [36].

Miller (1980) developed one of the earliest transient wellbore simulator, WELBORE. The program solves the equations for mass, momentum and energy with a partially implicit method. Unlike previous wellbore simulators a steady state is not assumed, i.e. the mass into the well does not necessary equal the mass out of it. She proposed using the model to study early transient changes in the wellbore. Moreover, by coupling it with a simple reservoir model, the early-time interaction of the well flow and reservoir flow during a well test in geothermal wells could be investigated [65].

Bilicki et al. (1981) constructed a one dimensional simulator, BROWN, with a single liquid feed point. The model starts calculating at the bottom of a well and continues upwards with a stepwise integration method. The liquid phase is assumed to be NaCl liquid solution but the vapor phase pure water. The authors disregarded the presence of non-condensible gases for they believed the effect on the properties of the working fluid could be ignored. One distinctive characteristic of the model is that the transition boundaries between the flow regimes are evaluated in an analytical manner using experimental results [30].

Barelli et al. (1982) have shown that if the presence of CO_2 is neglected the comparison of pressure and temperature profiles becomes insignificant. They described a steady state wellbore simulator that included a unique point of interest not found in other models, namely, they accounted for non-condensable gases and dissolved solids. It was found that an increase in CO_2 concentration brings about an increase in pressure but has little effect on temperature [45].

Ortiz-Ramirez (1983) developed a geothermal simulator, WF2, at Stanford University. His work was based on earlier efforts at Stanford University. The model assumes one dimensional and steady state flow with a single feed point. It was one of few simulators at that time which allowed calculations to start at the top or the bottom of a well [30, 73].

Bjornsson (1987) developed a geothermal wellbore simulator, HOLA, to simulate one or two phase flow in a vertical well with multiple feedzones. The motive for his work was that limited explorations had been carried out concerning the effects of multiple feedzones with different pressure potentials on wellbore performances [14]. Later, two other simulators, GWELL and GWNACL, were published. They are modified versions of HOLA that can handle H_2O-CO_2 and H_2O-NaCl systems, respectively [5].

Gunn and Freeston (1991) implemented a wellbore simulation package, WELLSIM, where three codes ,WFSA, WFSB and STFLOW, were combined into one. The code WFSA (Well Flow Simulator A) can model the presence of dissolved solids, multiple feedzones and fluid-rock heat exchange. It is not capable of modeling the presence of gases but WFSB (Well Flow Simulator B) was designed specifically to model gassy wells. WFSB is however not able to model multiple feedzones. STFLOW (Steam

Flow) was designed to model wells in vapor-dominant areas and can model saturated or superheated steam. WELLSIM includes all the features of the three codes and can therefore be used to analyze wells with different characteristics [29, 39, 41].

García-Valladares et al. (2006) conducted one dimensional steady and transient numerical model, GEOWELLS, to describe heat and fluid dynamic transport inside geothermal wells. Governing equations were solved with a fully implicit step by step method. The simulator, together with Orkiszewski relations, was applied to model the heat and fluid flow processes inside wells in Mexican geothermal fields. The simulator yielded predictions in good agreement with measured profiles of pressures and temperatures. Furthermore, the authors discussed the effect of input data uncertainties in GEOWELLS simulations [33].

Since the first wellbore simulator was published, scientist have striven for improving modeling techniques and renewing older work. Number of wellbore simulators have been discussed in published literature and it is needless to describe all in details here. Other known wellbore simulators include VSTEAM, GEOTEMP2, WELLCARD, PROFILI, SIMU93, SIMU2000, MULFEWS and SuperWell [10, 58, 66, 85–87, 91, 92].

2.2. Reservoir Simulators

Different assessment methods are used in geothermal resource management. These methods are either classified as volumetric assessment methods or dynamic modeling methods. Volumetric methods are commonly used for first stage assessment, but lack consideration for the response of the geothermal reservoir in question. Dynamic methods can be categorized into simple analytical models, lumped parameter models and numerical models. In simple methods the structure and properties of a geothermal system are greatly simplified. Simple modeling is a time saving and cost effective alternative and requires limited data about the geothermal system and its response. However, simple models can only simulate one aspect of a geothermal system's response, whereas numerical models can accurately simulate most aspects of the response to production. Detailed numerical modeling is the most powerful modeling method available and is generally the preferred technique to determine production potential of a geothermal reservoir. It is a time consuming and often expensive process and requires detailed data about the geothermal system. It is therefore important to evaluate the data, time and financial support available when choosing a modeling technique [7, 70].

The development of the first geothermal reservoir simulators took place in the 1970s. Whiting and Ramey (1969) were the first to construct a lumped parameter model

of the Wairakei geothermal system. Due to the availability of data, the Wairakei field in New Zealand was frequently used as a case study for models in development. It was the first high-temperature field to be substantially exploited, and scientists desired to understand the rapid decline in reservoir pressure that occurred soon after the generation started in 1958 [38, 71].

As the development of the lumped parameter models of Warakei continued, numerical modeling of geothermal systems started to evolve. Nowadays, numerical modeling is the most important part of geothermal management and has been a subject in number of studies. The methods used in most of these studies were developed within many pioneering groups, both in the public sector and the private industry; Lawrence Berkeley National Laboratory, Los Alamos National Laboratory, US Geological Survey, University of Auckland, GeothermEx and Unocal [70].

Commonly used reservoir simulators include STAR, TETRAD and TOUGH2 [79, 81, 96]. These are all three dimensional simulators that are capable of treating the complex structure of the reservoir as well as managing multi phase flows. TETRAD and STAR require rectangular meshes whereas TOUHG2 can handle general unstructured meshes, making TOUGH2 the most appealing option when taking on numerical modeling of a geothermal reservoir [70]. TOUGH2 is described in more detail in the section *The Forward Model TOUGH2* in Chapter 3.

Other known geothermal reservoir simulators, that are not as widely used, include PT, GEOTHER/HYDROTHERM, AQUA, GEMMA, SING, SIM.FIGS and FEFLOW [18, 24, 44, 53, 57, 68, 76].

2.3. Coupled Wellbore-Reservoir Simulators

Usually, the flow in the wellbore is simulated separately from the one in the reservoir. However, the flow in the wellbore cannot be considered in isolation; it must be coupled to the flow in the reservoir [25]. By coupling wellbore and reservoir simulators, more accurate modeling of the exploitation of a geothermal system is accomplished. Several attempts have been made to couple wellbore and reservoir simulators with different approaches [41].

Miller (1980) developed one of the earliest transient wellbore models. Her model included heat and mass transfer and was coupled to a simple reservoir model. She used the model to investigate the transient behavior of a single and two phase flow in wells during a well test, along with early interactions with the flow in the reservoir [65].

Coupling the wellbore and reservoir simulators can be achieved in two ways, explicitly or implicitly. The first explicit coupling was described by Hagdu et al. (1995). They coupled the wellbore simulator WFSA to the reservoir simulator TOUGH. TOUGH was used to compute the reservoir pressure, temperature, enthalpy, density and kinematic viscosity for each feedzone. WFSA then evaluated the mass flow rate at the deepest feedzone in an iterative process with a first guess for the wellbore pressure. WFSA computed the flow parameters up the wellbore till the next feedzone was detected. Heat and mass balances yielded new flow parameters at this feedzone along with the feed mass flow rate. This procedure was continued for all the feedzones until the wellhead was reached. The computed wellhead pressure was compared to a specified wellhead pressure and if they significantly differed, the iterative process was continued with a different guess value for the wellbore pressure at the deepest feedzone [41].

Murray and Gunn (1993) described an implicit coupling between the reservoir simulator TETRAD and the wellbore simulator WELLSIM. The wellbore simulator was run in advance with a constant wellhead pressure for a range of enthalpies and mass flow rates in order to generate tables of wellbore pressures. Separate tables were generated for each well or group of wells that had the same characteristics. TETRAD determined the flow conditions at the shallowest feedzone and used the tables to evaluate wellhead parameters by interpolation. The flow from deeper feedzones was then calculated by TETRAD using one of the wellbore hydraulic gradient option implemented in the code [67].

The reservoir simulator TOUGH2 is also capable of utilizing wellbore tables when considering a coupled wellbore flow. However, this capability in TOUGH2 is restricted to wells with a single feedzone and can only handle wellbore pressure effects due to change in mass flow rates and enthalpies [81].

More recently, attempts have been made to couple the reservoir simulator TOUGH2 and the wellbore simulator HOLA. Baht et al. (2005) described a fully explicit coupled model between TOUGH2 and HOLA. Their main goal was to add the capability of treating multiple feedzones in the wellbore to the coupled wellbore flow in TOUGH2. Baht et al. followed a similar path to Hagdu et al. A call was made to HOLA at the start of each timestep which iterated to calculate flow rates and enthalpies at various feedzones and at the wellhead. They concluded that a coupled reservoir-wellbore model certainly predicts more accurately than a non-coupled one [12].

Rivera Ayala (2010) described an implicit coupling of TOUGH2 and HOLA through wellbore tables. He compared two options for fluid production in TOUGH2; wells on deliverability against specified bottomhole pressure and wells on a deliverability against specified wellhead pressure. In the second option the wellbore tables of flowing bottomhole pressure were used. He concluded, using the Namafjall geothermal

field in Iceland, that more energy output is attained when wells are modeled as variable well bottom pressure and constant wellhead pressure sinks [83].

By using the implicit method of generating wellbore tables prior to reservoir simulation, the computational time can be significantly reduced and many numerical convergence difficulties avoided. On the other hand, explicit coupling is more accurate because the wellhead conditions are calculated directly by the wellbore simulator [93].

At the moment, no single simulator that is capable of simulating all aspects of geothermal power generation exists [17]. Future steps will hopefully involve development of a simulator that is able to simulate the reservoir, the wellbore, the gathering system and the power plant in a coupled manner. However, care must be taken not violate the main rule of geothermal resource management, keeping models as simple as possible.

3. Theoretical Background

In this chapter the theoretical background for this study will be discussed. First the flow within the wellbore is described, where the expression of governing equations for single and two phase flow proposed by Pálsson (2011) is used. Secondly the physical theory and mathematical approaches implemented in the reservoir simulator TOUGH2, the optimization program iTOUGH2 and the iTOUGH2 universal optimization using the PEST protocol are presented, as explained by their creators Pruess et al. (1999), Finsterle (2007) and Finsterle (2010) respectively.

3.1. The Physical Model of FloWell

Two phase flow occurs frequently in our nature and is most common in geothermal reservoirs, wellbores and surface pipelines. Whether the flow contains two immiscible liquids, a liquid and a solid, a liquid and a vapor, or a solid and a vapor, the internal topology of the flow constantly changes as the phases interact, exchanging energy, momentum and often mass. Following sections describe the mathematical approaches behind the wellbore simulator FloWell, beginning with the most general principles governing the behavior of all matter, namely, conservation of mass, momentum and energy.

3.1.1. Single Phase Flow

The continuity equation derives from the conservation of mass, simply stated as

$$\frac{d}{dz}(\dot{m}) = 0 \tag{3.1}$$

Expressing this in terms of density, velocity of the fluid and cross sectional area of the pipe, and assuming that the pipe diameter is constant, the equation becomes

$$\frac{d}{dz}(\rho u) = 0 \tag{3.2}$$

By applying differentiation rule for a product of functions and using a version of the Chain Rule, because ρ is a function of p and h with continuous first partial derivatives, and p and h are differentiable functions of z, the relation can be written as

$$u\left(\frac{\partial\rho}{\partial p}\frac{dp}{dz}+\frac{\partial\rho}{\partial h}\frac{dh}{dz}\right)+\rho\frac{du}{dz}=0 \tag{3.3}$$

The energy equation is derived from the first law of thermodynamics. The law states that energy can be transformed from one form to another, but can neither be created nor destroyed [22]. The equation contains a kinetic energy part, gravitational potential energy part and thermal energy part so the relation becomes

$$\frac{d}{dz}\left(\dot{m}\left(\frac{u^2}{2}+gz+h\right)\right)+\dot{Q}=0 \tag{3.4}$$

By using the product rule for the differentiation, the continuity equation to eliminate one part of the equation and implementing the Chain Rule for partial derivatives, the energy equation can be written as

$$\dot{m}u\frac{du}{dz}+\dot{m}\frac{dh}{dz}+\dot{m}g+\dot{Q}=0 \tag{3.5}$$

The momentum equation is a statement of Newton's second law. It relates the sum of forces acting on an element of fluid to its rate of change of momentum [22]. The momentum equation can be written as

$$\rho u\frac{du}{dz}+\frac{dp}{dz}+\rho g+\frac{\rho f}{2d}|u|u=0 \tag{3.6}$$

where the terms in the equation represent inertia, pressure changes, hydrostatic pressure and head losses. Possible equations for the friction factor, f, are the Blasius relation for smooth pipes

$$f=\frac{0.316}{Re^{1/4}} \tag{3.7}$$

and the Swamee-Jain [22] relation for pipes with roughness

$$f=\frac{0.25}{\left(log_{10}\left(\frac{\epsilon}{3.7d}+\frac{5.74}{Re^{0.9}}\right)\right)^2} \tag{3.8}$$

where Re is the dimensionless Reynolds number defined as

$$Re=\frac{\rho u d}{\mu} \tag{3.9}$$

The continuity, energy and mass equations for single phase flow can be assembled to a single system;

$$\begin{bmatrix}\rho & u\frac{\partial\rho}{\partial p} & u\frac{\partial\rho}{\partial h}\\ \dot{m}u & 0 & \dot{m}\\ \rho u & 1 & 0\end{bmatrix}\frac{d}{dz}\begin{bmatrix}u\\p\\h\end{bmatrix}+\begin{bmatrix}0\\\dot{m}g+\dot{Q}\\\rho g+\frac{\rho f}{2d}|u|u\end{bmatrix}=\begin{bmatrix}0\\0\\0\end{bmatrix} \tag{3.10}$$

This first order set can either be solved by finite difference methods or numerical integration from the well bottom to the top or vice versa.

3.1.2. Two Phase Flow

The laws governing two phase flow are identical to those for single phase flow. However, when two phases are present in a wellbore the flow will take on more complex fluidic behavior causing the governing equations to be more complicated. The steam quality, x, is one of the additional parameters needed for two phase flow calculations. It is the ratio of the mass of vapor to the total mass of liquid and vapor. This ratio is a function of the depth, z, and is constantly increasing as the fluid mixture flows up the well due to boiling in deeper sections of the well.

$$x = \frac{\dot{m}_g}{\dot{m}_l + \dot{m}_g} \tag{3.11}$$

In separated flow models it is assumed that the phases flow side by side with different velocities, u_l and u_g. Pálsson (2011) expresses the flow velocity in the well as if the liquid is flowing alone in the pipe, but with the total mass flow rate of liquid and vapor. This uniform velocity is written as

$$u = \frac{\dot{m}}{\rho_l A} \tag{3.12}$$

The actual velocities of liquid and vapor phases, u_l and u_g can be directly related to the flow velocity, u, described as follows.

$$u_l = \frac{\dot{m}_l}{\rho_l A_l} = \frac{(1-x)\dot{m}}{\rho_l(1-\alpha)A} = \frac{1-x}{1-\alpha}u \tag{3.13}$$

$$u_g = \frac{\dot{m}_g}{\rho_g A_g} = \frac{x\dot{m}}{\rho_g \alpha A} = \frac{x}{\alpha}\frac{\rho_l}{\rho_g}u \tag{3.14}$$

where α is the void fraction, defined later in the section.

In two phase flow the total mass flow consists of both liquid and vapor. Applying $\dot{m} = \dot{m}_l + \dot{m}_g$ to Eq. (3.1) for single phase flow, assuming constant diameter and using the definition of void fraction, the continuity equation can be expressed as

$$\frac{d}{dz}(\rho_l u_l(1-\alpha) + \rho_g u_g \alpha) = 0 \tag{3.15}$$

Further simplifications can be implemented by using the uniform velocity u instead of the actual velocities for vapor and liquid states;

$$\frac{d}{dz}(\rho_l u) = 0 \tag{3.16}$$

Finally, partial differentiation yields the following form of the continuity equation;

$$u\frac{\partial \rho_l}{\partial p}\frac{dp}{dz} + \rho_l \frac{du}{dz} = 0 \tag{3.17}$$

The energy equation can be written as

$$\frac{d}{dz}\left(\dot{m}_l\left(\frac{u_l^2}{2} + gz + h_l\right) + \dot{m}_g\left(\frac{u_g^2}{2} + gz + h_g\right)\right) + \dot{Q} = 0 \tag{3.18}$$

Noting that $\dot{m}h = \dot{m}_l h_l + \dot{m}_g h_g$, $\dot{m}_l = (1-x)\dot{m}$ and $\dot{m}_g = x\dot{m}$, as well as the uniform velocity u and introducing a simplicity factor, γ, along with its derivative, the energy equation becomes

$$\gamma u\frac{du}{dz} + \frac{u^2}{2}\frac{\partial \gamma}{\partial p}\frac{dp}{dz} + \left(1 + \frac{u^2}{2}\frac{\partial \gamma}{\partial h}\right)\frac{dh}{dz} + g + \frac{\dot{Q}}{\dot{m}} = 0 \tag{3.19}$$

where γ is defined as

$$\gamma = \frac{(1-x)^3}{(1-\alpha)^2} + \frac{\rho_l^2 x^3}{\rho_g^2 \alpha^2}$$
$$\frac{\partial \gamma}{\partial z} = \frac{\partial \gamma}{\partial p}\frac{dp}{dz} + \frac{\partial \gamma}{\partial h}\frac{dh}{dz}$$

For single phase flow the momentum equation, Eq. (3.6), can be expressed as

$$\frac{d}{dz}(\dot{m}u) + A\frac{dp}{dz} + \rho g A + \frac{\rho f A}{2d}u^2 = 0 \tag{3.20}$$

However in two phase flow, both velocities have to be accounted for in the inertial part of Eq. (3.20). Additionally, the density in the gravitational part should be the homogenous density based on the void fraction, $\rho_\alpha = (1-\alpha)\rho_l + \alpha\rho_g$. This results in

$$\frac{d}{dz}(\dot{m}_l u_l + \dot{m}_g u_g) + A\frac{dp}{dz} + ((1-\alpha)\rho_l + \alpha\rho_g)gA + \Phi^2\frac{\rho_l f A}{2d}u^2 = 0 \tag{3.21}$$

where Φ^2 is the friction correction factor for two phase flow, defined later in the section. Inserting Eq. (3.13) and Eq. (3.14) for u_l and u_g respectively, noting that $A_l = (1-\alpha)A$ and $A_g = \alpha A$ and introducing a simplicity factor, η, along with its derivative, the momentum equation can be written as

$$\begin{aligned}\eta\rho_l u\frac{du}{dz} + \left(1 + \rho_l u^2\frac{\partial \eta}{\partial p} + \eta u^2\frac{\partial \rho_l}{\partial p}\right)\frac{dp}{dz} + \rho_l u^2\frac{\partial \eta}{\partial h}\frac{dh}{dz} \\ + ((1-\alpha)\rho_l + \alpha\rho_g)g + \Phi^2\frac{\rho_l f}{2d}u^2 = 0\end{aligned} \tag{3.22}$$

where η is defined as

$$\eta = \frac{(1-x)^2}{1-\alpha} + \frac{\rho_l}{\rho_g}\frac{x^2}{\alpha}$$
$$\frac{\partial \eta}{\partial z} = \frac{\partial \eta}{\partial p}\frac{dp}{dz} + \frac{\partial \eta}{\partial h}\frac{dh}{dz}$$

Since the uniform velocity, u, is based on liquid properties the friction factor, f, in the momentum equation for two phase flow must be evaluated based on the liquid Reynolds number;

$$Re_l = \frac{\rho_l u d}{\mu_l} \tag{3.23}$$

As for the single phase flow, the continuity, energy and momentum equations can be assembled to one system that can either be solved by finite difference methods or numerical integration from the well bottom to the top or the well top to the bottom;

$$\begin{bmatrix} \rho_l & u\frac{\partial \rho_l}{\partial p} & 0 \\ \gamma u & \frac{u^2}{2}\frac{\partial \gamma}{\partial p} & \left(1+\frac{u^2}{2}\frac{\partial \gamma}{\partial h}\right) \\ \eta\rho_l u & \left(1+\rho_l u^2\frac{\partial \eta}{\partial p}+\eta u^2\frac{\partial \rho_l}{\partial p}\right) & \rho_l u^2\frac{\partial \eta}{\partial h} \end{bmatrix} \frac{d}{dz}\begin{bmatrix} u \\ p \\ h \end{bmatrix} + \begin{bmatrix} 0 \\ g+\frac{\dot{Q}}{\dot{m}} \\ \left((1-\alpha)\rho_l+\alpha\rho_g\right)g+\Phi^2\frac{\rho_l f}{2d}u^2 \end{bmatrix} = \begin{bmatrix} 0 \\ 0 \\ 0 \end{bmatrix} \tag{3.24}$$

Comparing this set of equations to the set of equations for single phase flow the increase of complexity is apparent. The two phase formulation has as an addtion the evaluations of x, α, Φ^2, γ and η and their derivatives.

Theoretical modeling of a two phase flow can often prove to be a troublesome process. The pressure drop and the void fraction are among the most important hydrodynamic aspects of a two phase flow and tend to increase the complexity of calculations intensively [94]. These complicating factors involved in two phase flow make the use of empirical and analytical equations fairly attractive. Empirical correlations are based on observations and experiments, where scientists try to measure the pressure drop and the void fraction. These experimental efforts often take place under a range of operating conditions for bounded set of fluids. Investigators studying a two phase flow often find it challenging to choose suitable correlations for their studies. That is mainly due to the fact that available correlations are limited to the range of test data that was used to form them. Some correlations may therefore yield poor results while others give better outcomes for the same operation conditions [37].

The void fraction is one of the critical unknown parameters involved in two phase flow calculations. The most widely used void fraction definition is the cross sectional

average void fraction, where the void fraction is defined as the fraction of the channel cross sectional area that is occupied by gas phase [90];

$$\alpha = \frac{A_g}{A_g + A_l} \tag{3.25}$$

Numerous void fraction correlations exist in technical literature but only a few will be considered in this study. The basic homogenous void fraction model is defined in [37, 90, 97] as

$$\alpha = \left[1 + \left(\frac{1-x}{x}\right)\left(\frac{\rho_g}{\rho_l}\right) S\right]^{-1} \tag{3.26}$$

where S is the *slip ratio* or the *velocity ratio*;

$$S = \frac{u_g}{u_l} \tag{3.27}$$

In the homogenous model it can be assumed that the phases travel at the same velocity yielding the slip ratios to be equal to one. Other models extend the simple homogenous flow model by using other derived relations as the slip ratio. Zivi (1964) proposed that the slip ratio was only dependant on the density ratio of the phases [37, 90, 97];

$$S = \left(\frac{\rho_l}{\rho_g}\right)^{1/3} \tag{3.28}$$

The Zivi void fraction expression can therefore be written as

$$\alpha = \left[1 + \left(\frac{1-x}{x}\right)\left(\frac{\rho_g}{\rho_l}\right)^{2/3}\right]^{-1} \tag{3.29}$$

Chisholm (1973) arrived at the following correlation for the slip ratio

$$S = \left(\frac{\rho_l}{\rho_x}\right)^{1/2} = \left(1 + x\left(1 - \frac{\rho_l}{\rho_g}\right)\right)^{1/2} \tag{3.30}$$

where ρ_x is the homogenous density based on steam quality defined as

$$\frac{1}{\rho_x} = \frac{x}{\rho_g}\frac{1-x}{\rho_l} \tag{3.31}$$

Similar to the Zivi void fraction the Chisholm correlation can be expressed as an extended homogenous model [37, 97];

$$\alpha = \left[1 + \left(\frac{1-x}{x}\right)\left(\frac{\rho_g}{\rho_l}\right)\left(1 + x\left(1 - \frac{\rho_l}{\rho_g}\right)\right)^{1/2}\right]^{-1} \tag{3.32}$$

One of the more complex void fraction correlation based on slip ratio is the one introduced by Premoli et al. (1970) [90, 97]. The correlation given in terms of the slip ratio, which can be related to the void fraction using Eq. (3.26) above, is

$$S = 1 + F_1 \left(\frac{y}{1 + yF_2} - yF_2 \right) \tag{3.33}$$

where

$$F_1 = 1.578 Re_l^{-0.19} \left(\frac{\rho_l}{\rho_g} \right)^{0.22} \tag{3.34}$$

$$F_2 = 0.0273 We_l Re_l^{-0.51} \left(\frac{\rho_l}{\rho_g} \right)^{-0.08} \tag{3.35}$$

$$y = \frac{1}{\left(\frac{1-x}{x}\right)\left(\frac{\rho_g}{\rho_l}\right)} \tag{3.36}$$

$$We_l = \frac{G^2 d}{\sigma \rho_l} \tag{3.37}$$

$$Re_l = \frac{Gd}{\mu_l} \tag{3.38}$$

One of the most widely used void fraction correlations is the correlation based on the work of Lockhart and Martinelli (1949). The Lockhart-Martinelli model is expressed in [97] as

$$\alpha = \left[1 + 0.28 \left(\frac{1-x}{x} \right)^{0.64} \left(\frac{\rho_g}{\rho_l} \right)^{0.36} \left(\frac{\mu_l}{\mu_g} \right)^{0.07} \right]^{-1} \tag{3.39}$$

Another well-known group of void fractions is based on the drift flux model. The drift flux model was developed principally by Zuber and Findlay (1965). They derived an expression to predict the void fraction, taking into account the non-uniformity in the flow and the drift velocity. The drift velocity is defined as the difference between the gas phase velocity and the two phase mixture velocity. Rouhani and Axelsson (1970) constructed a popular drift flux void fraction that included mass flux, surface tension and buoyancy effects. Their model can be defined as [33, 37, 97]

$$\begin{aligned} \alpha = \left[\frac{x}{\rho_g} \right] \Bigg[(1 + 0.12(1-x)) \left(\left(\frac{x}{\rho_g} \right) + \left(\frac{1-x}{\rho_l} \right) \right) \\ + \frac{(1.18(1-x))(g\sigma(\rho_l - \rho_g))^{0.25}}{G\rho_l^{0.5}} \Bigg]^{-1} \end{aligned} \tag{3.40}$$

In both the Premoli and Rouhani-Axelsson models, the void fraction is defined as a function of the surface tension. According to the IAPWS (The International Association for the Properties of Water and Steam), the relation for surface tension can be written as [54]

$$\sigma = 0.2358 \left(1 - \frac{T}{T_c} \right)^{1.256} \left(1 - 0.625 \left(1 - \frac{T}{T_c} \right) \right) \tag{3.41}$$

where T_c is the critical temperature, $T_c = 647.096\ K$.

Woldesemayat and Ghajar (2006) performed a comparison of the performance of 68 void fraction correlations on an extensive set of data. Their objective was to find a void fraction that could produce acceptable predictions for all inclination angles and different flow patterns. The Rouhani-Axelsson model showed good prediction capabilities in inclined and vertical flow. The Premoli correlation was the second after Rouhani-Axelsson to predict all data sets with very good accuracy. These two correlations are therefore highly recommended by Woldesemayat and Ghajar for two phase flow calculations in wellbores [97].

As for the void fraction, the two phase frictional pressure drop has been the subject of many experimental studies. Various relations for the friction correction factor exist but in this study two approximations will be considered; the model by Friedel (1979) and the model by Beattie (1973). The Friedel friction correction factor includes both the gravity effect by the Froude number and the effect of surface tension by the Weber number, and is defined as

$$\Phi^2 = E + \frac{3.24FK}{Fr^{0.045}We^{0.035}} \tag{3.42}$$

where

$$E = (1 - x^2) + x^2 \frac{\rho_l}{\rho_g} \frac{f_g}{f_l} \tag{3.43}$$

$$F = x^{0.78}(1 - x^2)^{0.24} \tag{3.44}$$

$$K = \left(\frac{\rho_l}{\rho_g}\right)^{0.91} \left(\frac{\nu_g}{\nu_l}\right)^{0.19} \left(1 - \frac{\rho_g}{\rho_l}\right)^{0.7} \tag{3.45}$$

$$Fr = \frac{\rho_l^2 u^2}{g\rho_x^2 d} \tag{3.46}$$

$$We = \frac{\rho_l^2 u^2 d}{\sigma \rho_x^2} \tag{3.47}$$

Two friction factors are present in the definition of the Friedel friction correction factor, the liquid friction factor f_l and the vapor friction factor f_g. These friction factors are based on corresponding Reynolds numbers, Re_l and Re_g;

$$Re_l = \frac{\rho_l u d}{\mu_l} \tag{3.48}$$

$$Re_g = \frac{\rho_g u d}{\mu_g} \tag{3.49}$$

Unlike the Friedel model, the Beattie [33] correlation is defined in a simpler manner:

$$\Phi^2 = \left(1 + x\left(\frac{\rho_l}{\rho_g} - 1\right)\right)^{0.8} \left(1 + x\left(\frac{3.5\mu_g + 2\mu_l}{(\mu_g + \mu_l)\rho_g} - 1\right)\right)^{0.2} \tag{3.50}$$

3.2. The Forward Model TOUGH2

TOUGH2 is a general numerical simulator for non-isothermal multi phase flow in porous and fractured media. Its main application area is geothermal reservoir management. TOUGH2 is one of the most sophisticated programs available and has been used in a considerable number of field studies worldwide.

3.2.1. Mass and Energy Balances

TOUGH2 calculates the thermodynamic conditions present in a predefined geothermal reservoir. This is accomplished by integrating basic mass- and energy balance equations over an arbitrary sub-domain V_n bounded by the surface Γ_n. The mass- and energy equations can be written in the general form

$$\frac{d}{dt}\int_{V_n} M^\kappa \, dV_n = \int_{\Gamma_n} \mathbf{F}^\kappa \cdot \mathbf{n} \, d\Gamma_n + \int_{V_n} q^\kappa \, dV_n \tag{3.51}$$

where M denotes mass per volume with $\kappa = 1, ..., NK$, or energy per volume with $\kappa = NK + 1$, and NK is the number of mass components. In this study a single mass component, pure water, is assumed so $\kappa = 1$ for the mass equation and $\kappa = 2$ for the energy equation. $\mathbf{F}$ represents the mass or heat flux, $\mathbf{n}$ is the normal vector on the surface element $d\Gamma_n$ and q is the mass generation for the sinks and sources. The mass accumulation term is given as

$$M^\kappa = \phi \sum_\beta S_\beta \rho_\beta X_\beta^\kappa \tag{3.52}$$

The total mass of component κ is calculated by summing over all phases, in this case, liquid and gas. S_β is the saturation of phase β and X_β^κ is the mass fraction of component κ present in phase β, ϕ is the rock porosity and ρ_β is the density of phase β. For a multi phase, single mass component, this relation can be simplified to

$$M = \phi \sum_\beta S_\beta \rho_\beta \tag{3.53}$$

For the energy balance equation, the heat accumulation can be written as

$$M^{NK+1} = (1 - \phi)\, \rho_R C_R T + \phi \sum_\beta S_\beta \rho_\beta v_\beta \tag{3.54}$$

where ρ_R and C_R are the rock density and specific heat and v_β the specific internal energy of phase β. The advective mass flux term in Eq. (3.51) is a sum over present phases;

$$\mathbf{F}^\kappa_{adv} = \sum_\beta X^\kappa_\beta \mathbf{F}_\beta \tag{3.55}$$

Using the multi phase version of Darcy's law, and ignoring mass transport by diffusion and hydrodynamic dispersion, the individual phase fluxes can be given as

$$\mathbf{F}_\beta = \rho_\beta \mathbf{u}_\beta = -k\frac{k_{r\beta}\rho_\beta}{\mu_\beta}\left(\nabla P_\beta - \rho_\beta \mathbf{g}\right) \tag{3.56}$$

where $\mathbf{u}_\beta$ is Darcy's velocity in phase β, k is absolute permeability, $k_{r\beta}$ is relative permeability to phase β and μ_β is viscosity. P_β is the fluid pressure in phase β, assuming no capillary pressure is present. The relative permeability represents the reduction in available permeability due to the fact that only a fraction of pore space is occupied by phase β [82]. In a simpler manner, it describes how the available absolute permeability is divided between the phases, liquid and gas [83]. The heat flux contains both conductive and convective components, and can be written as

$$\mathbf{F}^{NK+1} = -\lambda \nabla T + \sum_\beta h_\beta \mathbf{F}_\beta \tag{3.57}$$

The thermal conductivity is labeled as λ and h_β is specific enthalpy in phase β.

3.2.2. Space and Time Discretization

Using the integral finite differences method, Eq. (3.51) is discretized as

$$\int_{V_n} M^\kappa \, dV = V_n M^\kappa_n \tag{3.58}$$

where M^κ_n is the average value of M^κ over the volume V_n. Approximating the surface integrals in Eq. (3.51), the discrete sum of averages over the surface segments A_{nm} can be used;

$$\int_{\Gamma_n} \mathbf{F}^\kappa \cdot \mathbf{n} \, d\Gamma = \sum_m A_{nm} F^\kappa_{nm} \tag{3.59}$$

F^κ_{nm} is the average flux over the surface A_{nm} between elements n and m. This discretization approach is illustrated in Fig. (3.1). Substituting these two equations into the mass and energy balance equation, a first order differential equation is obtained;

$$\frac{dM^\kappa_n}{dt} = \frac{1}{V_n}\sum_m A_{nm} F^\kappa_{nm} + q^\kappa_n \tag{3.60}$$

The finite difference expression for the basic Darcy flux term in Eq. (3.56) across the interface between grid blocks n and m is

$$F_{\beta,nm} = -k_{nm}\left[\frac{k_{r\beta}\rho_\beta}{\mu_\beta}\right]_{nm}\left[\frac{P_{\beta,n}-P_{\beta,m}}{D_{nm}} - \rho_{\beta,nm}g_{nm}\right] \tag{3.61}$$

where $D_{nm} = D_n + D_m$ is the distance between nodal points n and m.

To obtain the numerical stability required for multi phase flow calculations the time is discretized as a first order finite difference in a fully implicit manner where the right hand side of Eq. (3.60) is expressed in terms of unknown thermodynamic parameters at time step $t^{k+1} = t^k + \Delta t$. This results in a set of coupled nonlinear equations;

$$R_n^{\kappa,k+1} = M_n^{\kappa,k+1} - M_n^{\kappa,k} - \frac{\Delta t}{V_n}\left\{\sum_m A_{nm}F_{nm}^{\kappa,k+1} + V_n q_n^{\kappa,k+1}\right\} = 0 \tag{3.62}$$

where $R_n^{\kappa,k+1}$ is the residual for each volume element. Solving for the residuals a Newton-Raphson iteration is used. The residuals at iteration step $p+1$ can be approximated using a Taylor series expansion;

$$R_n^{\kappa,k+1}\left(x_{i,p+1}\right) = R_n^{\kappa,k+1}\left(x_{i,p}\right) + \sum_i \left.\frac{\partial R_n^{\kappa,k+1}}{\partial x_i}\right|_p \left(x_{i,p+1} - x_{i,p}\right) + ... = 0 \tag{3.63}$$

where $x_{i,p}$ is an independent primary variable i at iteration p. Considering only the terms up to first order, the Taylor series becomes

$$-\sum_i = \left.\frac{\partial R_n^{\kappa,k+1}}{\partial x_i}\right|_p \left(x_{i,p+1} - x_{i,p}\right) = R_n^{\kappa,k+1}\left(x_{i,p}\right) \tag{3.64}$$

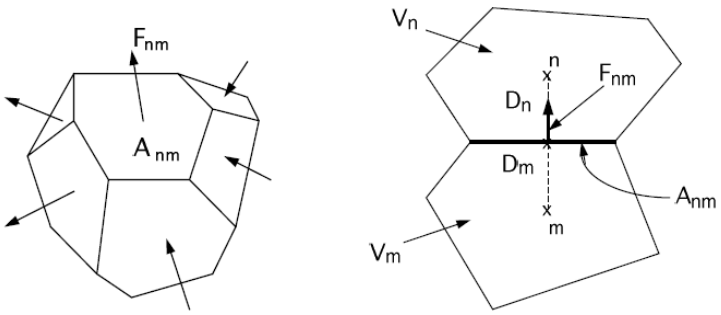

Figure 3.1: Space discretization and geometry data in the integral finite difference method [81].

All the $\partial R_n/\partial x_i$ terms in the so-called Jacobian matrix are estimated using numerical differentiation. The iteration is continued until the residuals are reduced below a predefined convergence tolerance, ε;

$$\left| \frac{R_{n,p+1}^{\kappa,k+1}}{M_{n,p+1}^{\kappa,k+1}} \right| \leq \varepsilon \tag{3.65}$$

In TOUGH2 the default value of the convergence tolerance is $\varepsilon = 10^{-5}$. To solve the linear equation system, the Lancoz-type bi-conjugate gradient solver with incomplete LU factorization as preconditioner is used.

3.2.3. User Features in TOUGH2

It is always recommended to have sufficient distance between the boundaries of a geothermal area and the production and the injection zone. This will ensure that the boundary conditions do not significantly effect the model's output. TOUGH2 offers two types of boundary conditions; Dirichlet and Neumann. The Dirichlet conditions prescribe thermodynamic conditions such as temperature and pressure, while the Neumann conditions prescribe fluxes of mass and heat crossing the boundaries. Both of these types can be time-dependent or time-independent.

The generation term in Eq. (3.51) can be specified in several ways. The simplest method is to specify constant injection or production flow rate from elements defined as the sinks and sources, regardless of the reservoir pressure. These flow rates can also be time-dependent where the user supplies the rates through tabular data. The time-dependent data is then subjected to an interpolation procedure to acquire discrete generation rates at calibration points. However, in a real well the production rate depends mainly on material properties of the reservoir, conditions of the well and the working fluid. By specifying a fixed production rate, dependent of time or not, removing mass at a higher rate than physically possible is sometimes attempted, leading to a convergence failure in the model.

A more reasonable way to specify the production of a fluid is by assuming that the wells operate on a deliverability against fixed bottomhole pressure, P_b, with a productivity index, PI. The mass generation rate of phase β can then be written as

$$q_\beta = H_\beta \cdot PI \cdot (P_{e,\beta} - P_b) \tag{3.66}$$

where the element phase pressure is larger than the wellbore bottomhole pressure, $P_{e,\beta} > P_b$. The variable H_β is defined as

$$H_\beta = \frac{k_{r\beta}}{\mu_\beta} \rho_\beta \tag{3.67}$$

The productivity index is a mathematical mean of expressing the ability of a reservoir to deliver fluids to the wellbore. Using the productivity index the flow into the well is proportional to the pressure difference between the well and containing element, allowing flow rate changes in time due to changes in reservoir pressure.

The last option in TOUGH2, which is probably the best approximation of a real well, is to use the coupled wellbore flow model. This option differs from the deliverability model by specifying a constant wellhead pressure instead of bottomhole pressure. A wellbore simulator is run prior to the reservoir simulation to calculate the bottomhole pressure. This is done for a range of generation rates and enthalpies, resulting in a table of bottomhole pressures. Using the tabular data of bottomhole pressures TOUGH2 performs wellbore pressure corrections, resulting in more accurate prediction by the forward model. Although better forecasts can be expected, this option is limited to wells with single feedzones and can only manage wellbore pressure effects from changing generation rates and enthalpies.

3.3. The Inverse Estimation Model iTOUGH2

Inverse problems often lead to difficult optimization routines with no straightforward solution. Therefore, no general method is at hand to solve all inverse problems. The most common formulation is based on system identification techniques and least-squares fitting of parameterized models to measured data. In brief, inverse modeling consists of estimating model parameters from measurements of system response at discrete points in time and space. A number of mathematical models and data processing techniques can be used to solve an inverse problem. A basic simulation package called iTOUGH2 is frequently used. iTOUGH2 is a computer program for parameter estimation and sensitivity and uncertainty analysis. The program contains various minimization algorithms for adjustment of model against measured data.

3.3.1. Objective Function

The numerical program iTOUGH2 is a great addition to geothermal resource management. It is compatible with the multi phase flow simulator TOUGH2, and its main task is parameter estimation by automatic calibration. The vector $\mathbf{p}$ of length n contains the parameters to be estimated by the inverse analysis. These parameters are the input parameters of the forward model, TOUGH2, and may represent hydrogeologic characteristics, thermal properties, initial or boundary conditions. Other parameters in the forward model, that are not to be estimated, are held fixed at

their best known value. The basic procedure in iTOUGH2 is to compare the calculated output from the forward model to measured data, while changing the value of selected input parameters. If a change in a parameter set results in a reduction in the objective function, the program has found a better estimation for the parameter.

A residual vector $\mathbf{r}$ of length m contains the differences between measured data and calculated model output at calibration points;

$$\mathbf{r} = \mathbf{z}^* - \mathbf{z}(\mathbf{p}) \tag{3.68}$$

where the measured data or observations at calibration points are summarized in the vector $\mathbf{z}^*$ and $\mathbf{z}(\mathbf{p})$ holds the corresponding model output.

No measurements are exact. The quality of measurements mostly depend on the accuracy of measuring equipment and the skills of the operator. The measurements errors may be assumed to be uncorrelated, normally distributed random variables with zero mean. The *a priori* distributional assumption about the residuals can be summarized in an $m \times m$ diagonal covariance matrix:

$$\mathbf{C}_{zz} = \begin{bmatrix} \sigma^2_{z_1} & 0 & 0 & 0 & \dots & 0 \\ 0 & \sigma^2_{z_i} & 0 & 0 & \dots & 0 \\ 0 & 0 & \sigma^2_{z_n} & 0 & \dots & 0 \\ 0 & 0 & 0 & \sigma^2_{z_j} & \dots & 0 \\ \vdots & \vdots & \vdots & \vdots & \ddots & \vdots \\ 0 & 0 & 0 & 0 & \dots & \sigma^2_{z_m} \end{bmatrix} \tag{3.69}$$

The j^{th} diagonal element is the variance representing the measurement error of observation z^*_j. The elements of the observation covariance matrix scale the data relative to quality, where accurate data is given more weight in the inversion of the matrix than data with greater measurement errors.

The objective function is a function of the residuals and therefore directly related to the measure of misfit between the model and the data. Since it has been assumed that the measurement errors are uncorrelated, normally distributed variables with zero mean, the objective function can be derived from maximum likelihood considerations. If sufficient data points exist, the objective function to be minimized is the sum of the squared residuals, weighted by the inverse of the variance σ^2_i;

$$S = \mathbf{r}^T \mathbf{C}^{-1}_{zz} \mathbf{r} = \sum_{i=1}^{m} \frac{r_i^2}{\sigma^2_{z_i}} \tag{3.70}$$

By minimizing this weighted least squares objective function the maximum likelihood estimates, or the best estimates of the parameter set, are obtained. To increase the robustness of an inversion iTOUGH2 offers additional objective functions. The least squares estimation is the default choice in iTOUGH2 and Levenberg-Marquardt algorithm is the standard method to solve nonlinear least square problems.

3.3.2. Minimization Algorithms

The objective function is a measure of misfit between data and the corresponding model output. This fit can often be improved by changing the parameter set $\mathbf{p}$. The minimization algorithms in iTOUGH2 handles this task. iTOUGH2 offers several options for the minimization routines. They are:

- Gauss-Newton
- Levenberg-Marquardt
- Downhill Simplex
- Simulated Annealing
- Grid Search

The default choice is the Levenberg-Marquardt minimization algorithm. It has been found to perform well with most iTOUGH2 applications and is therefore also chosen for the inverse analysis in this study. The Levenberg-Marquardt algorithm is an iterative method based on quadratic approximation of the objective function. The objective function is obtained from the first three terms of the Taylor series expansion;

$$S\left(\mathbf{p}_{k+1}\right) \approx S\left(\mathbf{p}_k\right) + \mathbf{g}_k^T \Delta\mathbf{p}_k + \frac{1}{2}\Delta\mathbf{p}_k^T \mathbf{H}_k \Delta\mathbf{p}_k \tag{3.71}$$

where $\mathbf{p}_k$ is the parameter set of iteration k. The minimum of the objective function is attained if $\Delta\mathbf{p}_k$ minimizes the quadratic function

$$\Phi\left(\Delta\mathbf{p}\right) = \mathbf{g}_k^T \Delta\mathbf{p} + \frac{1}{2}\Delta\mathbf{p}^T \mathbf{H}_k \Delta\mathbf{p} \tag{3.72}$$

The vector $\mathbf{g}_k$ is the gradient vector and $\mathbf{H}_k$ is the Hessian matrix;

$$\mathbf{g}_k = -2\mathbf{J}_k^T \mathbf{C}_{zz}^{-1} \mathbf{r}_k \tag{3.73}$$

$$\mathbf{H}_k = 2\left(\mathbf{J}_k^T \mathbf{C}_{zz}^{-1} \mathbf{J}_k + \mathbf{B}\right) \tag{3.74}$$

The Jacobian matrix is defined as

$$\mathbf{J} = -\frac{\partial \mathbf{r}}{\partial \mathbf{p}} = \frac{\partial \mathbf{z}}{\partial \mathbf{p}} = \begin{bmatrix} \frac{\partial z_1}{\partial p_1} & \cdots & \frac{\partial z_1}{\partial p_n} \\ \vdots & & \vdots \\ \frac{\partial z_m}{\partial p_1} & \cdots & \frac{\partial z_m}{\partial p_n} \end{bmatrix} \tag{3.75}$$

When the minimum of the quadratic function in Eq. (3.72) has been reached, the following assertion can be stated:

$$\mathbf{H}_k \Delta\mathbf{p}_k = -\mathbf{g}_k \tag{3.76}$$

Combining Eq. (3.73), (3.74), and (3.76), and replacing $\mathbf{B}$ with an $n \times n$ diagonal matrix $\lambda_k \mathbf{D}_k$, the calculated parameter update results in

$$\Delta \mathbf{p}_k = \left(\mathbf{J}_k^T \mathbf{C}_{zz}^{-1} \mathbf{J}_k + \lambda_k \mathbf{D}_k\right)^{-1} \mathbf{J}_k^T \mathbf{C}_{zz}^{-1} \mathbf{r}_k \tag{3.77}$$

The matrix $\mathbf{D}_k$ is given by $D_{jj} = \left(\mathbf{J}_k^T \mathbf{C}_{zz}^{-1} \mathbf{J}_k\right)_{jj}$, for $j = 1, ..., n$. The Levenberg parameter, λ, controls the step size chosen in the algorithm. At first the Levenberg parameter is chosen relatively large leading to small steps along the gradient of the objective function. Each time a reduction in the objective function occurs the Levenberg parameter is reduced by a factor of $1/v$; v being the Marquardt parameter. On the other hand, if the objective function is increased, the Levenberg parameter is increased by v. If a step is successful, the new updated parameter set becomes

$$\mathbf{p}_{k+1} = \mathbf{p}_k + \Delta \mathbf{p}_k \tag{3.78}$$

The algorithm searches for a lower objective function until a stopping criteria has been met. To identify when the minimum of the objective function has been reached, iTOUGH2 uses any the following convergence criteria:

- Number of iteration steps exceeds a specified number.
- Number of forward runs with TOUGH2 exceeds a specified number.
- Number of unsuccessful uphill steps exceeds a specified number.
- Normalized step size is smaller than specified tolerance.
- Norm of the gradient vector is smaller than specified tolerance.
- Objective function is smaller than specified tolerance.

3.3.3. Sensitivity and Error Analysis

As well as supporting parameter estimation, the program provides some statistical information about the estimation error and the uncertainty of the forward model predictions. Even if a good match is obtained between the measured data and the model output it does not necessarily mean that the best estimates are acceptable. The parameters may be highly correlated causing the results from the parameter estimation to be untrustworthy. The Jacobian matrix and the covariance matrix provide the basis for a detailed sensitivity and error analysis. The Jacobian matrix in Eq. (3.75) holds the sensitivity coefficients. To be able to compare them to one another the coefficients are scaled by the standard deviation of the observation, σ_z, and the expected parameter variation, σ_p;

$$\tilde{J}_{ij} = J_{ij} \frac{\sigma_{p_j}}{\sigma_{z_i}} = \frac{\partial z_i}{\partial p_j} \frac{\sigma_{p_j}}{\sigma_{z_i}} \tag{3.79}$$

Now, one can directly compare the contribution of each observation to the estimation of each parameter. The overall contribution of a data set is given by

$$c_k = \sum_{j=1}^{n} \sum_{\substack{i=1 \\ i \in k}}^{m} |\tilde{J}_{ij}| \tag{3.80}$$

where k indicates the number of data sets. By calculating the sum of each column, the measure of parameter sensitivity is obtained;

$$b_j = \sum_{i=1}^{m} |\tilde{J}_{ij}| \tag{3.81}$$

A high b_j value indicates that parameter j is more likely to reach an estimation uncertainty of σ_{p_j} than another parameters with a lower value on b_j. The estimated error variance, s_0^2, is a measure of goodness-of-fit;

$$s_0^2 = \frac{\mathbf{r}^T \mathbf{C}_{zz}^{-1} \mathbf{r}}{m - n} \tag{3.82}$$

If the estimated error variance is too large, the model does not match the data sufficiently, causing the estimated parameters to be meaningless. However, if a good match is obtained, the measure of goodness-of-fit is not sufficient to decide if the inverse problem has been reasonably solved. The results must also be subjected to residual analysis and some other additional terms. The covariance matrix of the estimated parameters can be given as

$$\mathbf{C}_{pp} = s_0^2 \left(\mathbf{J}^T \mathbf{C}_{zz}^{-1} \mathbf{J} \right)^{-1} \tag{3.83}$$

This matrix is one of the most important variables in evaluating the results from the inverse modeling problem. The diagonal elements are the variances σ_p^2, the lower triangular matrix shows the covariances and the upper triangular matrix holds the corresponding correlation coefficients. The correlation coefficients are hard to interpret physically so a matrix of direct correlations is included in the error analysis. The direct matrix reveals the dependence of pairs of parameters where values close to -1 and 1 indicate strong correlation.

The residual analysis can be used to evaluate whether some parts of the model need to be modified. It shows potential trends in the residuals, indicating possible systematic errors in the model or data. The iTOUGH2 output file provides a scatter plot of the residuals. By visually inspecting the plot, systematic errors in the model are usually easy to detect since the residuals are expected to be randomly distributed around the center line.

The sensitivity, error and residual analysis provide valuable knowledge about the solution of the inverse problem. The analyses describe possible uncertainty in the

estimation, errors in available data or in the model itself, and the importance of individual observations and parameters. This information is then used to distinguish if a good match between data and the model output has been reached and if the estimated parameters are believable.

3.3.4. iTOUGH2-PEST

iTOUGH2 is usually run in combination with TOUGH2, a forward simulator for non-isothermal multi phase flow in porous and fractured media, but can also be linked to non-TOUGH2 models. In that way the iTOUGH2 can be used as an inverse analyzing tool for models such as the wellbore simulator FloWell.

To be able to link non-TOUGH2 models with iTOUGH2, a protocol called PEST has been implemented in iTOUGH2. The protocol enables interaction between the non-TOUGH2 model and iTOUGH2 through a clear and simple communication format. The optimization routine and the analysis procedure in iTOUGH2 remains the same, it is only the communication format that is borrowed from PEST. The iTOUGH2-PEST structure is shown in Fig. (3.2).

In the PEST Template File the input variables, which are subjected to parameter estimation, are identified. The input variables are written to the Input File and updated throughout the inverse analysis. The PEST Instruction File is used to extract output variables that will be compared to measured data. These variables are calculated by the forward Non-TOUGH2 Model and stored in the Output File.

To start the parameter estimation with the PEST protocol an iTOUGH2 Input File is run with a corresponding executable file. A parameter-selection command is used in the iTOUGH2 Input File to indicate that the parameters refer to the Non-TOUGH2 Model and will be adjusted through the PEST Template File. In the iTOUGH2 Input File a guess value is assigned to the parameters to be estimated and observation data is defined along with executable instructions. The guess values for the parameters are the Input Parameter Set which are written to the Input File.

The iTOUGH2 Input File calls for the Non-TOUGH2 Model to run with the guess values for the parameters in the Input File. The Non-TOUGH2 Model then calculates output parameters at calibration points. Adjustment of the output parameters against observation data is performed using the iTOUGH2 capabilities, which are the local and global algorithms, the sensitivity, residual and error and uncertainty analyses. This will give an estimation of new input parameters (updated parameters) for the Non-TOUGH2 Model. The inverse analysis continues until stopping criteria has been met. Available stopping criteria are listed in section 3.3.2.

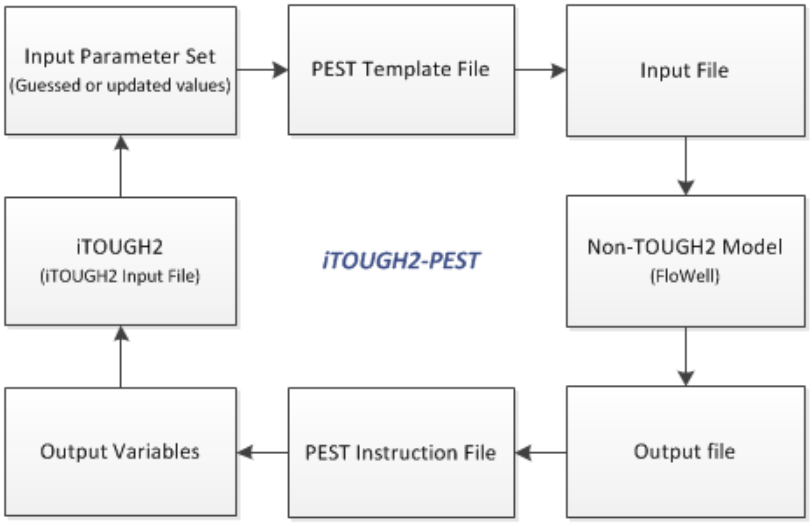

Figure 3.2: The iTOUGH2-PEST structure [28].

4. The Wellbore Model FloWell

The following sections are devoted to the discussion of the wellbore model FloWell, available data and comparison between simulated results and measured data.

4.1. Basic Architecture of the Model

For this study, a numerical wellbore simulator has been developed and named FloWell. A wellbore model is often described as a vertical or inclined pipe with liquid flow in the deeper zones which flashes in the upper zones when pressure and temperature drop. From the flashing zone and up the flow consists of two phases, liquid and vapor. As the mixture progresses up the well the distribution of phases becomes rather complex due to the slippage between them [1]. This phenomena is often described with flow regimes, where different regimes indicate different friction between the phases and the pipe wall. Many wellbore models define the flow problem in terms of flow regimes but that is not the case in FloWell [41]. FloWell is built around Eq. (3.1)-(3.50) defined in the section *The Physical Model of FloWell* in Chapter 3. MATLAB is used as a programming language and the continuity, energy and momentum equations are solved directly using numerical integration without any consideration to flow regimes. To evaluate the differential equations the *ode23* function built in MATLAB is used. The function uses second and third order Runge-Kutta formulas simultaneously to obtain a solution [89]. The depth interval is adjusted by the integration function and at each depth node the function produces velocity, pressure and enthalpy values.

To perform a simulation with FloWell the following input parameters are needed:

- The geometry of the well such as the inner diameter and the depth of the well.
- The bottomhole pressure or the wellhead pressure.
- The enthalpy of the working fluid in the well.
- The total mass flow at the wellhead.
- The roughness of the pipe walls in the well.

The geometric parameters are usually easily obtained. When the drilling of a well has come to an end the well design is verified and diameters and lengths of the casings may be determined, as well as the final depth of the well. Other input parameters require more effort. After a well has been drilled, well testing and measurements are performed. The basic measurements are pressure and temperature logs or profiles. These measurements give an estimate of the enthalpy and the amount of fluid coming out of the well. FloWell utilizes this information to calculate the density, viscosity and steam quality at each step in the numerical integration.

It is often challenging to estimate the wall roughness of a geothermal well. Before production, the wall roughness is a known standard value. After production starts, scaling occurs in the well, changing the initial value of the roughness. Scaling can increase the roughness but it may as well smooth out the wall of the well. As scaling occurs, layers are added to the pipe wall causing reduction in the well inner diameter. In this study, both in the validation of FloWell and in the case study of Reykjanes geothermal field, no scaling is assumed, and standard values for diameters and wall roughness, corresponding to casing materials, are used.

The main core of FloWell is the simulation itself, that is solving the differential equations. The wellbore simulator is capable of the following additional features:

- Modeling liquid, two phase and superheated steam flows.
- Allowing users to choose between various friction, friction correction factor and void fraction correlations.
- Performing wellbore simulations from the bottomhole to wellhead section, or from the wellhead to the bottom of the well.
- Providing simulated results, such as pressure and temperature distribution as well as steam quality, friction, velocity, enthalpy and void fraction at each depth increment.
- Providing graphical plots of simulated pressure and temperature profiles.

FloWell offers several options for friction factor, friction correction factor and void fraction correlations. These options are described in Chapter 3. As a run is initiated with FloWell, the user is asked to choose between a simulation for a smooth well or if well roughness should be accounted for. Next a friction correction factor model is determined and finally the model for the void fraction. Options available in FloWell are illustrated in Fig. (4.1).

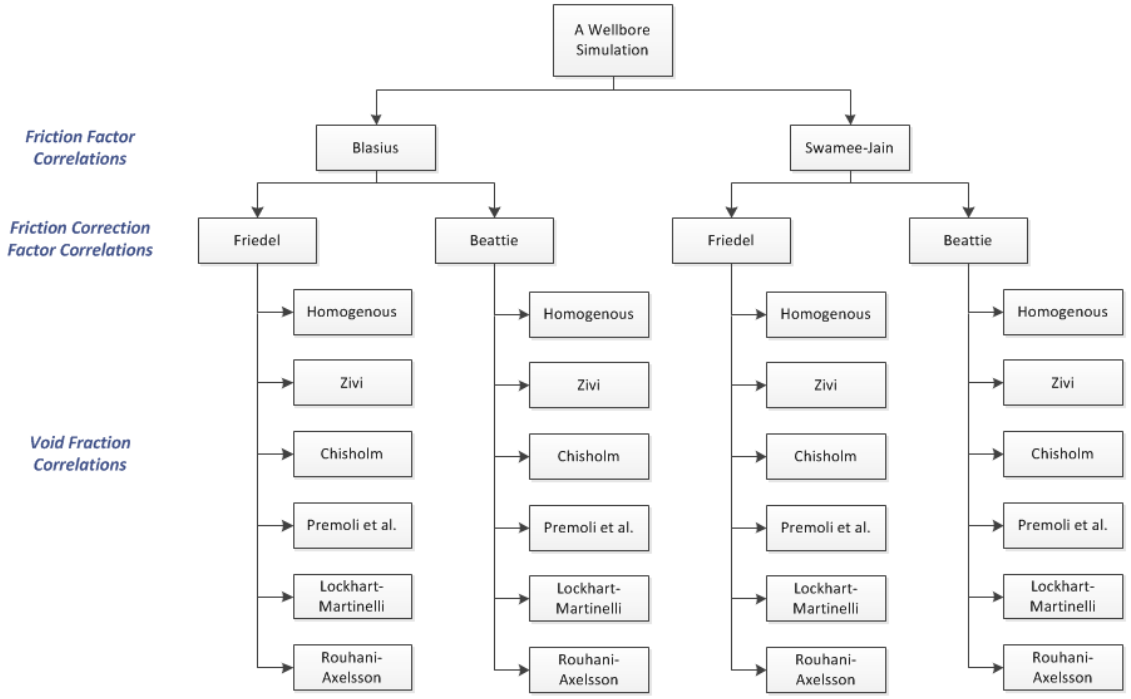

Figure 4.1: Available options for the friction factor, friction correction factor and void fraction correlations in FloWell.

As of now, FloWell offers the above options for empirical correlations but future steps include implementing a wider range of correlations.

Some general assumptions have been made in the development of the simulator. It is assumed that:

- The flow is steady and one dimensional.
- Multiple changes of the wellbore geometry, such as diameters and roughness, do not occur.
- Simulations will be restricted to wells with single feedzones.
- The fluid is pure water and IAPWS Industrial Formulation 1997 is used for the thermodynamic properties of liquid and vapor phases [55]. The dynamic viscosity is obtained from the IAPWS Formulation 2008 for the viscosity of ordinary water substance [56].
- Phases are in thermodynamic equilibrium.
- Fluid properties remain constant within a step.
- The presence of non-condensable gases and dissolved solids is ignored.

To validate the wellbore simulator FloWell, the simulated output needs to be compared to measured data. Comparison is essential for the credibility of the simulator but many factors can affect the outcome of the simulation. The accuracy of the wellbore simulator depends mainly on:

- The amount and reliability of measured data available.
- The accuracy of any estimated data, such as well roughness and in some cases well diameter which may have been reduced by scaling.
- The validity of correlations coded into the simulator, i.e. friction, friction correction factor and void fraction correlations.

Moreover, inaccurate prediction can be caused by the use of physical properties of pure water that do not represent actual thermodynamic behavior of the geothermal fluid.

FloWell can be used individually to simulate the behavior of producing geothermal wells. The program is also designed to be coupled to a reservoir simulator in a moderately simple way. Coupling of the wellbore simulator FloWell and the reservoir simulator TOUGH2 is described in detail in Chapter 5.

4.2. Verification and Validation of FloWell

Simulating geothermal wells can provide vital information about the geothermal reservoir and is an essential tool in geothermal resource management. Verification and validation are processes that help to ensure that simulators are correct and reliable. Validation is usually achieved through model calibration, that is comparing results from the simulation to actual system behavior. If a simulation does not provide valid representations of the actual system, conclusions derived from the simulation can prove to be erroneous and may result in poor decision making [74].

4.2.1. Review of Available Data and Well Testing

To validate FloWell, data from two geothermal fields, Reykjanes and Svartsengi, in the Reykjanes peninsula in Iceland is used. Fig. (4.2) shows where these geothermal fields are located. The Icelandic energy company HS Orka provided data for the validation of FloWell. HS Orka operates the power plants at Reykjanes and Svartsengi along with managing electric power sale. HS Orka carries out well testing for each well soon after drilling when the well has stabilized and reached full formation

heat. Reports are available describing these well tests in detail. They include a short description about the well design, results from temperature and pressure logs, well enthalpy and production potential estimate and fluid chemical composition analysis. In these reports the temperature and pressure profiles are illustrated in figures. Data points can be extracted from these figures and compared to simulations with FloWell. This offers some uncertainty, for the original data from the logs is not included in the reports and manually extracting data points from figures can cause the data to be slightly shifted relative to the original data. However, this uncertainty is not considered great compared to errors involved in the actual temperature and pressure logs. These measurement errors are reviewed later in the section.

The history of geothermal energy utilization in the Reykjanes peninsula can be traced back to the year 1956, when the first research wellbore was drilled in Reykjanes. The drilling of several other research wellbores followed but it was not until 2006 that production of energy started from the Reykjanes Power Plant. In all, 30 wells have been drilled in Reykjanes geothermal field with 13 of them connected to the power plant [50]. Producing wells at Reykjanes are listed in Table (4.1) along with the main parameters required for simulations with FloWell.

Table 4.1: Main parameters for producing wells at Reykjanes [15, 43, 46–49, 59, 61].

Wells	Drilling year	Total depth [m]	Depth of production casing [m]	Wellhead pressure [bar-a]	Total mass flow [kg/s]	Well Enthalpy [kJ/kg]
RN-11	2002	2248	689	41	50	1300
RN-12	2002	2506	854	38	110	1300
RN-13B	2007	2531	818	41	22	1590
RN-14B	2007	2426	-	-	-	-
RN-15	2004	2507	-	-	-	-
RN-18	2005	1815	750	-	-	-
RN-19	2005	2248	-	-	-	-
RN-21	2005	1713	609	41	34	1206
RN-22	2006	1680	728	43	34	1370
RN-23	2006	1928	701	44	29	1379
RN-24	2007	2115	708	29	39	1216
RN-27	2008	1503	754	49	9	2795
RN-28	2008	1119	765	47	10	2805

Emphasis is put on using data from wells at Reykjanes and to account for as many wells as possible. However, reports from temperature and pressure logs are not available for all wells currently in production at Reykjanes. As can be seen in Table (4.1), sufficient data is at hand for wells RN-11, RN-12, RN-13B, RN-21, RN-22, RN-23, RN-24, RN-27 and RN-28. For more comprehensive validation of FloWell,

data from three wells at Svartsengi is included. Main parameters for these wells are listed in Table (4.2).

Table 4.2: Main parameters for wells SV-21, SV-22 and SV-23 at Svartsengi [16, 23, 60].

Wells	Drilling year	Total depth [m]	Depth of production casing [m]	Wellhead pressure [bar-a]	Total mass flow [kg/s]	Well Enthalpy [kJ/kg]
SV-21	2001	1475	844	15	70	1030
SV-22	2008	862	385	23	10	2800
SV-23	2008	698	493	23	12	2801

Some of the wells at Reykjanes and Svartsengi are directionally drilled. Care must be taken when analyzing reports discussing temperature and pressure measurements in these wells because downhole data is generally plotted as a function of measured depth along the wellbore. Before this data can be compared to results from FloWell it must be corrected so that the depth represents true vertical depth. Knowing the rate of angle buildup, the desired angle and the depth where the angle buildup starts this correction can be performed using simple trigonometric functions. Equations for calculation of characteristic points of a theoretical vertical profile can also be found in the *Data Drilling Handbook* [32].

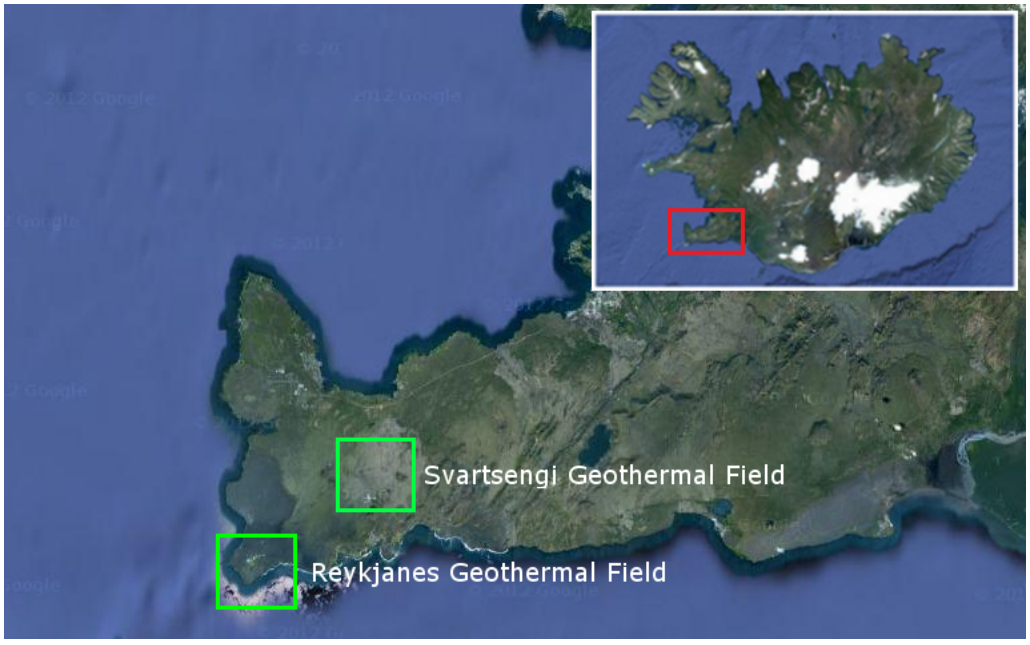

Figure 4.2: Location of geothermal fields used in the validation of FloWell [34].

When a geothermal well has been drilled, collecting data from the well is the next step. The most common measurements in the well are temperature and pressure logs. These measurements are performed with the well remaining in same condition throughout the measurement period and over the full depth of the well, if possible. The choice of a logging device depends mainly on test objectives, expected downhole conditions, well design, the fluid type in the well and the availability of the devices [38].

The company Iceland Geosurvey handles most of the well logging in Iceland. The company owns and operates a temperature and pressure logging tool, *K10*, from Kuster Company. It is a high temperature and pressure recording instrument that is operated subsurface. The measurement device is slipped through a holder fixed at the wellhead to protect the sensitive electronics to the high geothermal temperatures. As it is lowered down the well it measures temperature and pressure. The pressure transducer senses the wellbore pressure through the protective tube, while the *RTD* (Resistance Temperature Detector) sensor is exposed to the wellbore for temperature sensing. When *K10* reaches the well bottom it is pulled up, measuring the temperature and pressure again on the way up the well. It is not possible to retrieve data from the device while it is in the well, it must be done once the device reaches the surface [61, 80].

The logging tool can operate in a geothermal environment for up to 6 hours at temperature 300°C and up to 4 hours at temperature 350°C. It can measure pressure up to 345 bar with 0.024% accuracy. The temperature is measured with 0.15% accuracy and the minimum sample interval of the tool is 1 second. It is not advised to run the device faster than 45 m/min [62].

Although the *K10* is very accurate there are other parameters involved in the well logging procedure that contribute greatly to potential errors in downhole temperature-pressure data. After well completion, the well is shut and allowed to heat to full formation temperature. During the heat-up process the temperatures and pressures are measured several times in the well but reliable temperature and pressure logging cannot be performed in the well until the heat-up process is completed. In geothermal fields in Iceland, the pressure and temperature profile measurements are usually performed prior to the connection of the well to the power plant. It is important that the well remains in the same state throughout the test but before a well is connected to production it can often prove to be unstable, especially if it has not reached full formation temperature, causing the test results to be unreliable [38].

Another factor regarding possible errors is the wireline used to convey the measurement instrument. As the device is lowered deeper into the well, the length of the wireline will increase due to thermal expansion. The lengthening can vary up to several meters. This can be spotted when logs are compared, for they are often displaced by a few meters relative to each other. The data can also become offset

with respect to depth because measurements are recorded while the logging tool is moving down and up the well [38]. Finally, it is possible that the logging tool itself influences the flow in the wellbore, leading to incorrect interpretation of conditions in the well.

Several methods exist to estimate the flow rate and enthalpy. For wells that have not been connected to a power plant, the method by Russell James is commonly used. Applying this method, the critical pressure (lip pressure) is measured as the two phase mixture, produced in the well test, is led into a silencer (atmospheric pressure separator). The liquid flow from the silencer is measured with a V-notch while the steam is released to the air. From the critical pressure and the liquid flow rate, the total mass flow rate and enthalpy can be calculated using derivation of the James equation;

$$\dot{m}_t = 1835000 \cdot A \cdot \frac{P_c^{0.96}}{h^{1.102}} \tag{4.1}$$

where $\dot{m}_t$ is the total mass flow, P_c is the critical pressure in bar-a, h is the enthalpy in kJ/kg and A is the cross sectional area of the pipe to the silencer. Using the steam quality, the total mass flow can also be calculated by

$$\dot{m}_t = \dot{m}_l \frac{h_g - h_l}{h_g - h} \tag{4.2}$$

Knowing the liquid mass flow rate and the critical pressure, Eq. (4.1) and (4.2) can be solved together to obtain the total mass flow and the flowing enthalpy [38, 61].

After a well has been connected to production a tracer flow test is more practical to calculate the total mass flow rate and enthalpy from a well. Liquid and gas phase tracers, different from the brine found in the well, are injected to the two phase flow from the wellbore. Samples are then collected at sufficient distance from the injection point, and the concentration of the injected tracers measured. The dilution of the tracers indicate the mass flow rate of liquid and steam;

$$\dot{m}_l = \frac{\dot{m}_T}{B_l} \tag{4.3}$$

$$\dot{m}_g = \frac{\dot{m}_T}{B_g} \tag{4.4}$$

where $\dot{m}_T$ is the tracer injection mass flow rate and B is the concentration of tracer in liquid and vapor phases, respectively. If the pressure at a sampling point is known, the flowing enthalpy can be solved from Eq. (4.2) [38].

4.2.2. Validation of FloWell

FloWell offers a considerably wide selection of empirical correlations for two phase calculations as illustrated in Fig. (4.1). Which correlation performs best is a question many scientists and researches struggle to answer. More often than not, there is no one right answer to this question as it can prove to be difficult to find one correlation to simulate the diverse characteristics found in geothermal wells.

Utilizing the features iTOUGH2 has to offer, a measure of how each correlation performs in simulating the pressure and temperature profiles in a well can be found. Since FloWell is a non-TOUGH2 model, an inverse run with iTOUGH2-PEST is initialized to calculate an objective function with Eq. (3.70). The objective function (see definition in section 3.3.1) describes how a simulation with FloWell fits measured data, in this case data points from temperature and pressure logs. If, for example, the objective function calculated using the void fraction correlation by Rouhani-Axelsson is lower than the one found with the Homogenous correlation, the Rouhani-Axelsson correlation is more likely to simulate the expected behavior of the well.

The objective function is calculated for each well and all available correlations described in Fig. (4.1). The calculated objective functions are compared within each well and the correlation which yields the lowest objective function is identified. With that, a ranking of the correlations can be established for each well. These individual rankings can be summarized to find an overall ranking for the wells. The overall ranking can be presented in percentages that show how often a correlation performs the best or the worst in all wells. The simulations for the following analysis are performed down to the bottom of the production casing since all fluid flow into a geothermal well occurs below that point. Several feedzones are present in a well but since FloWell is a single feedzone simulator the most reliable simulations would be the ones that only reach the bottom of the production casing. Simulating further down the well is also an option but it may invite unreliable predictions. Results are summarized in Fig. (4.3).

From Fig. (4.3) it can be seen that there is no significant difference in using the Blasius or Swamee-Jain equation to calculate the friction factor. The Blasius equation produces a better simulation in 54% of the cases while the Swamee-Jain equation predicts better in 46% of them. The same applies to the friction correction factor, where the models by Friedel and Beattie each give better results for around half of the cases. For the void fraction correlations, the models by Zivi and Lockhart-Martinelli never produce the best simulations while the rest of the models, the Homogenous, Chisholm, Premoli et al. and Rouhani-Axelsson, take turns at simulating the behavior in the wells most accurately.

Since there is no significant difference in using the Blasius equation instead of the Swamee-Jain equation or the Friedel model in place of the Beattie model, it is interesting to analyze how a void fraction performs regardless of friction factor and friction correction factor. In Table (4.3) the results for the void fraction correlations in Fig. (4.3) are summarized along with other placements.

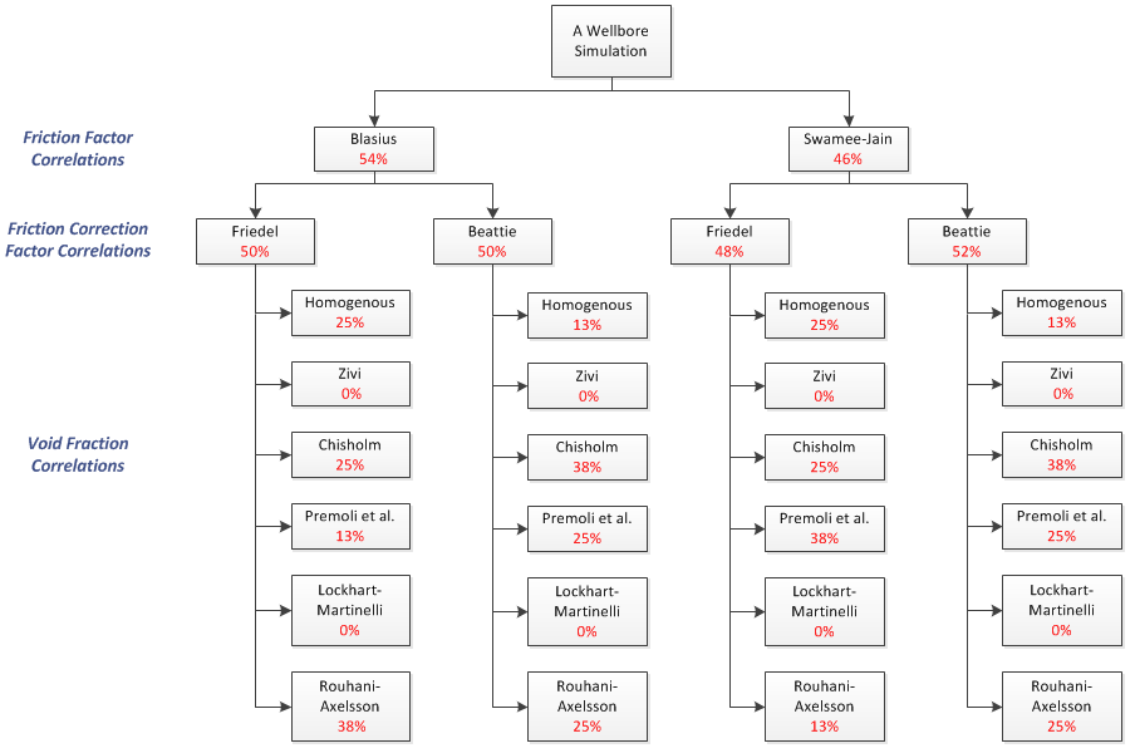

Figure 4.3: Ratio of which a correlation yields the lowest objective function for simulations with FloWell down to the bottom of the production casing.

Table 4.3: Ratio, in percentages, of how often a void fraction correlation ranks 1st to 6th when simulating with FloWell down to the bottom of the production casing.

Rank	Homogenous	Zivi	Chisholm	Premoli et al.	Lockhart-Martinelli	Rouhani-Axelsson
1st	19	0	31	25	0	25
2nd	0	0	0	38	31	31
3rd	6	0	34	0	19	41
4th	3	16	6	22	50	3
5th	28	31	28	13	0	0
6th	44	53	0	3	0	0

From the table it is clear that the model by Chisholm most often yields results closest to measured data. The model by Premoli et al. is the one that is most often

in second place, the model by Rouhani-Axelsson is most often in third place and the model by Lockhart-Martinelli is most often in fourth place. The model by Zivi is the one that produces the worst predictions, placing most often in the last two places. To further summarize the results, Table (4.4) describes how often a correlation ranks among the top three and bottom three, respectively.

Table 4.4: Ratio, in percentages, of how often a void fraction correlation ranks in the top three and in the bottom three when simulating with FloWell down to the bottom of the production casing.

Rank	Homogenous	Zivi	Chisholm	Premoli et al.	Lockhart-Martinelli	Rouhani-Axelsson
1st-3rd	8	0	22	21	17	32
4th-6th	25	33	11	13	17	1

When simulating down to the bottom of the production casing the correlation by Rouhani-Axelsson ranks most often in the top three while the model by Zivi ranks most often the lower three.

Although simulating down to the bottom of the well is not as accurate as simulating to the bottom of the production casing, it is interesting to examine whether or not the results deviate from the ones shown above. The results are summarized in Table (4.5).

Table 4.5: Ratio, in percentages, of how often a void fraction correlation ranks in the top three and in the bottom three when simulating with FloWell down to the bottom of the well.

Rank	Homogenous	Zivi	Chisholm	Premoli et al.	Lockhart-Martinelli	Rouhani-Axelsson
1st-3rd	2	20	26	30	6	16
4th-6th	31	14	7	3	27	18

For simulations down to the bottom of a well, the model by Premoli et al. produces simulations that are most often in the top three, with the top one being the closest to measure data. Predictions by the Homogenous correlation are most often placed in the bottom three and therefore the worst fit to measured data. Compared to the results above, the model by Zivi seems to perform better when simulating all the way down to the bottom.

To better understand how FloWell performs, visual results are of great help. Wells RN-11, RN-12, RN-21, RN-24 and SV-21 have similar characteristics. They are vertical wells with low enthalpy fluid and steam fraction between 9-13% at the wellhead. Simulations for wells RN-12 and SV-21 can be seen in Fig. (4.4) and (4.5). For these simulations the Blasius equation and the model by Friedel are used

to calculate the friction factor and friction correction factor. The figures show both simulations down to the bottom of the production casing and to the bottom of the well.

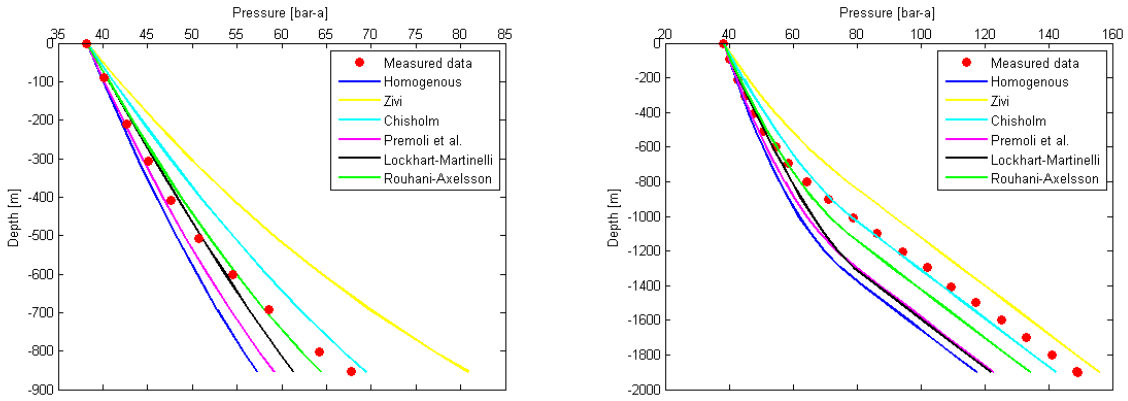

Figure 4.4: Simulations with FloWell for well RN-12 down to the bottom of production casing (left) and to the bottom of the well (right), using the Blasius equation and the model by Friedel.

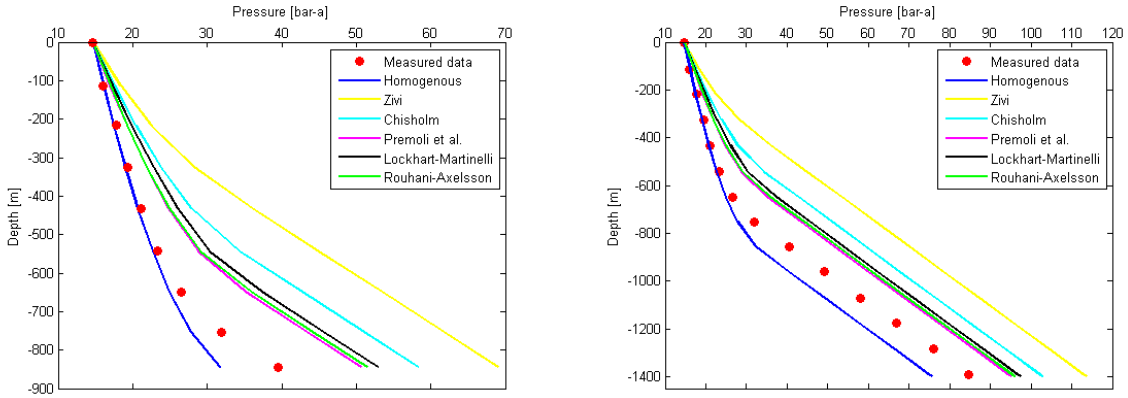

Figure 4.5: Simulations with FloWell for well SV-21 down to the bottom of production casing (left) and to the bottom of the well (right), using the Blasius equation and the model by Friedel.

For well RN-12 the Rouhani-Axelsson and the Chisholm void fraction correlations perform the best. For well SV-21 the Homogenous correlation shows simulations closest to the measured data. The Homogenous correlation usually yields adequate simulations for wells with a low steam fraction, for it assumes that the phases travel at the same velocity. This is the case in well SV-21, the steam fraction in the well is between 9-10%, while the steam fraction in well RN-12 is little over 13%.

Wells RN-13B, RN-22 and RN-23 have also similar characteristics. They are directionally drilled wells, contain fluid with a little higher enthalpy than wells described above and steam fraction between 15-18%. As these wells are directionally drilled, it is necessary to correct the depth points given in available reports so they represent true vertical depth. Simulations for well RN-22 are shown in Fig. (4.6), along with corrected and uncorrected data points. Same correlations are used for the friction factor and friction correction factor as before.

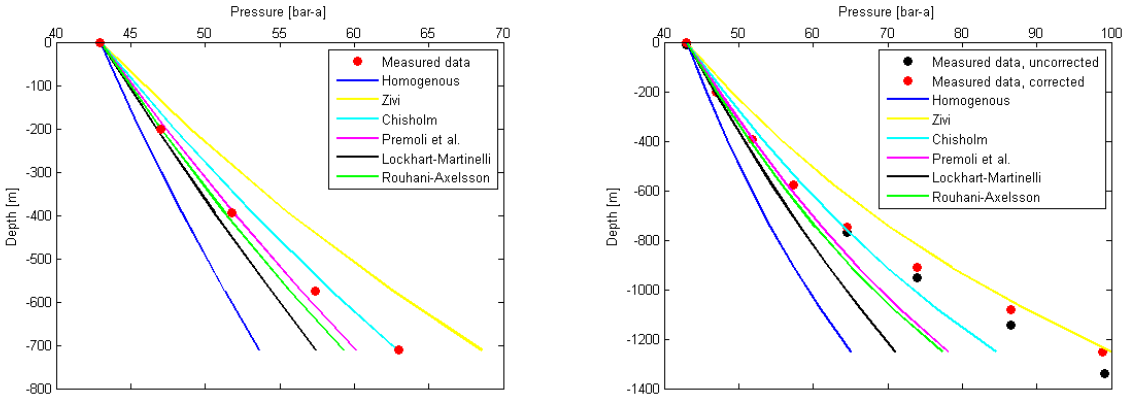

Figure 4.6: Simulations with FloWell for well RN-22 down to the bottom of production casing (left) and to the bottom of the well (right), using the Blasius equation and the model by Friedel.

The Chisholm and Premoli et al. perform the best when simulating well RN-22. Judging by the figure, FloWell seems to simulate the uncorrected data points better than the corrected ones. Possible explanation for this is the contribution of uncertainties involved in the correction process and in the measured data itself.

The downhole conditions in a well can be rather sensitive to changes in wellhead parameters. Well RN-13B is a good example of this. In Table (4.1) the enthalpy gathered from an available report about the well testing in RN-13B is estimated to be around 1590 kJ/kg. Using this value for the enthalpy, along with the wellhead pressure and estimated mass flow rate, FloWell yields simulations which do not imitate the known pressure profile in the well. The fluid flashes before it enters the well and two phase flow is present in the well from the bottom to the top. By changing the enthalpy value, simulations that better fit measured data can be obtained. This may indicate that the enthalpy in the well is overestimated, but it is also possible that other uncertainties involved in the well testing play a part in producing inadequate simulations. This phenomena is illustrated in Fig. (4.7).

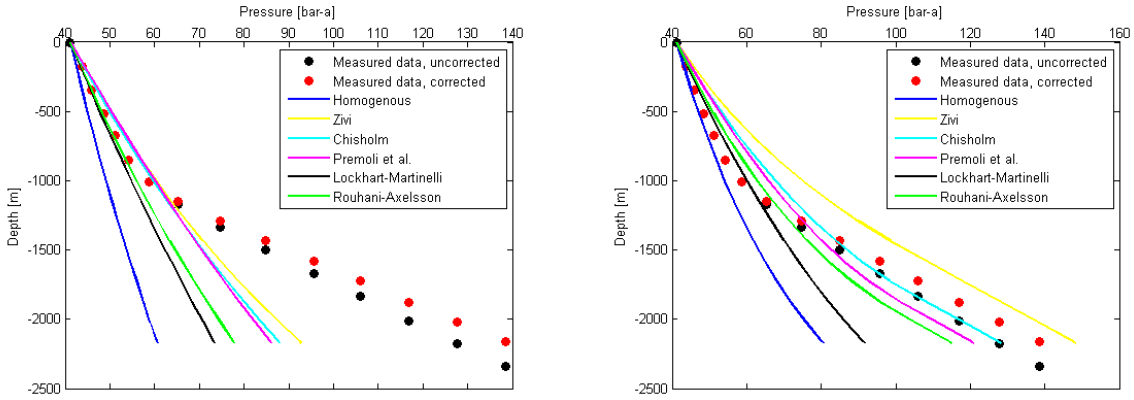

Figure 4.7: Simulations with FloWell for well RN-13B down to the bottom of the well using the Blasius equation and the model by Friedel, for the original enthalpy 1590 kJ/kg (left) and the enthalpy 1400 kJ/kg (right).

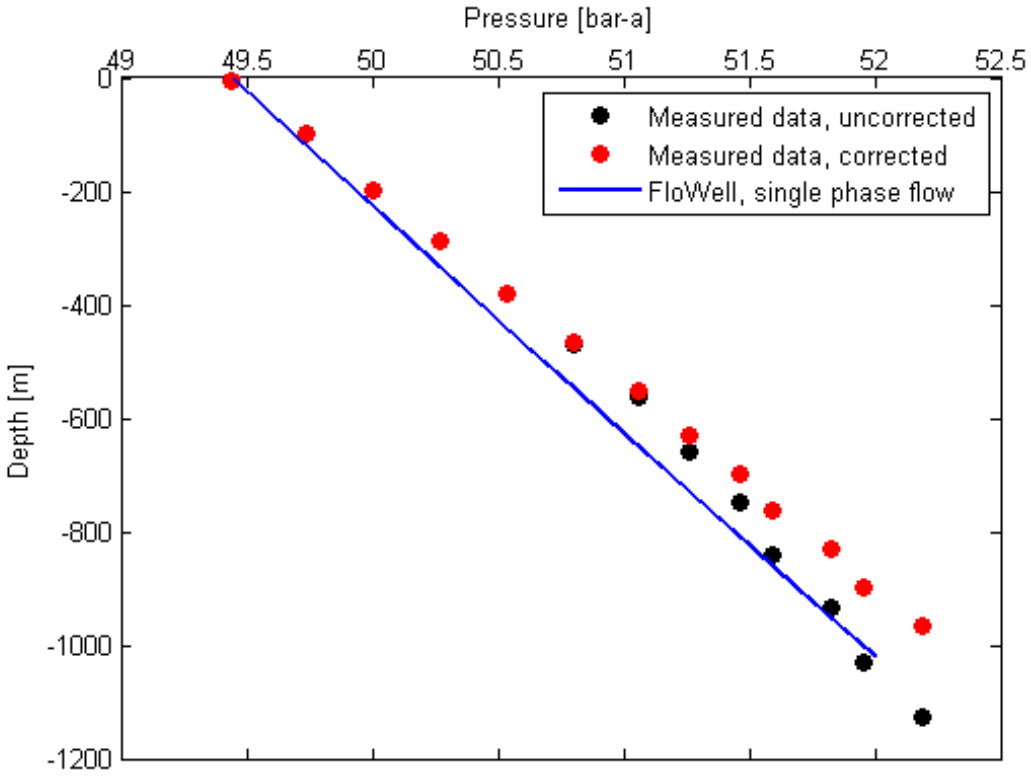

Figure 4.8: Simulation with FloWell for well RN-27 down to the bottom of the well.

FloWell is not only able to simulate two phase flow but also to account for superheated steam. Several wells at Reykjanes and Svartsengi produce saturated steam and some even superheated steam. Among these wells are RN-27, RN-28, SV-22 and SV-23. They are all directionally drilled wells and produce fluid with high enthalpy. RN-27 is one of the wells that displays superheated steam. A simulated pressure profile along with corrected data is shown in Fig. (4.8).

Since FloWell is also capable of starting at the bottom of a well and calculating up, it is interesting to see a simulation up the well versus down the well. In Fig. (4.9) these two options are compared for well SV-21. From the figure it can be seen that considerable difference is between simulating up the well and down the well. Despite this difference, the homogenous correlation still performs best and the model by Zivi the worst. From this discussion the question which option is more accurate arises. As it is easier to measure wellhead parameters than downhole ones, wellhead conditions are constantly being monitored and noted. From that alone it may be concluded that simulating down the well is more accurate but if carefully measured parameters exist at the top and at the bottom it may prove difficult to favor one over the other.

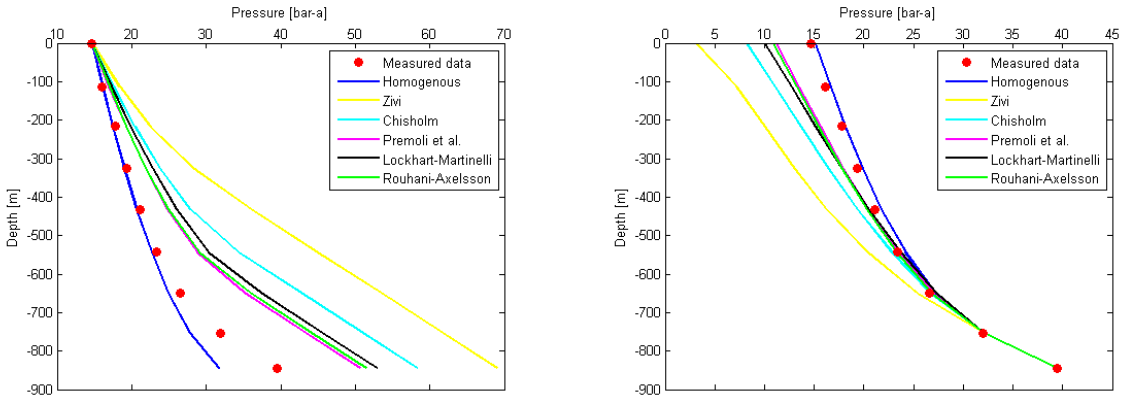

Figure 4.9: Simulations with FloWell for well SV-21, starting at the top and simulating down to production casing (left) and starting at the bottom of production casing and simulating up (right).

As seen above, FloWell manages to simulate the behavior of geothermal wells to some extent. No correlation simulates the exact pressure profile in a well while some are closer to it than others. It is intriguing to use inverse analysis with iTOUGH2-PEST to improve parameters in the void fraction correlations so simulations with FloWell better fit measured data. Before initializing a run with iTOUGH2-PEST, the measured pressure profile is defined as observations and a parameter to be evaluated in a chosen void fraction correlation is identified. Using the Homogenous model to calculate the void fraction in well RN-11, FloWell yields a simulation that is not very

close to the known pressure profile. It is assumed that the slip ratio is equal to one in the Homogenous correlation, meaning that the liquid and steam travel with the same velocity up the well. This assumption limits the performance of the correlation when simulating wells with significant amount of steam. If inverse analysis is applied to well RN-11 and the slip ratio evaluated, several iterations with iTOUGH2-PEST result in a new value for the slip ratio, *S=1.68*. Using this value instead of one in the Homogenous correlation, almost a perfect match to the measured data is obtained with FloWell. Fig. (4.10) shows both a simulation with the original Homogenous correlation and a simulation where the slip ratio has been exchanged for a new value for well RN-11. Similarly, inverse analysis can be applied to parameters in other correlations to produce a better fit to measured data.

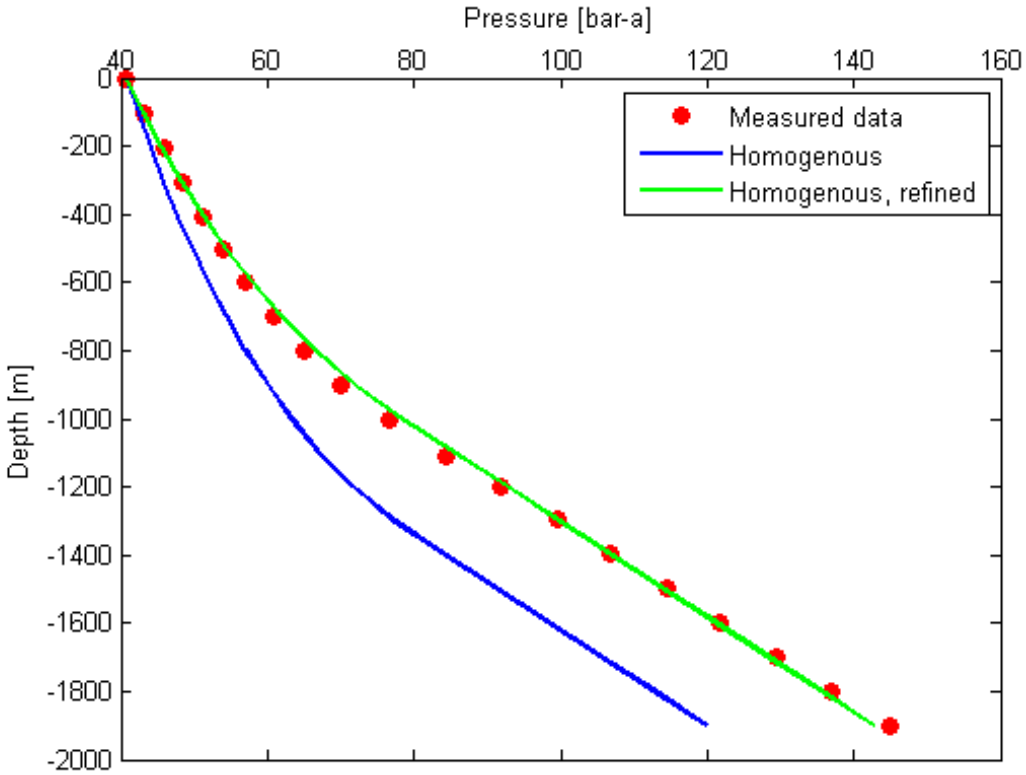

Figure 4.10: Simulations with FloWell for well RN-11 with the original Homogenous model (blue) and with improved slip ratio (green).

Although the results hint that some of the correlations perform better than others, the results are not conclusive and a choice of correlations needs to be evaluated on a case to case basis. It should be kept in mind that if great uncertainties are involved in measured data necessary for simulations no gain is to be had by choosing a complex correlation over a simpler one.

In appendix A, visual results of simulated pressure profiles in the wells listed in Tables (4.1) and (4.2) are presented. The results include simulations for all compositions of available correlations in FloWell illustrated in Fig. (4.1), as well as simulations both to the bottom of production casing and to the bottom of the well.

5. The Coupled FloWell-TOUGH2 Model

Geothermal reservoir engineers and other model designers have made several attempts to couple reservoir and wellbore models, explicitly and implicitly. In explicit coupling, a call is made from the reservoir model to the wellbore simulator at each timestep while the wellbore simulator is run prior to the reservoir model in implicit coupling. The general opinion is that more accurate simulations of geothermal systems can be obtained using coupled wellbore-reservoir model rather than a non-coupled one.

In this study, a different approach is used. In addition to designing a coupled wellbore-reservoir model, an inverse analysis with continually measured wellhead parameters as observations is applied to the coupled model to improve the model design and keep it up to date. Most reservoir engineers that have experience working with the reservoir simulator TOUGH2 are familiar with the inverse analysis program iTOUGH2 and many of them use it on a regular basis for model calibration. Usually, the emphasis is on calibrating the reservoir model, but the method suggested here is to apply an inverse analysis on the wellbore simulator as well. This is to be done in an iterative manner where measured wellhead conditions are used to calibrate the reservoir model to find estimates for the bottomhole pressures in wells. These bottomhole pressures are then used to calibrate the wellbore simulator. This iteration process is explained in detail in following paragraphs.

Wellhead conditions are monitored 24 hours a day and usually stored in a database at the power company in question. By constantly observing wellhead conditions tremendous amount of information is gathered about the behavior of wells and consequently the reservoir behavior. One of the main focuses in this study is to utilize the measured wellhead parameters to a greater extent than has been done so far, by using them as an input to the coupled model and to calibrate the model with an inverse analysis. As new wellhead parameters are measured they are imported into the coupled model and an iterative inverse analysis process is initiated. This results in continuous improvements being made to the model design in the reservoir simulator and in the wellbore simulator.

The basic methodology behind the coupled model is illustrated in Fig. (5.1). The parameters that are measured or estimated at the wellhead, the mass flow rate, enthalpy and pressure, are the input to the wellbore simulator FloWell. FloWell calculates the bottomhole pressures in the wells using available correlations for the friction factor, the friction correction factor and the void fraction. To couple FloWell to TOUGH2 the bottomhole pressures are inserted into the input file for TOUGH2. An inverse analysis by iTOUGH2 on the reservoir model returns new values for the bottomhole pressures in the wells. Lastly, these new values are used in a second inverse analysis performed on the wellbore simulator by iTOUGH2-PEST to obtain a new estimate on parameters in void fraction correlations. From this point, the whole process is repeated where FloWell calculates new bottomhole pressures with the improved void fraction correlation. This iteration is continued until a stopping criteria has been met.

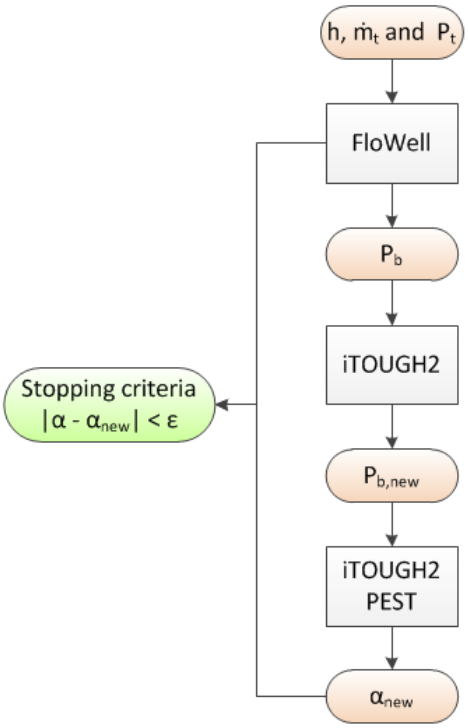

Figure 5.1: The basic ideology for the coupled FloWell-TOUGH2 model.

Although the basic ideology seems simple enough, the total coupling and calibration process is considerably more complicated. How the models are coupled and improved depends mainly on what data is available for calibration and what parameters are to be evaluated. The coupling and calibration can be done in several ways and the method introduced here is one suggestion.

The model design is best explained by taking a regular power plant with several producing wells that has been operated for i+1 years as an example. Historical data about the rate of production and the pressure drawdown in the reservoir is available, as well as continually measured data at the top of the wells. The detailed model design for this case is shown in Fig. (5.2). The modeling procedure has been divided into steps for easier understanding.

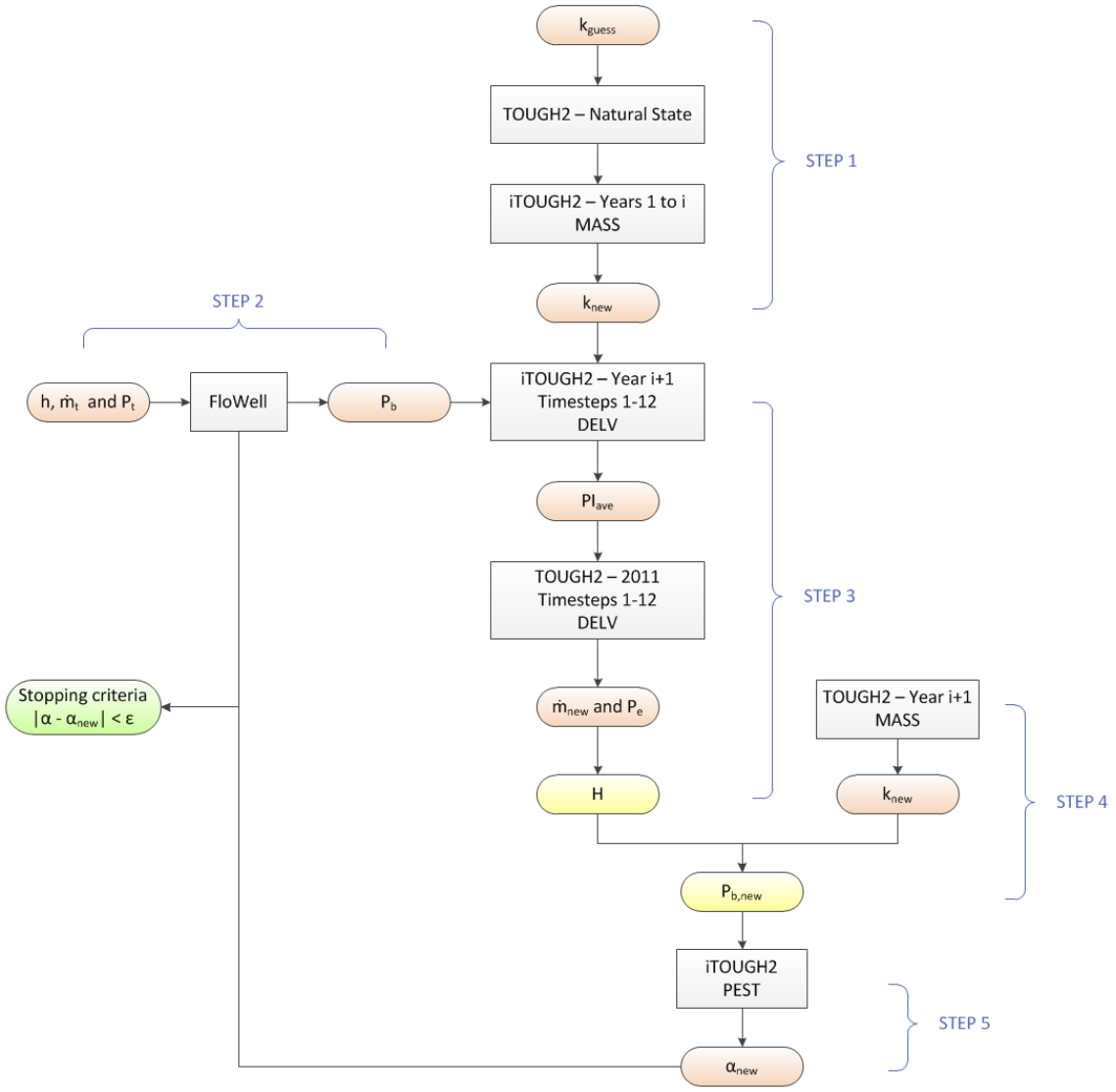

Figure 5.2: The detailed model design for the coupled FloWell-TOUGH2 model.

In the first step a conceptual model is constructed for the reservoir in question. In this conceptual model physical properties such as porosity, density and permeability of the rock structure are identified. Many parameters can be identified with confidence while others are more difficult to determine. The permeability is usually one

of the parameters selected for inverse estimation with iTOUGH2 since it can prove hard to identify.

Before simulating the response of the reservoir to production, initial conditions for pressure and temperature in every element of the model have to be established. That is done by obtaining the natural state of the reservoir before exploitation started by simulating without any production wells and a reasonable value for the permeability (k_{guess}) until a steady state has been reached. Suppose historical data describing the pressure drawdown in the reservoir exists for year 1 to year i of the exploitation period. After a TOUGH2 model has been set up for years 1 to i, this data can be used to calibrate the model in order to obtain a fairly good estimate for permeability (k_{new}) of the rock structure in the reservoir. By changing the permeability in the TOUGH2 model, the initial conditions are no longer valid and new conditions have to be obtained by running the natural state simulation again.

In step 2 it is assumed that measured wellhead conditions, mass flow rates ($\dot{m}_t$), enthalpies (h) and pressures (P_t), are available for every month of the year i+1. These parameters are used as inputs into FloWell, which calculates the bottomhole pressures (P_b) in producing wells in the reservoir.

Desirably, the next move would be to insert the calculated bottomhole pressures and the measured mass flow rates at the wellheads directly into the TOUGH2 model. However, TOUGH2 does not offer an option in which a mass flow rate and a bottomhole pressure for a well can both be used as inputs. To be able to insert bottomhole pressures from FloWell into TOUGH2, wells have to be defined as DELV types but if one wishes to define exact mass flow rates from wells, the MASS option has to be used. When using the DELV option in TOUGH2 it is assumed that wells operate on deliverability against specified bottomhole pressures and productivity indices. Running TOUGH2 with a bottomhole pressure and a productivity index specified for a well, a matching mass flow rate for the well is evaluated.

In the model design presented here, the DELV type is used to couple FloWell with TOUGH2. In step 3, the calculated bottomhole pressures from FloWell are entered to the reservoir model that has been arranged for year i+1 and guess values assigned to the productivity indices (PI) of the wells. This reservoir model is thought as a continuation to the reservoir model in step 1 where the new estimate on the permeability is used. By using mass flow rates as observations to calibrate the TOUGH2 model and to find new estimates for the productivity indices that suites the bottomhole pressure and mass flow rate for each well, the flow rates have now been linked to the coupled model. This calibration has to be performed in twelve timesteps where each timestep represents one month. In total the timesteps add up to one year, year i+1 in production. The reason for this is that TOUGH2 does not allow the user to define time-dependant bottomhole pressures, the pressures have to be fixed throughout the simulation.

Dividing the simulation into steps to account for varying bottomhole pressures results in twelve new estimates for the productivity index of each well to be obtained. As it is custom to denote only one productivity index for a well an average is taken of the twelve values (PI_{ave}). The average values of the productivity indices, one average value for each well, are now inserted into the TOUGH2 model instead of the guess values and a forward run in twelve timesteps executed as before. After each run, pressures in the elements where wells are defined (P_e) are extracted from the output report from TOUGH2, along with mass flow rates ($\dot{m}_{new}$). These extracted mass flow rates can differ from the actual mass flow rates measured at the wellheads mainly because of two reasons. Firstly iTOUGH2 is not always able to match the observed mass flow rate completely, and secondly using the average value in a forward run causes the mass flow rate to deviate even further from the observed value.

At this stage, the parameters $\dot{m}_{new}$, P_b, P_e and PI_{ave} have all been identified. Using Eq. (3.66) the variable H can be calculated.

$$H = \frac{\dot{m}_{new}}{PI_{ave} \cdot (P_e - P_b)}$$

For this study it is not all-important to distinguish H further but for curious readers the variable is dependent on the density and viscosity of the fluid and the relative permeability as expressed in Eq. (3.67).

As step 3 has been concluded, a coupled FloWell-TOUGH2 model exists where measured pressures and mass flow rates at wellheads serve as main inputs into the coupled model. In step 4 a new estimate for the permeability that describes year i+1 is found with iTOUGH2. Similarly to step 1, the MASS option in TOUGH2 is used and values for mass flow rates observed at the wellheads inserted into time-dependent tables. Since forward runs with MASS should not differ much from runs with DELV, the element pressures found in step 3 are used as observations for the inverse analysis in step 4. The inverse analysis results in permeability that yields element pressures that are close to the ones used as observations. These new element pressures can then be used along with correct mass flow rates, the productivity indices and the variable H found in step 3 to achieve new bottomhole pressures ($P_{b,new}$);

$$P_{b,new} = P_{e,new} - \frac{\dot{m}_t}{PI_{ave} \cdot H}$$

The final step involves the calibration of FloWell with iTOUGH2-PEST. The new bottomhole pressures calculated in step 4 are used as observations in the inverse analysis and the parameters chosen for evaluation are variables in void fraction correlations. The variable chosen varies with void fraction correlation, for example if the homogenous model is used for simulations the slip ratio would be a probable parameter for estimation. The reason why the void fraction is selected for parameter

estimation is that it is one of the most critical parameters in wellbore simulations and is therefore often the subject of geothermal researches. When the void fraction has been manipulated so bottomhole pressures match the ones from step 4 the first iteration has been completed. This new void fraction is inserted into FloWell and the procedure repeated until the difference between the new void fraction and the one in the iteration before is negligible.

After a new permeability has been found in step 4 it is advisable to run the natural state again because the initial conditions are no longer valid. However, in this case it can be justified to skip it because the change in the permeability over one year is expected to be insignificant. As mentioned above this coupling procedure and calibration described here is one suggestion but this can also be accomplished a different manner. In step 4 the simulation time spans one year to shorten the computational time. Another way would be to apply inverse analysis to a TOUGH2 model where the simulation covers the whole operation time of the power plant, namely years 1 to i+1. In step 3 the simulations are divided into months, but if more continuous data was available longer time periods would be more desirable. Step 3 does not only serve as a procedure to couple FloWell to TOUGH2, the development of the productivity index throughout year i+1 also yields interesting information. Although dividing the simulation time into twelve steps is necessary, the resulting twelve productivity indices can describe what is happening in the wells. If for example a great change is observed in a productivity index for a well between months it can indicate that scaling has began to block the flow from the reservoir to the well.

By concluding steps 1-5 in Fig. (5.2), a calibrated coupled wellbore-reservoir model has been developed which can be further used for forecasting scenarios to predict how the reservoir reacts to production in the future.

6. Case Study for Reykjanes Geothermal Field

The following sections are devoted to the discussion of the case study of Reykjanes geothermal field where a conceptual model and a numerical model of Reykjanes are introduced along with numerical results.

6.1. Conceptual model

The Reykjanes peninsula, situated at the south-western end of Iceland, is an onshore continuation of the Mid-Atlantic Ridge. The active volcanic zone of Iceland extends from the peninsula right across the country. The peninsula became active 6-7 million years ago when a major ridge jump initiated spreading of the Mid Atlantic Ridge. Due to this spreading, earthquakes are frequent in the area and usually occur at depths of 1-5 km. These earthquakes are essential to maintain or increase the permeability of the rock so the water recharge to the heat sources can be conserved. The peninsula features series of sub-parallel eruptive fissures and normal faults, spaced approximately 5 km apart. The fissure swarms have all been active in historic time and consist of shear fractures (normal faults), extension fractures (gaping fissures with no shear displacement) and fractures that exhibit both shear and extension [31].

The general topography of the Reykjanes peninsula has been shaped by sub- and postglacial fissure eruptions that created the northeast trending hyaloclastite ridges and crater rows. No central volcanos have been developed in Reykjanes so the heat sources for the high temperature fields in the peninsula are considered to be dyke swarms. The uppermost geological layers consist mainly of sub-aerial basaltic formations, followed by a series of hyaloclastite tuff formations intersected with sedimentary layers which extend down to 900 m. Below, down to at least 3000 m, layers of pillow lava become dominant along with intrusions that have forced their way into the lava over an extended period of time [4, 31, 69]

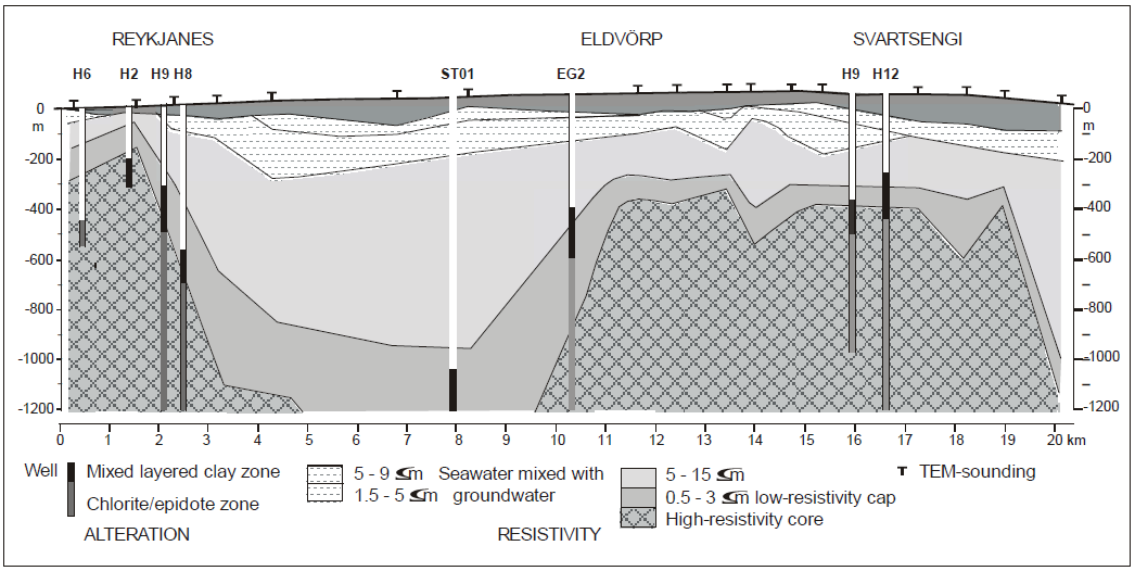

Figure 6.1: Resistivity cross-section of Reykjanes in the west to Svartsengi-Eldvörp in the east along with alteration zoning in wells [3].

Reykjanes geothermal field is among six high temperature areas found along the Reykjanes Peninsula, as shown in Fig. (4.2). The others are the Eldvörp area, the Svartsengi area, the Krýsuvík-Trölladyngja area, the Brennisteinsfjöll area and the Hengill area [21, 69]. High temperature fields in Iceland display similar resistivity structures which is featured by a lower resistivity cap at the top and outer margins of the reservoir and underlain by a more resistive core. TEM resistivity measurements performed in 1996-1997 on the outer part of the Reykjanes peninsula revealed the resistivity structure of the high-temperature geothermal fields in the peninsula, Reykjanes, Svartsengi and Eldvörp, as illustrated in Fig. (6.1). The measurements showed the surrounding rocks having resistivities ranging from 5-15 Ωm and the geothermal reservoirs as a low resistivity cap with resistivities of the order 0.5-3 Ωm. High resistivity core appears beneath the geothermal fields with resistivities from 7 Ωm to 15 Ωm [3]. In the geothermal fields located on the Reykjanes peninsula, the temperatures follow the boiling point curve with depth in the uppermost 400-1000 m but at greater depth they are about constant, indicating good vertical permeability [4]. Two fissure zones are believed to control the permeability in the Reykjanes geothermal field. One of them lies from Rauðhólar through the hot spring area next to Gunnuhver while the other one stretches out under the Grey Lagoon with a north-west direction [50].

Although geothermal waters in Iceland generally have lower content of dissolved solids than waters in similar areas in the world, Reykjanes produces water with quite high concentration of dissolved solids. The cause is that the recharge water to the reservoir consist mainly of seawater which is then modified chemically through interaction with the basaltic rock. The saline-water system in the Reykjanes peninsula

indicates different correlation between alteration and resistivity from that in fresh-water systems. In fresh-water systems the boundary between the low resistivity cap and the resistive core correlates with the boundary between the smectite-zeolite zone and the mixed-layered clay zone but in Reykjanes the boundary seems to be within the mixed-layered clay zone, indicating different alteration zoning in saline systems as shown in Fig. (6.1) [3].

From resistivity measurements reaching down to 1000 m it is believed that the geothermal system at Reykjanes covers about 10 km^2 in area. Interpretations of satellite pictures indicate however that the geothermal system becomes considerably more extensive with depth, where large parts of the system may lie beneath the ocean floor far south of the Reykjanes Peninsula. In 2008, MT-measurements were performed to explore the resistivity deep down in the earth crust. Results from the MT-measurements indicate that the geothermal reservoir itself reaches down to at least 5000 m [31].

Temperature distribution in geothermal fields is essential in conceptual modeling. Maps of formation pressures in cross sections through the reservoir in Reykjanes are shown in Fig. (B.1)-(B.3) in Appendix B. Fig. (B.1) shows that the temperature in the reservoir has reached 260°C at 700 m and the highest temperature in wellbores in Reykjanes is found in well RN-10, 320°C. A temperature reversal is detected in RN-17 at 1000 m and the figure indicates that the well marks the edge of the reservoir to the south. In Fig. (B.2) the temperature has reached 300°C in RN-22 and RN-23 with RN-18 at the boundary of the reservoir to the north. Lastly, in Fig. (B.3) it is clear that RN-19 and RN-20 mark the boundary of the reservoir to the east and RN-16 to the west [50].

Well RN-10 was drilled in Reykjanes geothermal field in 1998 to explore potential power production in the area. The Reykjanes Power Plant was designed based on scaling results from well RN-10 along with other operational findings from previous drilled research wellbores, the first one being drilled in the year 1956. The power plant began producing 100 MW_e in May 2006 with two 50 MW_e twin steam turbines with sea cooled condensers. HS Orka plans to expand the power production by 50 MW_e in coming years as well as increase injection to support the pressure in the reservoir [52].

Little is known about the pressure change in the Reykjanes reservoir before power production started in the area but the data available indicates that the drawdown in pressure was hardly more than 2 to 3 bar prior to production [50]. The geothermal reservoir in Reykjanes reacts similarly to production to the one located in Svartsengi, which has been operated since 1976. In 2009 the production at Reykjanes had caused the pressure in the reservoir to decrease by 19 bar on average. Equivalent to Svartsengi, this reduction in pressure resulted in formation of a steam pillow at the depth of 800-1200 m. Due to this steam formation, less fluid mass is needed for the

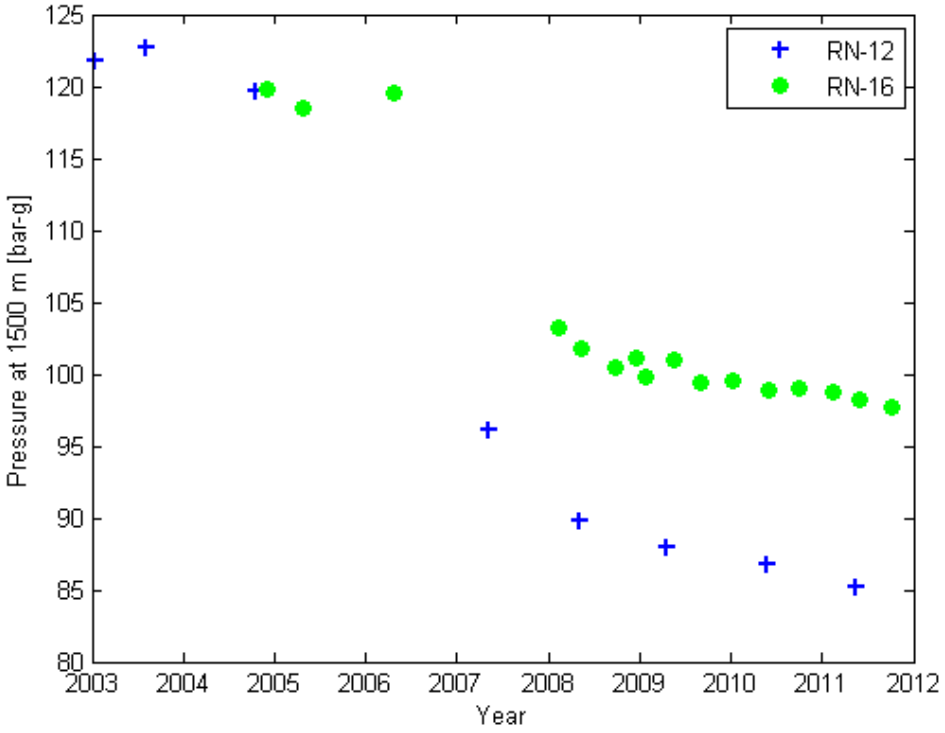

Figure 6.2: Pressure at depth 1500 m in wells RN-12 and RN-16 in Reykjanes in the years 2002 to 2011.

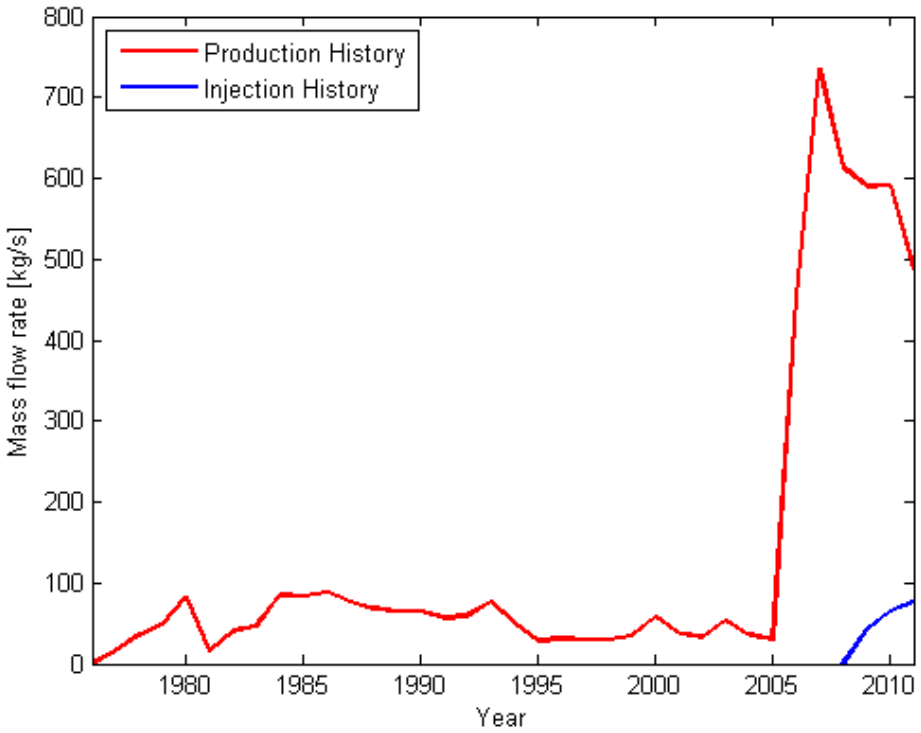

Figure 6.3: Total production in Reykjanes geothermal field from 1976 to 2011.

power production resulting in less being extracted from the reservoir, which leads to less drawdown in pressure in the reservoir. Newly started injection of brine from separators in the power plant also helps to maintain the pressure in the reservoir. [31]

Fig. (6.2) displays pressures at depth 1500 m in wells RN-12 and RN-16 in Reykjanes for years 2002-2011. RN-12 is a production well located near the center of the reservoir while RN-16 is a surveillance well situated at the boundaries. During the first months of production, steep decline in pressure is detected which continues until spring 2007. Pressure measurements in 2011 show however that substantial reduction in the rate of pressure drawdown occurs in the years 2008-2011. In total, from beginning of year 2006, the pressure drawdown in the center of the reservoir has reached the maximum of 36 bar while at the boundaries the drawdown is much less or 21 bar. This goes hand in hand with the magnitude of mass being extracted from the reservoir. The total production history for Reykjanes Power Plant can be seen in Fig. (6.3), reaching back to the year 1976. The production reaches a maximum value in 2007 when the most decline in pressure is detected, and gradually decreases to the present day, resulting in less drawdown in pressure [51]. Even though the production rate has the most effect on the drawdown, the fact that the production area itself only covers roughly 1 km^2, while the geothermal area is assumed to expand over several square kilometers, may influence the pressure. If the production load were distributed over a larger area it is possible that less pressure drawdown may have been detected [31].

6.2. Numerical model

The numerical model of Reykjanes geothermal field is designed based on the methodology behind the coupled model and the conceptual model of Reykjanes described in previous sections. The numerical model can be broken down into four main parts:

(i) A natural state model defining the Reykjanes geothermal reservoir prior to any production from the area.

(ii) A reservoir model to simulate the production history ranging from the year 1977 to the year 2010 in Reykjanes along with calibration of the model against measured pressure drawdown in the reservoir over the production period.

(iii) A coupled wellbore-reservoir model where wellhead measurements in 2011 are used to calibrate both the wellbore and the reservoir model.

(iv) A forecasting model using the results from parts (i)-(iii) where different scenarios are simulated to predict the reservoir's response the next 15 years.

The mesh design and most of the physical properties of the rock structure in the Reykjanes reservoir are the same for all four parts. The parts mainly differ in the choice of well types in TOUGH2, simulation time and intended use. The following sections are devoted to the discussion of generalities of the numerical model and the particularities of each part.

The main programming language used for the numerical model is MATLAB but a call is made to the programs TOUGH2, iTOUGH2 and iTOUGH2-PEST as needed. Lilja Magnúsdóttir, a PhD candidate at Stanford University, has designed a model to construct the element mesh and the input file for a simulation with TOUGH2 directly with MATLAB as well as some postprocessing methods. In this study her work is utilized, but with some improvements in order to adapt the model to the case study under review.

6.2.1. General Features

The mesh design is based on the conceptual model of Reykjanes geothermal field. Fig. (6.4) shows the overall mesh used. The mesh covers 10x10 km area or 100 km^2. The outermost elements are fairly large with boundary conditions that describe the state farthest away from the geothermal reservoir. Nearing the center of the reservoir, the element size decreases. Fig. (6.5) displays the innermost core of the geothermal reservoir along with placements of wells at Reykjanes geothermal field. Especially fine mesh is assigned for the core because more extensive knowledge is available about wells, fissures and faults and higher gradients are expected to occur there. Each dot represents a wellhead at Reykjanes and although the figure indicates that several wells share the same element, some wells are directionally drilled resulting in the extraction of fluid taking place in different elements for each wellbore.

The mesh consists of 2064 elements where 344 elements are defined inactive and mass and energy flows through 6884 connections between the elements. The numerical model of Reykjanes geothermal field consists of 12 layers, each with 172 elements and a thickness of 300 m. The horizontal mesh remains the same for each layer. Fig. (6.6) shows the stratification of the numerical model where layers are named in alphabetical order. Layers A and L represent the caprock and baserock of the reservoir and are defined inactive to maintain the temperature and pressure at the top and at 3.6 km depth. Layer B is above the depth of a production casing in a typical well at Reykjanes. Layers C and D contain the uppermost feedzones while layers E,F,G and H form the actual reservoir. No feedzones are located in layers I,J and K but inflow of hot fluid is thought to occur in layer K, believed to originate below the layer.

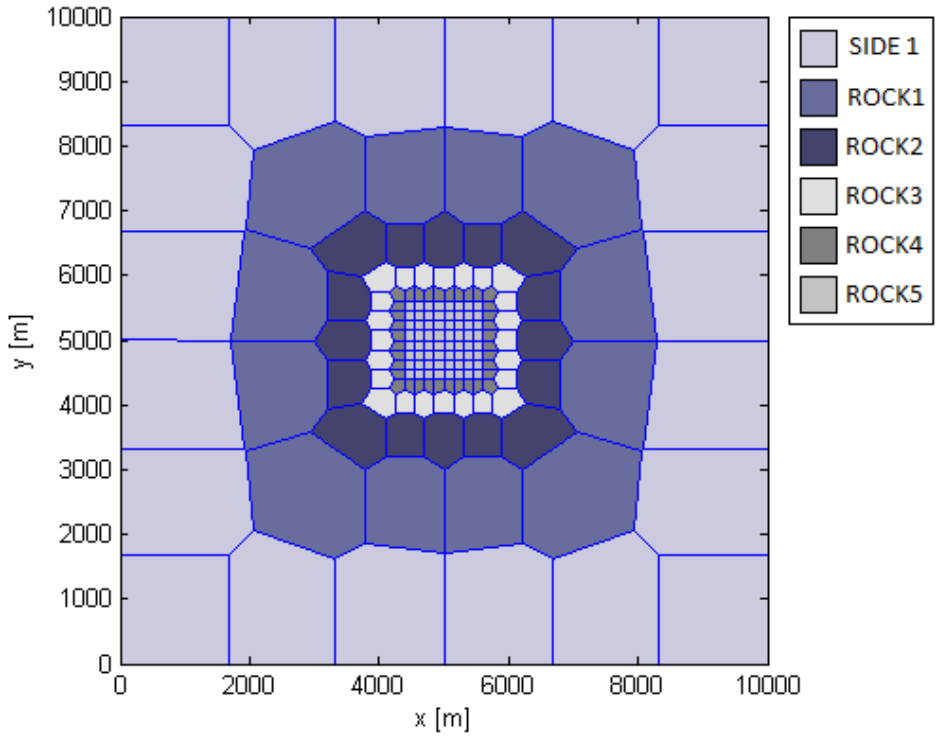

Figure 6.4: Horizontal mesh of the Reykjanes numerical model.

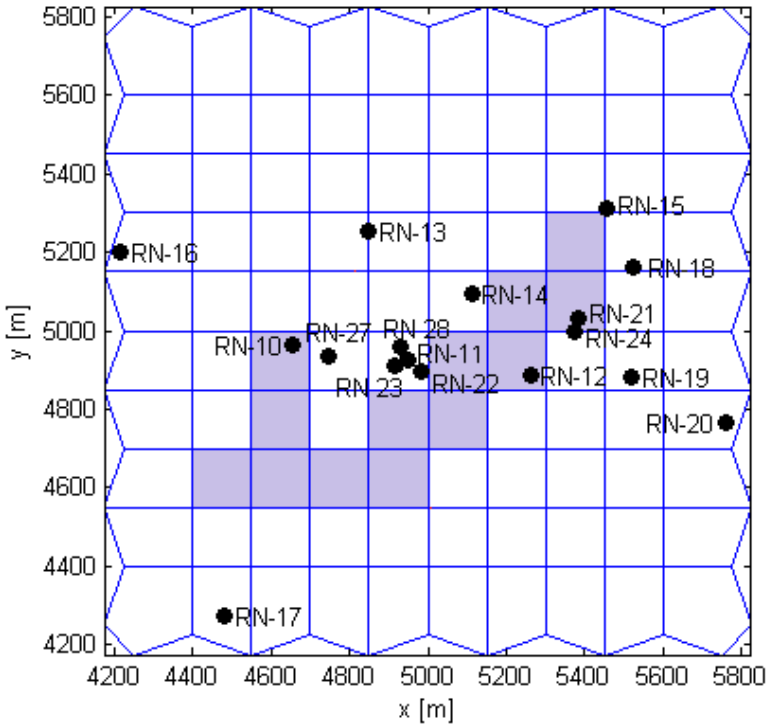

Figure 6.5: Placements of wells at Reykjanes geothermal field where purple elements represent upflow of geothermal fluid in layer K.

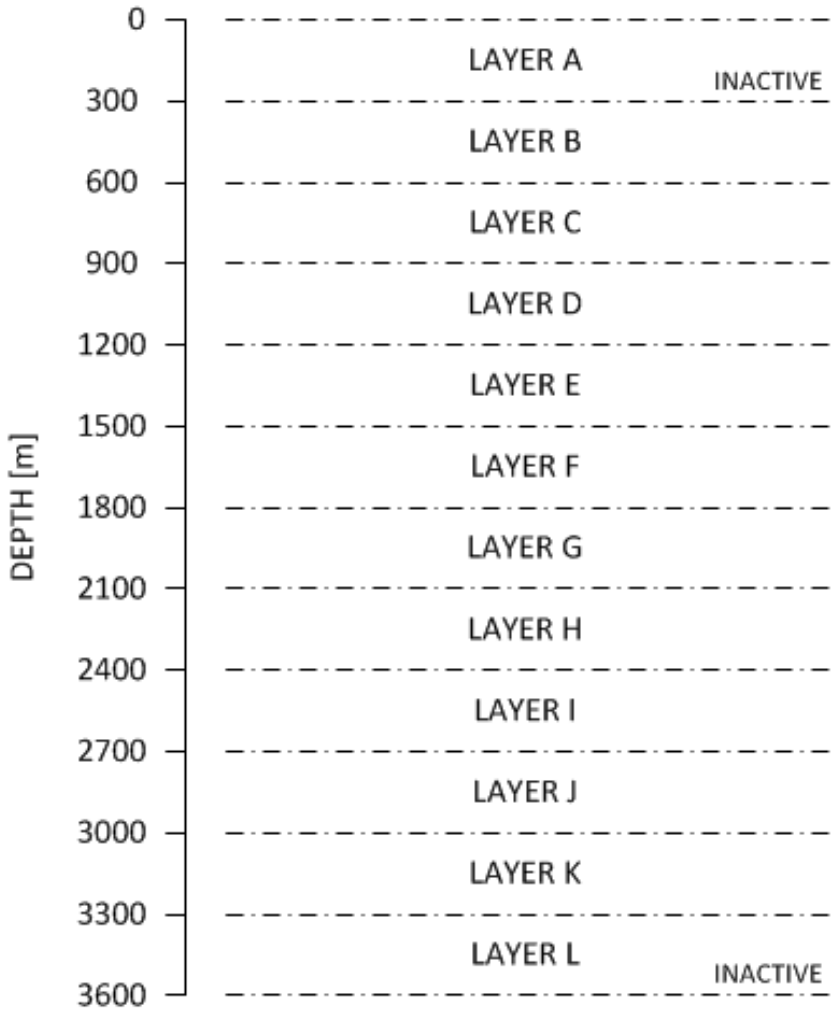

Figure 6.6: Stratification of the Reykjanes numerical model.

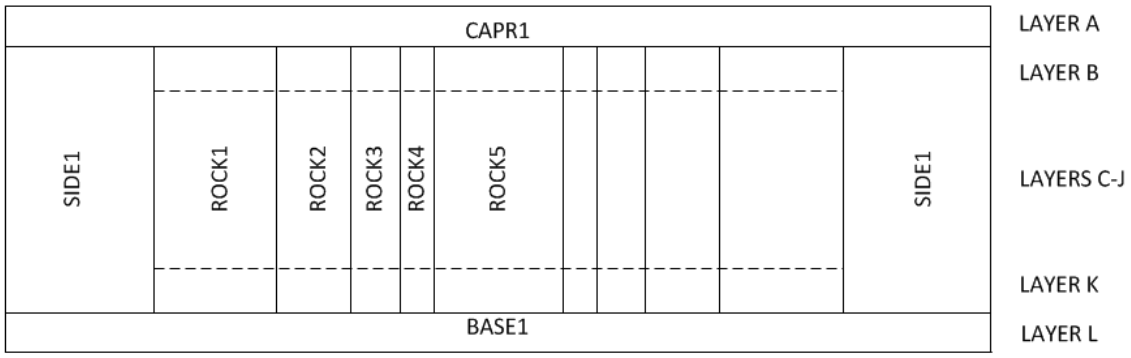

Figure 6.7: Vertical cross section of the Reykjanes numerical model.

The extraction of fluid takes place at the greatest feedzones in the wells. These feedzones are located in layers C to H where the shallowest feedzones are placed at 750 m depth and the deepest feedzones at 2250 m depth. The locations of the feedzones are restricted to the center of the layers so the depth to the feedzones are not as accurate relative to estimated depth according to temperature and pressure logs.

In the development of a numerical model, the geothermal field under observation is divided into rock types and each type assigned physical properties such as density, porosity and permeability. The rock types for the Reykjanes geothermal field can be seen in Fig. (6.4) but are further illustrated with a vertical cross section of the reservoir in Fig. (6.7). Layers A and L have the rock type names CAPR1 and BASE1 and the boundary of the Reykjanes geothermal field SIDE1. The surroundings of the reservoir are called ROCK1 and ROCK2 and the margin or the boundary of the main reservoir are represented with ROCK3 and ROCK4. The rock type name ROCK5 has been assigned to the actual reservoir where current production takes place in Reykjanes. All in all, 8 unique rock types exist within the mesh.

The approach of dividing the numerical model into vertical sections, each section representing a rock type with specific physical properties, is taken to simplify the numerical model and use as few rock types as possible. If more accurate results are sought, further division into rock types is recommended, especially if fissures and faults are to be analyzed for they are known to have permeabilities different from others in geothermal areas.

The physical properties that are believed to be constant for all rock types in Reykjanes geothermal field are listed in Table (6.1). These values are assumed to be similar to the Reykjanes model by Hjartarson and Júlíusson [50].

Table 6.1: Constant physical properties of rocks types in the Reykjanes model.

Physical properties	
Rock density	2650 kg/m^3
Thermal conductivity	2 W/m°C
Heat capacity	1000 kJ/kg
Porosity	10%

The heat capacity is assumed to be the same for all rock types except for one representing the boundaries of the geothermal field. There, an extremely large value for the heat capacity is assigned to the rock type (SIDE1) to maintain a constant linear heat gradient of 100°C/km.

Linear relative permeability curves are used with immobile liquid and vapor saturations of 0.4 and 0.05, respectively, and perfectly mobile liquid and vapor saturations

of 0.95 and 0.65, respectively. As for calculations in the wellbore simulator, the fluid in the numerical model is assumed to be pure water. Therefore the equation-of-state module EOS1 in TOUGH2 is chosen for reservoir calculations, but the module provides thermodynamic properties for pure water in its liquid, vapor and two phase states.

The permeability in a rock type can be different in x,y and z direction. For simplicity and to facilitate calculations in the inverse program iTOUGH2 by reducing number of unknowns, the permeability in x and y direction in this model is assumed to be the same. Furthermore, permeability close to zero is assigned to the top and the bottom layer in all directions to hinder water recharge into the system from the top or below. For permeability distribution in other rock types in the numerical model, comparable values to the values introduced in Hjartarson and Júlíusson [50] are used. They concluded that the permeabilities for the surroundings are close to 2-7 mD in the horizontal direction and 0.01-0.05 mD in the vertical direction. For rock types outside of fissure swarms but in the center of the reservoir the horizontal permeabilites are thought to be in the range of 2-20 mD and vertical permeability 0.01-1 mD. The highest permeability is encountered in fissures in the center of the reservoir or 2-200 mD in horizontal direction and 5-500 mD in vertical direction.

6.2.2. The Natural State Model

As presented in step 1 in the model design illustrated in Fig. (5.2), the natural state of the Reykjanes reservoir must be accomplished before any further analysis on the reservoir can be carried out. The natural state of the reservoir can be obtained by simulating with TOUGH2 for an extended period of time until a steady state has been reached. That is when the heat and mass entering the reservoir are equal to heat and mass released through the boundaries and no change is observed in thermodynamic variables. The natural state is intended to describe the reservoir before exploitation started so no production wells are defined in the TOUGH2 model. An upflow of hot geothermal fluid is believed to occur deep in the reservoir in the two main fissures presented in the conceptual model of Reykjanes. To describe this upflow a total of 80 kg/s of pure water with enthalpy of 1500 kJ/kg is injected into 13 elements in layer K above the inactive baserock, illustrated in Fig. (6.5). This upflow is adjusted so observed formation temperature and pressure are obtained but after exploitation has started the upflow is held constant in all simulations.

The initial conditions for temperature and pressure in the natural state simulation is is set at 15°C and 14.7 bar-a for the impermeable and inactive top layer and at 345°C and 263.5 bar-a for the bottom layer. This corresponds to a 100°C/km heat gradient which is commonly used in reservoir management in Iceland [50]. After an acceptable natural state model of the Reykjanes reservoir has been achieved the

formation temperatures and pressures from the natural state simulation are used as initial conditions for simulations describing the production period.

6.2.3. The Historical Model for the Years 1977-2010

This part is a continuation to the natural state model as shown in step 1 in Fig. (5.2). A reservoir model is constructed that simulates the reservoir's behavior to the production observed in the year 1977 to 2010. The yearly average production rates for individual wells for the years 1977-2010 are documented in [2] but the total extracted mass and injection are illustrated in Fig. (6.3). Since the production rates are available the wells are defined as MASS types with time dependent generation rates. It is not guaranteed that a TOUGH2 run with the physical properties listed in the conceptual model of Reykjanes yields the actual reservoir response and substantial uncertainty can be involved in the permeability distribution evaluation. The permeability distribution in the reservoir model is therefore calibrated with iTOUGH2 to match measured data over the production period. The historical data is the drawdown in pressure in wells RN-12 and RN-16 presented in Fig. (6.2). Limited pressure data is available about the Reykjanes reservoir prior to the power generation start in 2006 but it is believed that the pressure drawdown is no more than 3 bar. In the calibration model it is assumed that the pressure in the reservoir declines logarithmically with time from 1977 until the power production starts. When a reasonable match has been obtained the newly estimated permeability is interpreted as a representative of the actual permeability in the reservoir and the calculated reservoir conditions used as initial conditions for further simulations.

6.2.4. The Coupled FloWell-TOUGH2 Model

The coupling procedure of FloWell and TOUGH2 is described in steps 2-5 in the modeling design displayed in Fig. (5.2). Along with the coupling procedure, a calibration of both the wellbore simulator and the reservoir simulator takes place. The coupling and calibration are implemented with data measured at wellheads in the year 2011. Today, thirteen wells are producing in the Reykjanes geothermal field. It would prove to be very time consuming to calibrate the coupled model considering all producing wells in Reykjanes. Therefore six wells are chosen for the calibration, namely RN-12, RN-15, RN-18, RN-19, RN-21 and RN-24. Vertical wells are deliberately chosen over inclined ones because of more accurate data available. However, all wells are defined in the TOUGH2 model to account for the exact total mass extraction in 2011, the chosen wells as DELV types in TOUGH2 and other wells as MASS types. Doing so, wells defined as MASS types are not coupled through FloWell to TOUGH2 and pressure variations observed at wellheads do not influence

the calculations in TOUGH2.

Mass flow rates and enthalpies in the six wells, estimated for every month of 2011, are used as observations in iTOUGH to calibrate the productivity index of the wells. In the historical model, the overall permeability structure is calibrated, but to further reduce computational time it is focused on calibrating only the permeability at the center of the reservoir. To improve the model design in FloWell a parameter in the Rouhani-Axelsson void fraction correlation has been chosen. The parameter is marked with red in the following equation.

$$\alpha = \left[\frac{x}{\rho_g}\right]\left[(1+0.12(1-x))\left(\left(\frac{x}{\rho_g}\right)+\left(\frac{1-x}{\rho_l}\right)\right)+\frac{(1.18(1-x))(g\sigma(\rho_l-\rho_g))^{0.25}}{G\rho_l^{0.5}}\right]^{-1} \tag{6.1}$$

6.2.5. The Forecasting Model

The purpose of designing a reservoir model is to use it to predict the future response of the reservoir to different production scenarios. In this study, four different production scenarios were modeled for the Reykjanes geothermal field. All scenarios involve simulations up to the year 2027.

- **Scenario 1**: Maintaining the same total production and injection rates as in the year 2011.
- **Scenario 2**: Maintaining the same total production rate as in the year 2011 and increasing the injection rate to 30% of the total extracted mass.
- **Scenario 3**: Increasing the production capacity of the power plant by 50 MW_e and maintaining the injection rate as in the year 2011.
- **Scenario 4**: Increasing the production capacity of the power plant by 50 MW_e and the injection rate to 30% of the total extracted mass.

HS Orka intends to increase the production capacity of the Reykjanes power plant by 50 MW_e and the magnitude of injection into the reservoir to 30-50% of the total extracted mass. In scenarios 3 and 4 it is analyzed how the reservoir responds to increase in production and if the reservoir can sustain such boost in production. Enlargement of this magnitude involves a new turbine to be added to the preexisting turbine unit and new wells to be drilled and connected to the turbine. However, in order to simulate the increase in production in the simplest manner it is assumed that the capacity of each of the two preexisting turbines is increased by half, or 25 MW_e. Consequently, the steam production from each preexisting well is increased by half. In scenario 4 the magnitude of injection is greatly exaggerated, thus using only well RN-20B for injection is not enough. Therefore, it is decided to add injection

to well RN-17B in scenario 4. The production and injection rates for each scenarios are listed in Table (6.2).

Table 6.2: Production and injection rates for scenarios in the forecasting model.

Wells	Scenario 1	Scenario 2	Scenario 3	Scenario 4
Production rates				
RN-11	64.9	64.9	97.4	97.4
RN-12	78.8	78.8	118.2	118.2
RN-13B	31.1	31.1	46.7	46.7
RN-14B	33.3	33.3	49.9	49.9
RN-15	17.9	17.9	26.9	26.9
RN-18	27.4	27.4	41.0	41.0
RN-19	19.7	19.7	29.6	29.6
RN-21	34.0	34.0	50.9	50.9
RN-22	9.1	9.1	13.6	13.6
RN-23	75.2	75.2	112.9	112.9
RN-24	46.7	46.7	70.0	70.0
RN-27	28.0	28.0	42.0	42.0
RN-28	22.3	22.3	33.5	33.5
Injection rates				
RN-20B	77.8	150	77.8	110
RN-17B	0	0	0	110

In all scenarios it is assumed that the enthalpy of the fluid in the wells as estimated in 2011 is maintained throughout the prediction period. However, prolonged production can enhance the formation of a steam pillow and increased injection can cause cooling, which in both cases influences the enthalpy. In the forecasting model the forward simulator TOUGH2 is used. FloWell is excluded in this part but the permeability distribution found in the historical and the coupled FloWell-TOUGH2 models is used for the predictions. In the TOUGH2 model, the wells are defined as MASS types and flow of geothermal fluid is forced out of the wells. Therefore, the forecasting model is not fit to estimate how many wells have to be drilled to maintain the magnitude of steam for the power generation in the prediction period. Rather, the focus is on observing the response of the reservoir to the different production scenarios.

6.3. Numerical Results

6.3.1. The Natural State Model

The results for the natural state model are presented in Fig. (C.1)-(C.8) in Appendix C. The change in thermodynamic variables becomes negligible after approximately 100.000 years and therefore it may be expected that a steady state has been reached in the reservoir. Heat entering the reservoir is equal to the one being discharged and the model is believed to describe the state of the Reykjanes reservoir in 1977, before exploitation started. The natural state model simulates the formation temperature and pressure reasonably well in some wells but inadequately in others.

An acceptable pressure distribution has been obtained in all wells, but achieving proper temperature distribution has proven to be a greater challenge. An overall temperature of 260°C is detected at 700 m in all wells, which corresponds to what is stated in the conceptual model of the Reykjanes geothermal field. A very good match is obtained for the temperature distribution in wells RN-09, RN-12 and RN-21. Fig. (C.3) and (C.8) display a satisfactory match between simulated temperature and formation temperature in wells RN-11 and RN-24, but a temperature reversal is present at depths 2500-3500 m. This temperature reversal can partly be explained by the definition of upflow of hot geothermal fluid in layer K in the numerical model. The upflow is defined in elements situated directly beneath wells RN-09 and RN-12 where even temperature distributions in the wells are observed. However, no upflow is defined in elements beneath wells RN-11, RN-15, RN-19 and RN-24, which may cause the uneven temperature distribution at greater depths.

In well RN-10 a reasonable match is gained, except for the temperature being to low at depth 1200-2500 m. At this depth range the desired temperature is 320°C but observed temperature is 300°C. The model yields unsatisfactory temperature distribution for wells RN-15 and RN-19, which are located close to the boundary of the reservoir. This can mainly be blamed on the simplicity of the reservoir model. In all, a conclusion can be drawn that the natural state model yields acceptable temperature and pressure distributions in wells at the center of the reservoir, but less accurate simulations can be expected in wells farther away from the center.

6.3.2. The Historical Model for the Years 1977-2010

The historical model describes the response of Reykjanes reservoir to exploitation from the year 1977 to 2010. This part mainly involves calibration of the historical model in order to use it in forecasting scenarios in the following section. The pa-

rameter estimation with iTOUGH2 is performed on the permeability distribution of the rock structure in Reykjanes reservoir. New estimates for the permeability in xy-direction and z-direction are found for the rock types, SIDE1 and ROCK1-5 illustrated in Fig. (6.7). The permeability is kept constant close to zero in the base- and caprock to prevent inflow of water into the reservoir from the top or the bottom. The number of unknowns are kept to a minimum to simplify the computational procedure. Therefore, the rock types that represent the surroundings of the reservoir, ROCK1 and ROCK2, and the rock types that represent the boundaries of the reservoir, ROCK3 and ROCK4, are assumed as one rock type, respectively. The measured pressure drawdown in wells RN-12 and RN-16 is used as observations and a better fit to the measured data indicates a decrease in the calculated objective function.

Parameter estimation results are shown in Table (6.3) along with initial values for the permeability distribution. After only four iterations with iTOUGH2 the objective function had decreased to 94% of the initial value. The permeability at the boundary of the geothermal field (SIDE1) was reduced in both xy- and z-direction, much less in the latter. The same goes for the permeability at the boundaries of the reservoir (ROCK3+4), but opposite behavior is noticed for the main reservoir (ROCK5). For the surroundings of the reservoir (ROCK1+2) the permeability was reduced in xy-direction but a slight increase is detected in z-direction.

Table 6.3: Parameter estimation results for the historical model and initial values for the permeability distribution [mD].

	SIDE1	ROCK1+2	ROCK3+4	ROCK5
Guessed xy-permeability	2.00	20.00	20.00	100.00
Guessed z-permeability	0.010	1.00	1.00	200.00
Estimated xy-permeability	0.41	4.48	6.04	97.48
Estimated z-permeability	0.0097	1.66	0.97	117.77

The permeability in most geothermal reservoirs is not constrained within a uniform aquifer but distributed as an array of fractures that intersect the well at few points [38]. In this study the rock structure was roughly divided into sections and the presence of known fractures ignored. Therefore it cannot be stated that the permeability distribution introduced here reflects the actual distribution, but is rather presented as a rough estimate.

The simulated pressure drawdown for wells RN-12 and RN-16 with the new estimates for the permeability distribution is shown in Fig. (6.8) and (6.9). In both wells the historical model simulates the 3 bar pressure drawdown quite accurately. The model also produces acceptable simulations of the steep decline in pressure of 36 bar in the center of the reservoir and considerable lesser decline of 21 bar at the boundaries of

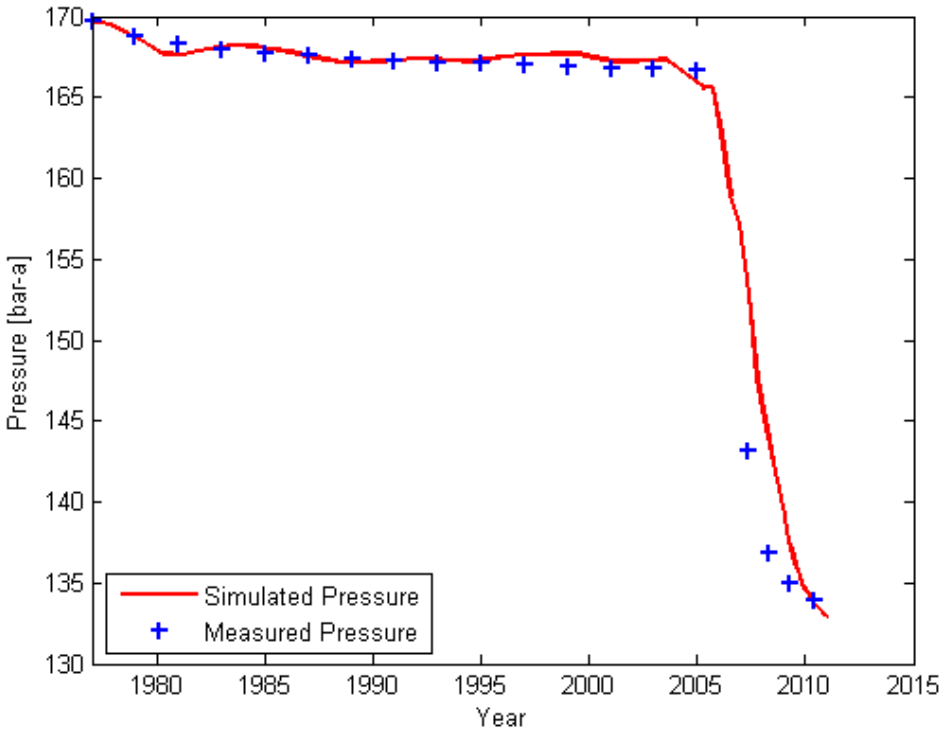

Figure 6.8: Simulated pressure drawdown vs. measured drawdown in well RN-12.

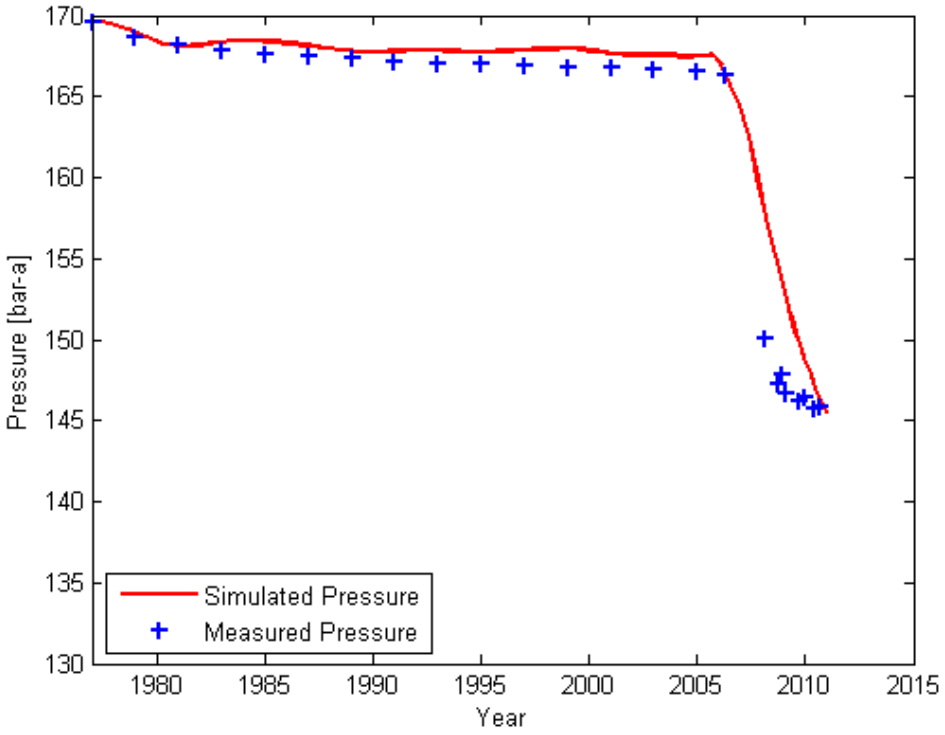

Figure 6.9: Simulated pressure drawdown vs. measured drawdown in well RN-16.

the reservoir. The total pressure drawdown is correctly simulated in both cases, although the curve of the pressure drawdown from the years 2006-2010 should be a little steeper in the latter case.

In the sensitivity and error analysis provided in the iTOUGH2 output file, information about the estimation error and the uncertainty in the model's simulations is available. The sensitivity analysis indicates that observations in wells RN-12 and RN-16 contribute equally to the minimization of the objective function. The sensitivity of the objective function with respect to each parameter denotes that the permeability of SIDE1 and ROCK5 in xy-direction and ROCK3+4 in z-direction contribute the most to the objective function while other parameters are not as sensitive.

The error analysis yields that the permeability of SIDE1 in z-direction is the most independent parameter whereas the permeability of SIDE1 and ROCK1+2 in xy-direction is strongly correlated to all the other parameters. The eigenanalysis of the covariance matrix supports the error analysis and the permeability of ROCK1+2 is identified as the most uncertain parameter. Although the matrix of direct correlations reveals that some parameters are strongly correlated, the result are not surprising since only two data sets are used as observations. If observations existed in other rock types (SIDE1, ROCK1 and ROCK2) less correlation of parameters should be expected. Other than the relative high correlation between parameters there is no indication of an unsuccessful parameter estimation.

6.3.3. The Coupled FloWell-TOUGH2 Model

The coupled FloWell-TOUGH2 model handles both the coupling procedure and the calibration of the coupled model. As described in the modeling design in Fig. (5.2) the iteration process is started by coupling FloWell to TOUGH2. Calculated bottomhole pressures are inserted to the reservoir model along with guess values for the productivity index of the wells. For this study a guess value of $3.0 \cdot 10^{-12}$ m^3 is assigned to all the wells. The reservoir model is then calibrated using observed mass flow rates and enthalpies at the wellheads, yielding new estimates of the productivity indices in all wells for each month in 2011. The average of the productivity indices over the year 2011 is assumed to represent the actual productivity of each well. Along with the productivity indices, the permeability of ROCK5 in xy- and z-direction is calibrated. Only the permeability of the center of the reservoir is considered in order to minimize the number of unknowns since the total process is very computationally expensive.

The permeabilities calculated in the historical model are used as guess values for ROCK5 but are fixed for other rock types. The inverse estimation of the reservoir model produces new bottomhole pressures which can be used to calibrate the wellbore simulator. A parameter, shown in red in Eq. (6.1), in the Rouhani-Axelsson void fraction correlation is chosen for the inverse estimation with iTOUGH2-PEST. The results for the coupled FloWell-TOUGH2 model are presented in Tables (6.4)-(6.6).

Table 6.4: Results for the productivity indices for each well in the coupled FloWell-TOUGH2 model [10^{-12} m^3].

Wells	Iteration 1	Iteration 2	Iteration 3	Iteration 4	Iteration 5
RN-12	2.283	2.283	2.275	2.267	2.267
RN-15	0.303	0.302	0.301	0.300	0.300
RN-18	1.275	1.275	1.275	1.275	1.275
RN-19	0.523	0.524	0.524	0.524	0.524
RN-21	1.342	1.342	1.342	1.342	1.342
RN-24	1.117	1.108	1.100	1.100	1.100

Table 6.5: Results for the void fraction for each well in the coupled FloWell-TOUGH2 model.

Wells	Iteration 1	Iteration 2	Iteration 3	Iteration 4	Iteration 5
RN-12	0.120	0.120	0.119	0.119	0.119
RN-15	0.119	0.117	0.115	0.114	0.114
RN-18	0.118	0.117	0.118	0.118	0.118
RN-19	0.121	0.121	0.122	0.122	0.122
RN-21	0.121	0.121	0.121	0.121	0.121
RN-24	0.118	0.114	0.111	0.111	0.111

Table 6.6: Results for the permeability of ROCK5 in the coupled FloWell-TOUGH2 model [mD].

	Permeability in xy-direction for ROCK5	Permeability in z-direction for ROCK5
Iteration 1	97.41	114.30
Iteration 2	97.93	113.77
Iteration 3	98.47	113.25
Iteration 4	97.65	113.77
Iteration 5	97.55	114.30
Iteration 6	97.60	114.56
Iteration 7	97.60	114.30
Iteration 8	97.57	114.30

It takes approximately five iterations for the average of the productivity indices in the reservoir model and the void fraction in the wellbore model to reach equilibrium. The iteration process yields productivity indices in the range of 0.300-2.267·10^{-12} m^3 for wells in consideration and an estimation of 0.111-0.122 for the parameter in the Rouhani-Axelsson void fraction correlation. For the permeability it takes around eight iterations to reach steady state. Minor changes are observed for the permeability of ROCK5, especially for the permeability in xy-direction. This is not unexpected since the simulation time only spans one year. It is also not unusual for a model parameter to fluctuate between values around the best estimate when optimizing several parameters in an iteration procedure.

When examining the productivity index between months in 2011 for wells RN-12, RN-15, RN-18, RN-19, RN-21 and RN-24 no great changes were encountered. However, if well RN-11 is taken into consideration considerable changes between months were detected. This could indicate some management difficulties in well RN-11, the well could for example be damaged or blocked by scaling, which would need further inspection.

6.3.4. The Forecasting Model

The following discussion is devoted to the results obtained in the four scenarios presented in section 6.2.5. Predictions of pressure drawdown in the center of the Reykjanes reservoir (well RN-12) and at the boundaries (well RN-16) are illustrated in Fig. (6.10) and (6.11). Scenarios are distinguished by colors where dotted lines represent cases with increased injection. In scenario 1 the total extracted mass and injection are kept constant at values observed in 2011. The figures show that in scenario 1 the pressure drawdown decelerates and the pressure in the reservoir is close to achieving equilibrium with just a total of 3-4 bar decline in pressure for the prediction period. By increasing the injection, the pressure in the reservoir starts to rise again as displayed for scenario 2. In scenario 3 the power generation is boosted up to 150 MW_e, with almost no injection taking place. Approaching five years of simulation a decline of 18 bar in the reservoir and 12 bar at the boundaries is observed. After five years of simulation a convergence failure is encountered in TOUGH2. This failure could indicate that the absolute pressure is dropping down to zero in one or more elements. If that happens the water recharge into the elements becomes insufficient and consequently it will be attempted to remove mass at a higher rate than physically possible. When adding considerably to the injection in scenario 3 less decline is detected and after 15 years of simulation the total drawdown in pressure is equal to the total drawdown after 5 years in scenario 3. As expected, the changes in production and injection influence the center of the reservoir more than the boundaries since most of the production occurs at the center.

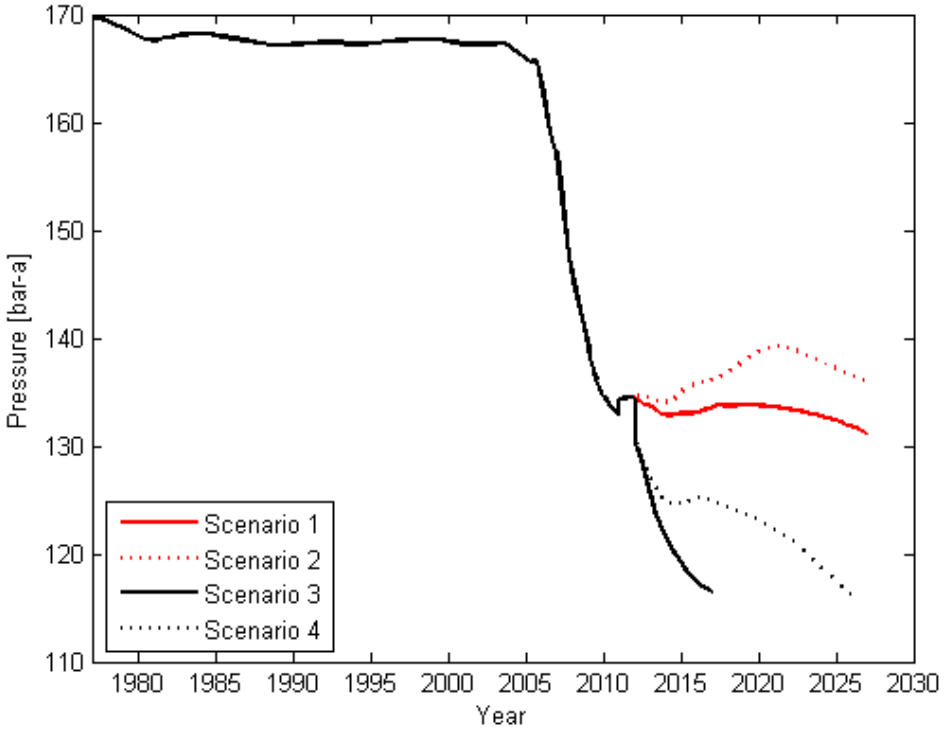

Figure 6.10: Pressure drawdown in well RN-12 in the forecasting scenarios.

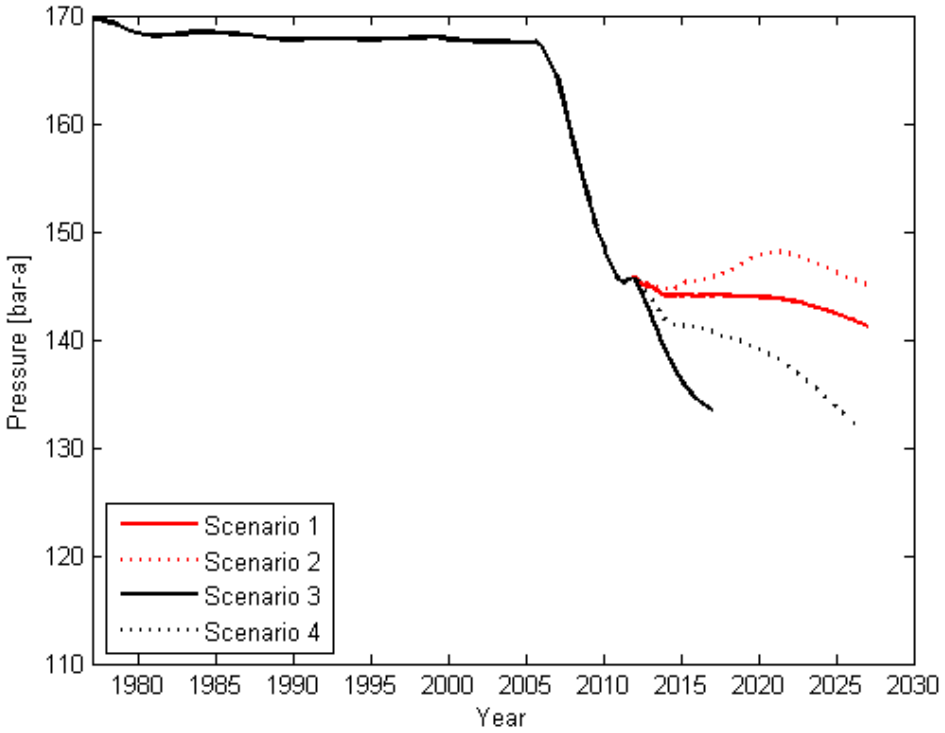

Figure 6.11: Pressure drawdown in well RN-16 in the forecasting scenarios.

Fig. (6.12) shows the development of the average enthalpy for the years 1977 to 2027. From the figure it can be concluded that the greater the production is from the reservoir, the greater the average enthalpy of the geothermal fluid becomes. Increasing the production causes the pressure to drop to a greater extent. As the pressure drops, boiling starts in shallow feedzones in the wellbores and the enthalpy increases. However, the injection in scenarios 2 and 4 supports the pressure in the reservoir and hinders boiling to occur, which yields lower enthalpy. Wells with shallow feedzones are more likely to display greater changes in enthalpy than wells with deeper feedzones. This phenomena is illustrated in Fig. (6.13) where great changes in enthalpy are encountered in well RN-23, which has feedzones located at 700-1100 m depth, while very little changes are observed in well RN-12, which main feedzone is at approximately 2000 m depth.

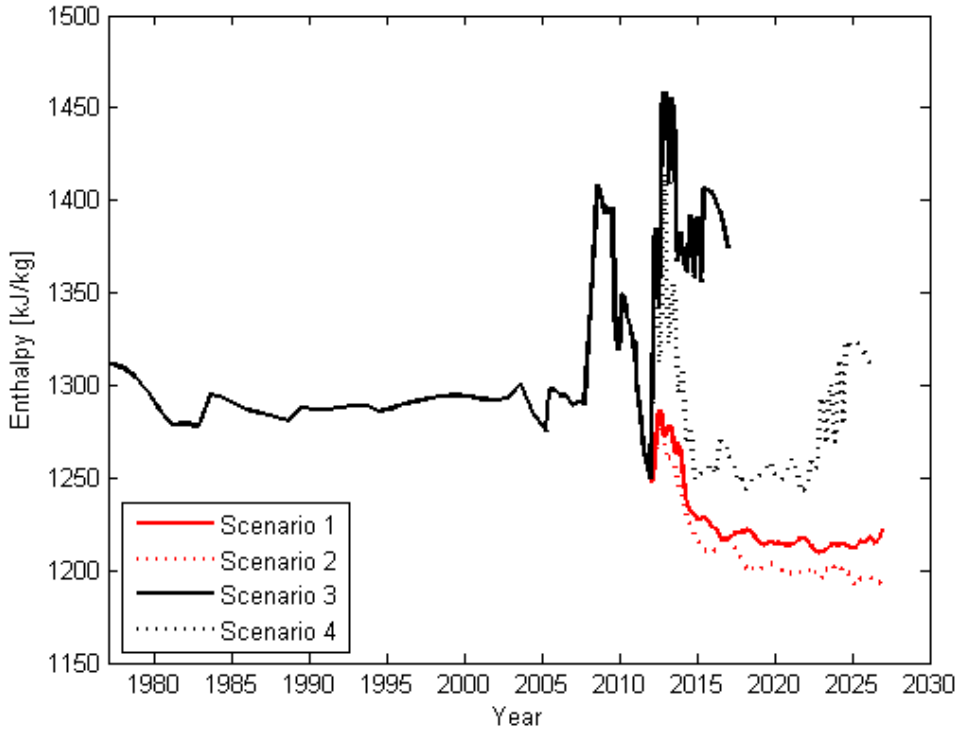

Figure 6.12: The average enthalpy development in wells in Reykjanes in the forecasting scenarios.

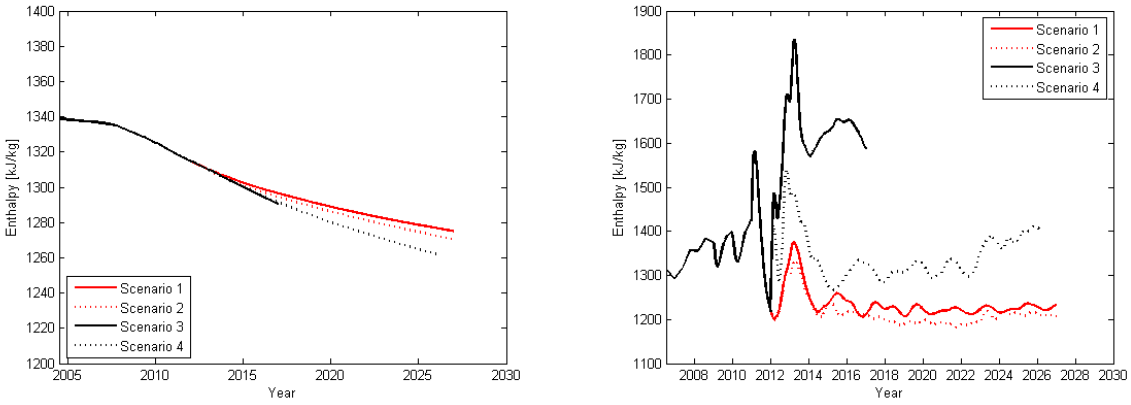

Figure 6.13: Enthalpy development in wells RN-12 (left) and RN-23 (right) in the forecasting scenarios.

From the results, the importance of injection into geothermal fields becomes apparent. The injection preserves the pressure in the reservoir, but because of less boiling at shallow depths lower average enthalpy is observed. Although lower enthalpy yields less steam for power production, the pressure support from the injection is considered more important because it keeps existing wells in production.

As noted above, scenario 3 causes convergence failure in TOUGH2. This shows the importance of physically meaningful boundary conditions and that specifying a constant production rate can be debated because in a real well desired production rate cannot be specified. The production rate depends on the geothermal fluid and physical properties of the reservoir, as well as the geometry and conditions of the production well. Defining wells as MASS types and increasing the production rates of the wells displays that the recharge to the reservoir cannot keep up with the rate of extraction. This also indicates that existing wells at Reykjanes may not support increased production from the reservoir and new wells covering larger area must be drilled. It should be mentioned that calculations of production rates needed for power generation of 150 MW_e are based on the state of the geothermal fluid observed in 2011. The calculated production rates are then fixed throughout the prediction period. However, increased production causes the pressure to drop and boiling to start in the reservoir, yielding geothermal fluids with higher enthalpy. More steam can be obtained from fluids with higher enthalpy than the ones with lower enthalpy so the total mass of geothermal fluid needed for power production diminishes. Therefore, the pressure drop due to increased production will eventually result in less mass extraction from the reservoir. From this discussion it can be assumed that scenarios 3 and 4 display the worst-case scenario of the production from the reservoir is increased and that this increased production may even sustain greater power generation than 150 MW_e.

7. Conclusions

The focus of this work was to develop a model that can simulate the flow in a geothermal reservoir as well as the flow in a production well in a coupled manner using measured wellhead conditions as main inputs. The coupling procedure can be implemented in various ways, but since the idea was to use measured wellhead conditions a specific model design was suggested. The program TOUGH2 was used to simulate the behavior of a reservoir while a new model was designed to simulate two phase flow in a wellbore.

The wellbore simulator FloWell created for this study is a single feedzone and one dimensional simulator that utilizes bottomhole or wellhead pressures, mass flow rates and well enthalpies to solve general equations for conservation of mass, momentum and energy. The validation of FloWell displayed that in most wells the simulations were in good agreement with pressure logs from wells at Reykjanes and Svartsengi geothermal fields. Furthermore, a comparison was made between available void fraction correlations in FloWell, resulting in the Rouhani-Axelsson correlation fitting the data best in most cases while the Zivi correlation produced the worst fit. Despite these results it is difficult to favor one correlation over the others, to reach conclusive results more extensive data must be obtained and tested with FloWell.

A detailed numerical model of the Reykjanes geothermal field in Iceland including the coupled wellbore-reservoir model was constructed. The formation temperature and pressure data available for the natural state of the Reykjanes reservoir, as well as exploitation and pressure drawdown history ranging from 1977 to 2010, served as groundwork in the creation of the numerical model. An acceptable pressure distribution was obtained in all wells and a reasonable match for the temperature distribution in wells located at the center of the reservoir. However, for wells at the boundaries of the reservoir achieving proper temperature distribution proved to be a greater challenge. The exploitation and pressure drawdown history of the Reykjanes reservoir was used to find new estimates for the permeability in xy-direction and z-direction in the rock types SIDE1 and ROCK1-5. The new estimates yielded an excellent fit to the pressure data, but since the rock structure of Reykjanes was only roughly divided into sections it cannot be stated that these estimates reflect the actual permeability distribution.

Measured wellhead conditions for each month of the year 2011 were used to couple the numerical model to FloWell. The coupling procedure was carried out in an iterative manner where the model design in FloWell and in the numerical model was improved by calibration with iTOUGH2. The parameters improved were the productivity indices of the wells, a variable in the Rouhani-Axelsson void fraction correlation and the permeability in the center of the reservoir. After five iterations the coupling procedure resulted in new estimates for the productivity indices and for the variable in the Rouhani-Axelsson correlation in all wells. Since the coupling procedure covered only one year little change was observed in the permeability in the center of the reservoir.

The calibrated numerical model was used in forecasting scenarios to predict the reservoir's response to future exploitation. Four scenarios were considered where the production rates of the wells were either kept constant as observed in 2011 or increased to maintain a 150 MW_e power production, with an increase in injection or not. The results showed that with the same production and injection rates as in 2011 the drawdown in pressure decelerated but by adding to the injection rate the pressure in the reservoir was recovered to some extent. Increasing the power production but keeping the injection rate as in 2011 caused a convergence failure in TOUGH2, indicating that existing wells at Reykjanes could not support the boost in production from the reservoir. It should be mentioned that this could also hint that the production should be distributed onto more elements in the reservoir model. Increasing the injection as well as the production capacity resulted in a steady drawdown in pressure but the decline was not as steep as observed in 2006-2009. As the pressure dropped in the reservoir the average enthalpy of the geothermal fluid in the reservoir increased, but lower enthalpies were encountered when the injection was increased. With higher enthalpies more steam can be produced from the geothermal fluid. Seeing as the production rates were fixed throughout the simulations in the scenarios it can be assumed that they can sustain even greater power generation than 150 MW_e. Although fluids with higher enthalpies are considered more desirable, the injection into the reservoir is thought to be more valuable since it helps maintain the pressure in the reservoir.

In the future, several improvements could be made to the wellbore simulator FloWell, the coupled FloWell-TOUGH2 model and the numerical model of Reykjanes. The option of multiple feedzones in a well as well as diverse changes of a wellbore geometry could be incorporated into FloWell. Moreover, adding options for the void fraction and friction correction factor correlations would allow the simulator to become more user-friendly. Problems due to scaling could be considered when simulating the flow in wells, especially in wells in Reykjanes. The geothermal fluid in the area is very rich in salinity and along with the high temperatures found in the reservoir the magnitude of dissolved solids increases, contributing heavily to scaling. For the coupled FloWell-TOUGH2 model and the numerical model of Reykjanes it would be advisable to increase the simulation time when more measured wellhead

data becomes available. It would also be interesting to include all producing wells in Reykjanes in the coupling procedure and to use more than one void fraction correlation. Lastly, the modeling approach introduced in this study should be applied to other geothermal systems with as accurate data as possible to improve its performance and hopefully extend its application field.

Geothermal modeling has become a standard practice in resource management. It helps develop a greater understanding of geothermal systems and predict the response of reservoirs to exploitation. A coupled wellbore-reservoir simulator allows for more accurate modeling of geothermal systems which results in more credible predictions of responses to production. Today, large amount of data can be obtained from the wellheads and with this data accessible an opportunity arises to improve reliability in geothermal modeling. The coupling procedure suggested in this study, with measured wellhead conditions as main inputs, has proven to yield reasonable results for the Reykjanes geothermal field. Therefore, after further validation, the simulator might become a useful tool in future assessments of geothermal resources, both in Iceland and worldwide.

Bibliography

[1] Álavarez del Castillo, A. Santoyo, E. and García-Valladares, O. (2011), A new void fraction correlation inferred from artificial neural networks for modeling two-phase flows in geothermal wells. *Computers and Geosciences*, 41:25-39.

[2] Arnaldsson, A. and Myer, E.M. (2011). *Svartsengi-Reykjanes. Vinnslueftirlit fyrir árið 2010*. Vatnaskil Consulting Engineers, Reykjavík, Iceland.

[3] Arnarson, K., Karlsdóttir, R., Eysteinsson, H., Flovenz, Ó.G and Guðlaugsson S.Þ. (2008). *The Resistivity Structure of High-Temperature Geothermal Systems in Iceland*. Geothermal Training Programme, Orkustofnun, Reykjavík, Iceland.

[4] Arnórsson, S. (1995). Geothermal Systems in Iceland: Structure and Conceptual models - I. *Geothermics*, 24:561-602.

[5] Aunzo Z.P., Bjornsson G. and Bodvarsson, G.S. (1991). *Wellbore Models GWELL, GWNACL, and HOLA User's Guide*. Berkeley, University of California, USA.

[6] Awada, M.M and Muzychkab, Y.S. (2004). A Simple Asymtotic Compact Model for Two-Phase Frictional Pressure. In *Proceedings of IMECE*, Anaheim, California, USA.

[7] Axelsson, G. (2008). Production capacity of geothermal systems. In *Proceedings of the Workshop for Decision Makers on Direct Heating Use of Geothermal Resources in Asia*, Tianjin, China.

[8] Axelsson, G. (2003). Sustainable Management of Geothermal Resources. In *Proceedings of the International Geothermal Conference*, Reykjavík, Iceland.

[9] Barelli A., Corsi R., Del Pizzo, G. and Scaii C. (1982). A Two-Phase Flow Model for Geothermal Wells in the Presence of Non-Condensible Gas. *Geothermics*, 11(3):175-191.

[10] Battistelli, A., Rivera-R., J. and Ferragina, C. (1992). The Modelling of Flow in Geothermal Wells Applied to the Reservoir Engineering Study of the Asal Field Republic of Djibouti. In *Proceedings of the 13th Annual PNO-EDC Geothermal Conference*, Quezon City, Metro Manila, Philippines.

[11] Beattie, D.R.H. (1973). A note on the calculation of two-phase pressure losses. *Nuclear Engineering and Design*, 25:395-402.

[12] Bhat, A., Swenson, D. and Gosavi, S. (2005). Coupling the HOLA Wellbore Simulator with TOUGH2. In *Proceedings of the 30th Workshop on Geothermal Reservoir Engineering Stanford University*, Stanford, California, USA.

[13] Bilicki, Z., Kestin, J. and Michaelides, E.E. (1981). *Flow in Geothermal Wells: Part III Calculation Model for Self-Flowing Well.* Brown University, Report GEOFLO/5, DOE/ET/27225-8, Rhode Island, USA.

[14] Björnsson, G. (1987). *A Multi-Feedzone Geothermal Wellbore Simulator.* Berkeley, University of California, USA.

[15] Björnsson, G., Ólafsson, M., Jónasson, H. and Magnússon, Þ.M. (2004). *Vinnslurannsóknir á holum RN-9, RN-10, RN-11 og RN-12 á Reyjanesi árin 2002-2004.* ÍSOR, Reykjavík, Iceland.

[16] Björnsson, H., Friðriksson, Þ., Jónsson, P., Þorgilsson, G., Þórhallsson, S. and Tryggvason, H. (2008). *Upphleyping holu SV-22 og mælingar í blæstri í mars 2008.* ÍSOR, Reykjavík, Iceland.

[17] Blöcher G., Kranz S., Zimmermann G., Frick S., Hassanzadegan A., Moeck I., Brandt W., Saadat A. and Huenges E. (2010). Conceptual Model for Coupling Geothermal Power Plants with Deep Reservoirs. In *Proceedings of the World Geothermal Congress 2010*, Bali, Indonesia.

[18] Böðvarsson, G.S. (1982). *Mathematical modeling of the behavior of geothermal systems under exploitation.* Berkeley, University of California, Report LBL-13937, USA.

[19] Carella, R. (2001). The future of European geothermal energy: EGEC and the Ferrara Declaration. *Renewable Energy*, 24(3):397-399.

[20] Chisholm, D. (1973). Pressure gradients due to friction during the flow of evaporating two-phase mixtures in smooth tubes and channels. *International Journal of Heat and Mass Transfer*, 16:347–358.

[21] Clifton, A.E. and Schlische, R.W. (2003). Fracture Populations on the Reykjanes Peninsula, Iceland: Comparison with Experimental Clay Models of Oblique Rifting. *Journal of Geophysical Research*, 108(B2).

[22] Crowe, C.T., Elger D.F., Williams, B.C. and Robersson, J.A. (2010). *Engineering Fluid Mechanics.* John Wiley & Sons, Inc., New Jersey, USA.

[23] Danielsen, P.E., Giroud, N. and Júlíusson, E. (2007). *Upphleyping holu SV-21 í febrúar 2007 og mat á afköstum.* ÍSOR, Reykjavík, Iceland.

[24] Diersch, H.J.G. (2009). *DHI-Wasy Software FEFLOW. Finite Element Subsurface Flow & Transport Simulation System. Reference Manual.* Berlin, Germany.

[25] Dipippo, R. (2008). *Geothermal Power Plants. Principles, Applications, Case Studies and Environmental Impact.* Second Edition. Elsevier.

[26] Duns, Jr., H and Ros, N.C.J. (1963). Vertical flow of gas and liquid mixtures in wells. In *Proceedings of the 6th World Petroleum Gongress*, Frankfurt am Main, Germany.

[27] Finsterle, S. (2007). *iTOUGH2 Users's Guide.* Berkeley, University of California, USA.

[28] Finsterle, S. (2010). *iTOUGH2 Universal Optimization Using the PEST Protocol.* Berkeley, University of California, USA.

[29] Freeston, D.H. and Gunn, C. (1993). Wellbore Simulation - Case Studies. In *Proceedings of the 18th Workshop on Geothermal Reservoir Engineering Stanford University*, Stanford, California, USA.

[30] Freeston, D.H. and Hagdu, T. (1988). Comparison of Results from some Wellbore Simulators using a Data Bank. In *Proceedings of the 10th New Zealand Geothermal Workshop*, Auckland, New Zealand.

[31] Friðleifsson, G. Ó, Sigurðsson, Ó., Albertsson, A. Þórólfsson, G. and Blöndal, Á. (2009). *Sjálfbærni jarðhitans á Reykjanesi.* HS Orka, Reykjanesbær, Iceland.

[32] Gabolde G. and Nguyen J.P. (2006). *Drilling Data Handbook.* Eight edition. Éditions Technip, Paris, France.

[33] García-Valladares, O., Sánchez-Utpon, P. and Santoyo, E. (2006). Numerical modeling of flow processes inside geothermal wells: An approach for predicting production characteristics with uncertainties. *Energy Conversion and Management*, 47:1621-1643.

[34] Google Maps. (2012). Retrieved June 10th 2012 from https://maps.google.com /maps?q=iceland&hl=en&sll=37.0625,-95.677068&sspn=38.41771,86.57226 6&t=h&hnear=Iceland&z=6.

[35] Gould, T.L. (1974). Vertical Two-Phase Steam-Water Flow in Geothermal Wells. *Journal of Petroleum Technology*, 26:833-842.

[36] Goyal K.P., C.W. Miller and M.J. Lippmann. (1980). Effect of Wellhead Parameters and Well Scaling on the Computed Downhole Conditions in Cerro Prieto Wells. In *Proceedings of the 6th Workshop on Geothermal Reservoir Engineering Stanford University*, Stanford, California, USA.

[37] Graham, D.M, Newell, T.A. and Chato, J.C. (1997). *Experimental Investigation of Void Fraction During Refrigerant Condensation*. University of Illinois at Urbana-Champaign, USA.

[38] Grant, M.A and Bixley P.F. (2011). *Geothermal Reservoir Engineering*. Second edition. Elsevier.

[39] Gunn C. and Freeston D. (1991). An Intergrated Steady-State Wellbore Simulation and Analysis Package. In *Proceedings of 13th New Zealand Geothermal Workshop*, Auckland, New Zealand.

[40] Guo B., Lyons W.C and Ghalambor A. (2007). *Petroleum Production Engineering. A Computer-Assisted Approach*. Elsevier Science & Technology Books, Oxford, UK.

[41] Hagdu T., Zimmerman R. and Bodvarsson G. (1995). Coupled Reservoir-Wellbore Simulation of Geothermal Reservoir Behavior. *Geothermics*, 24(2):145-166.

[42] Hagedorn, A.R. and Brown, K.E. (1965). Experimental study of pressure gradients occuring during continuous two-phase flow in small-diameter vertical conduits. *Journal Petroleum Technology*, 17(4): 475-484.

[43] Halldórsdóttir, S., Eyjólfsdóttir, E.I., Jónsson, P. and Friðriksson, Þ. (2009). *Upphleyping holu RN-28, þrepapróf og mælingar í blæstri í október 2008*. ÍSOR, Reykjavík, Iceland.

[44] Hanano, M., Seth, M.S., 1995. Numerical modeling of hydrothermal convection systems including super-critical fluid. In *Proceedings of the World Geothermal Congress*, Florence, Italy.

[45] Hasan, A.R. and Kabir, C.S. (2010). Modeling two phase fluid and heat flows in geothermal wells. *Journal of Petroleum Science and Engineering*, 71:77–86.

[46] Hjartarson, A., Danielsen P.E. and Friðriksson, Þ. (2006). *Upphleyping holu RN-21 og mælingar í blæstri í mars 2006*. ÍSOR, Reykjavík, Iceland.

[47] Hjartarson, A. and Friðriksson, Þ. (2006a). *Upphleyping holu RN-22 og mælingar í blæstri í apríl 2006*. ÍSOR, Reykjavík, Iceland.

[48] Hjartarson, A. and Friðriksson, Þ. (2006b). *Upphleyping holu RN-24 og mælingar í blæstri í mars 2006*. ÍSOR, Reykjavík, Iceland.

[49] Hjartarson, A., Friðriksson, Þ., Bjarnason J.Ö. and Þórarinsdóttir, S. A. (2006). *Upphleyping holu RN-23 og mælingar í blæstri í maí 2006*. ÍSOR, Reykjavík, Iceland.

[50] Hjartarson, A. and Júlíusson, E. (2007). *Reiknilíkan af jarðhitakerfinu á Reykjanesi og spár um viðbrögð þess við 100 MW rafmagnsframleiðslu.* ÍSOR, Reykjavík, Iceland.

[51] HS Orka. (2011). *Financial Statements 2011.* HS Orka, Reykjanesbær, Iceland.

[52] HS Orka. (2009). *Stækkun Reykjanesvirkjunar og frekari nýting jarðhitavökva.* VSO Consulting, Reykjavík, Iceland.

[53] Hu, B. (1995). Reservoir simulation of the Yangbajian geothermal field in Tibet, China. In *Proceedings of the World Geothermal Congress*, Florence, Italy.

[54] IAPWS. (1994). *IAPWS Release on Surface Tension of Ordinary Water Substance.* The International Association for the Properties of Water and Steam, Orlando, USA.

[55] IAPWS. (2007). *Revised Release on the Iapws Industrial Formulation 1997 for the Thermodynamic Properties of Water and Steam.* The International Association for the Properties of Water and Steam, Lucerne, Switzerland.

[56] IAPWS. (2008). *Release on the Iapws Formulation 2008 for the Viscosity of Ordinary Water Substance.* The International Association for the Properties of Water and Steam, Berlin, Germany.

[57] Ingebritsen, S.E. and Sorey, M.L. (1985). Quantitative analysis of the Lassen hydrothermal system, north-central California. *Water Resources Research*, 21(6), 853–868.

[58] INTERCOMP. (1981). *Vertical steam-water flow in wells with heat transfer - VSTEAM, User's manual.* INTERCOMP Resource Development and Engineering, Inc., Houston, Texas, USA.

[59] Jónsson, P. and Eyjólfsdóttir, E.I. (2008). *Upphleyping holu RN-27 og mælingar í blæstri í júlí 2008.* ÍSOR, Reykjavík, Iceland.

[60] Jónsson, P. and Eyjólfsdóttir, E.I. (2009). *Upphleyping holu SV-23 og mælingar í blæstri í nóvember 2008.* ÍSOR, Reykjavík, Iceland.

[61] Jónsson, P. and Friðriksson, Þ. (2008). *Upphleyping holu RN-13B og mælingar í blæstri í oktober 2007.* ÍSOR, Reykjavík, Iceland.

[62] Kuster. (2012). *K10 PT Geothermal Instrument Operation & Service Manual.* Retrieved June 16th 2012 from http://www.kusterco.com/pdfs/K10 _Geothermal_Manual.pdf.

[63] Lockhart, R. W., and Martinelli, R. C. (1949). Proposed Correlation of Data for Isothermal Two-Phase, Two-Component Flow in Pipes. *Chemical Engineering Progress Symposium Series*, 45(1):39-48.

[64] Martinelli, R. C., and Nelson, D. B. (1948). Prediction of Pressure Drop during Forced-Circulation Boiling of Water. *Transactions of the ASHE*, 70(6):695-702.

[65] Miller, C.W. (1980). *Welbore User's Manual*. Berkeley, University of California, Report, no. LBL-10910, USA.

[66] Mitchell, R. F. (1982). *Advanced wellbore thermal simulator - GEOTEMP2*. Reaserch report SAND82-7003/1, Sandia National Labatories, Albuquerque, New Mexico, USA.

[67] Murray, L. and Gunn, C. (1993). Toward Integrating Geothermal Reservoir and Wellbore Simulation: TETRAD and WELLSIM. In *Proceedings of the 15th New Zealand Geothermal Workshop*, Auckland, New Zealand.

[68] Nakanishi, S., Kawano, Y., Todaka, N., Akasaka, C., Yoshida, M., Iwai, N. (1995). A reservoir simulation of the Oguni geothermal field, Japan, using MINC type fracture model. In *Proceedings of the World Geothermal Congress*, Florence, Italy.

[69] Ngaruye, J.C. (2009). *Geological and Geothermal Mapping of the Slagaarnarvatn Area, Reykjanes Peninsula, SW-Iceland*. Geothermal Training Programme, Orkustofnun, Reykjavík, Iceland.

[70] O'Sullivan M.J., Pruess K. and Lippmann M.J. (2001). State of the art of geothermal reservoir simulation. *Geothermics*, 30:395–429.

[71] O'Sullivan, M.J., Yeh, A. and Mannington, W.I. (2009). A history of numercial modelling of the Wairakei geothermal field. *Geothermics*, 38:155-168.

[72] Orkiszewski, J. (1967). Predicting Two-Phase Pressure Drop in Vertical Pipe. *Journal Petroleum Technology*, 19:829-838.

[73] Ortiz-Ramirez, J. (1983). *Two-phase flow in geothermal wells: Development and uses of a computer code*. Stanford University, Stanford, California, USA.

[74] Pace, D.K. (2004). Modeling and Simulation Verification and Validation Challenges. *Johns Hopkins APL Technical Digest*, 25(2).

[75] Pálsson, H. (2011). *Simulation of two phase flow in a geothermal well*. Lecture notes in the course VÉL203F Geothermal Reservoirs at the University of Iceland.

[76] Parini, M., Cappetti, G., Laudiano, M., Bertani, R., Monterrosa, M. (1995). Reservoir modeling study of the Ahuachapan geothermal field (El Salvador) in the frame of a generation stabilization project. In *Proceedings of the World Geothermal Congress*, Florence, Italy.

[77] Poettmann F. H., and Carpenter P.G. (1952). Multiphase Flow of Gas, Oil and Water through Vertical Strings with Application to the Design of Gas Lift Installation. *API Drilling and Production Practice*, 257-317.

[78] Premoli, A., Francesco, D., Prima, A. (1970). An empirical correlation for evaluating two-phase mixture density under adiabatic conditions. *In European Two-Phase Flow Group Meeting*, Milan, Italy.

[79] Pritchett, J.W. (1995). STAR: A geothermal reservoir simulation system. In *Proceedings of the World Geothermal Congress*, Florence, Italy.

[80] Probe Holdings, Inc. (2012). *Kuster^{TM} K10 Geothermal PT (Memory)*. Retrieved June 16th 2012 from http://www.probe1.com/products /HPHTgeothermal/geothermaltools/k10geothermalptmemory_copy1_copy1.aspx.

[81] Pruess, K. , Oldenburg, C. and Moridis, G. (1999). *TOUGH2 User's Guide, Version 2.0*. Berkeley, University of California, USA.

[82] Pruess, K. (2002). *Mathematical modeling of fluid flow and heat transfer in geothermal systems - An introduction in five lectures*. Geothermal Training Programme, Orkustofnun, Reykjavík, Iceland.

[83] Rivera Ayala, M. A. (2010). *Coupled geothermal reservoir-wellbore simulation with case study for the Námafjall field, N-Iceland*. University of Iceland, Reykjavík, Iceland.

[84] Rouhani, S.Z. and Axelsson, E. (1970). Calculation of void volume fraction in the sub cooled and quality boiling regions. *International Journal of Heat and Mass Transfer*, 13:383–393.

[85] Sánchez-Utpon, P. (1995). The Wellbore Simulator SIMU93. In *Proceedings of the World Geothermal Congress*, Florence, Italy.

[86] Sánchez-Utpon, P. (2000). The Wellbore Simulator SIMU2000. In *Proceedings of the World Geothermal Congress*, Kyushu-Tohoku, Japan.

[87] Takahashi, M. (1988) A Wellbore Flow Model in the presence of CO2 Gas. In *Proceedings of the 13th Workshop on Geothermal Reservoir Engineering Stanford University*, Stanford, California, USA.

[88] Takács, G. (2005). *Gas Lift Manual*. PennWell Corporation, Tulsa, Oklahoma.

[89] The MathWorks. (2011). ode23, ode45, ode113, ode15s, ode23s, ode23t, ode23tb, The MathWoks^{TM}, Inc.

[90] Thome, J.R. (2010). *Engineering Data Book III*. Wolverine Tube Inc, Alabama, USA.

[91] Timlin, M. (2008). SuperWell - A simple well bore flow simulator in spreadsheet format. In *Proceedings of the 33rd Workshop on Geothermal Reservoir Engineering Stanford University*, Stanford, California, USA.

[92] Tokita, H. and Itoi, R. (2004). Development of the MULFEWS Multi-Feed Wellbore Simulator. In *Proceedings of the 29th Workshop on Geothermal Reservoir Engineering Stanford University*, Stanford, California, USA.

[93] Tokita, H., Lima, E. and Hashimoto, K. (2005). A Middle-Term Power Output Prediction at the Hatchobaru Field by Coupling Multifeed Wellbore Simulator and Fluid-Gathering Pipeline Simulator to Reservoir Simulator. In *Proceedings of the World Geothermal Congress*, Antalya, Turkey.

[94] Tripletta K.A., Ghiaasiaana S.M., Abdel-Khalika S.I., LeMouela A., and McCorda B.N. (1999). Gas–liquid two-phase flow in microchannels: Part II: void fraction and pressuredrop. *International Journal of Multiphase Flow Volume*, 25(3):395–410.

[95] Upadhyay, R.N., Ham, J.D., Tomokoria, B.N. and Gulati, M.S. (1977). Comparison of the Calculated and Observed Pressure Drops in Geothermal Wells Producing Steam-Water Mixtures. In *Proceedings of the 52nd SPE Annual Fall Technical Conference and Exhibition*, Denver, Colorado, USA.

[96] Vinsome, P.K.W., Shook, G.M. (1993). Multi-purpose simulation. *Journal of Petroleum Science and Engineering*, 9(1):29–38.

[97] Woldesemayat M.A. and Ghajar, A.J. (2006). Comparison of void fraction correlations for different flow patterns in horizontal and upward inclined pipes. *International Journal of Multiphase Flow*, 33:347-370.

[98] Zivi, S.M.. (1964). Estimation of steady state steam void fraction by means of the principle of minimum entropy production. *The ASME Journal Heat Transfer*, 86:247–252.

[99] Zuber, N. and Findlay, J. (1965). Average volumetric Concentration in Two-Phase Flow Systems. *Journal of Heat Transfer*, 87:453.

A. Visual Results from the Validation of FloWell

Well RN-11

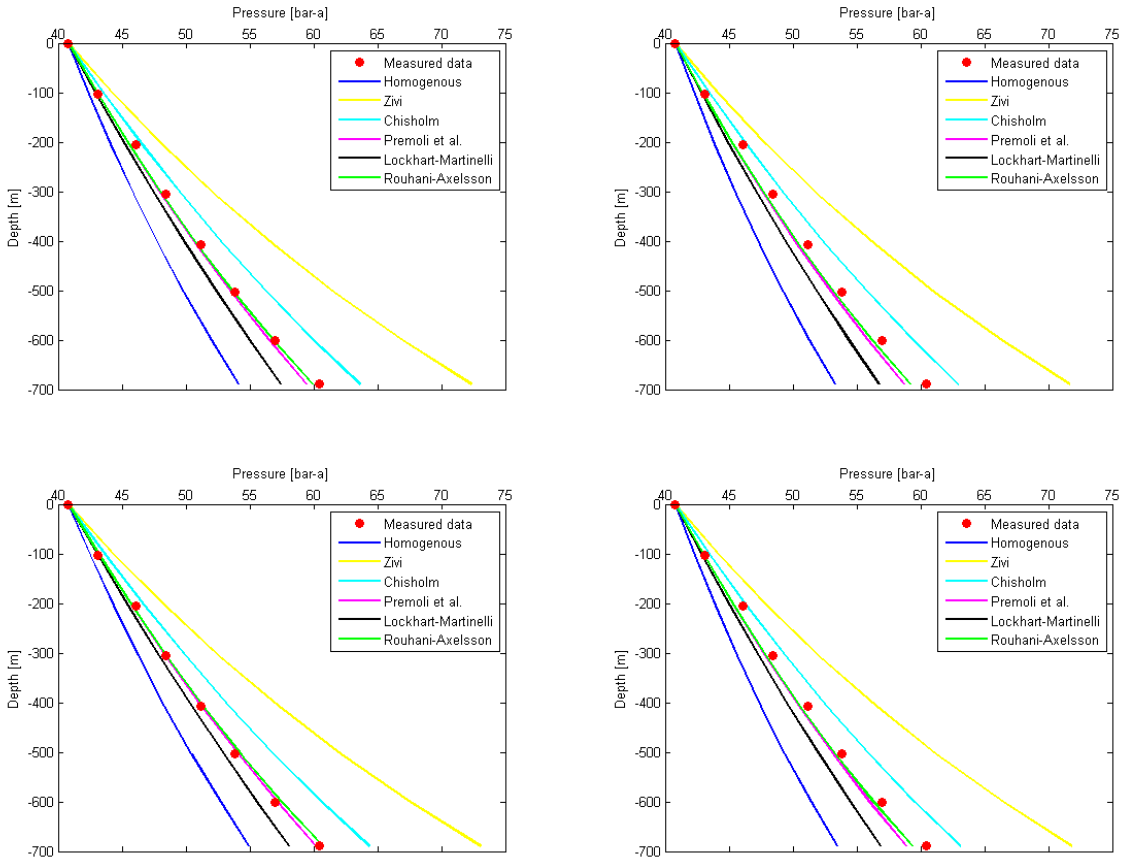

Figure A.1: Simulations for well RN-11 down to the bottom of the production casing; upper left corner: Blasius equation for friction factor and model by Friedel for friction correction factor, upper right corner: Blasius equation for friction factor and model by Beattie for friction correction factor, lower left corner: Swamee-Jain equation for friction factor and model by Friedel for friction correction factor, lower right corner: Swamee-Jain equation for friction factor and model by Beattie for friction correction factor.

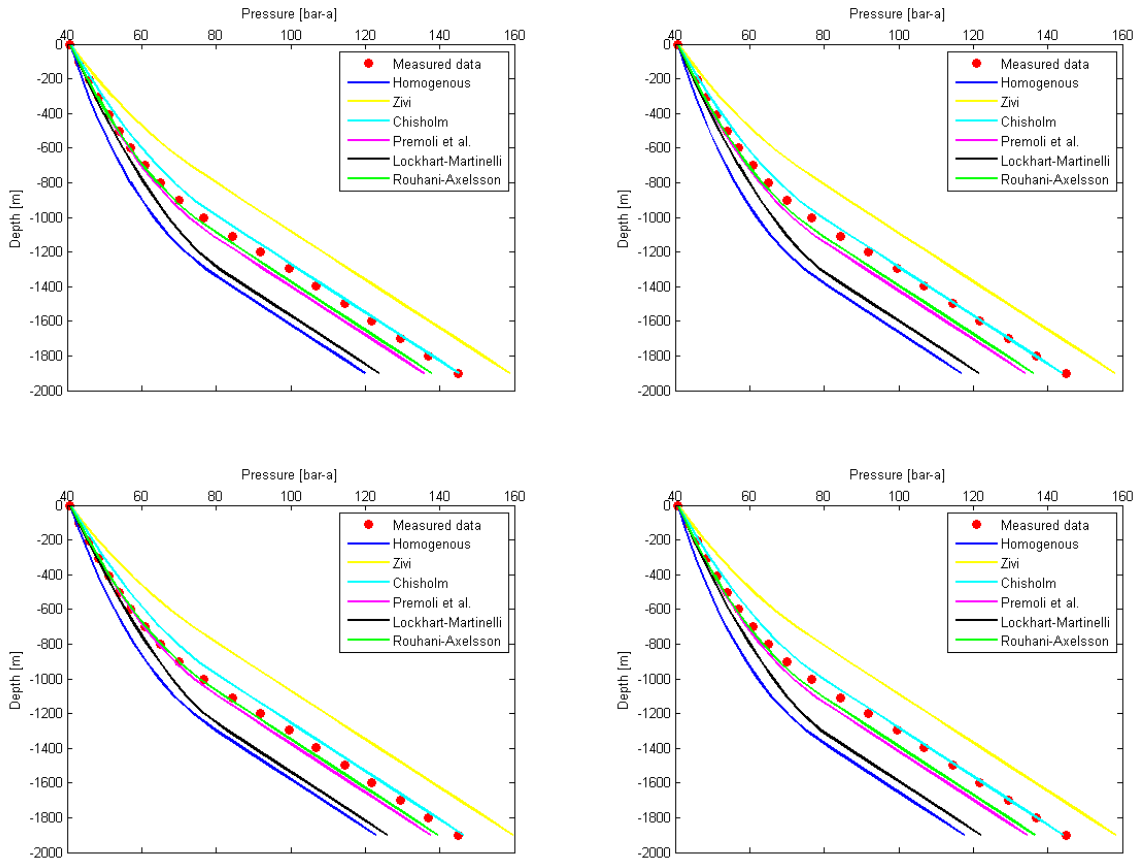

Figure A.2: Simulations for well RN-11 down to the bottom of the well; upper left corner: Blasius equation for friction factor and model by Friedel for friction correction factor, upper right corner: Blasius equation for friction factor and model by Beattie for friction correction factor, lower left corner: Swamee-Jain equation for friction factor and model by Friedel for friction correction factor, lower right corner: Swamee-Jain equation for friction factor and model by Beattie for friction correction factor.

Well RN-12

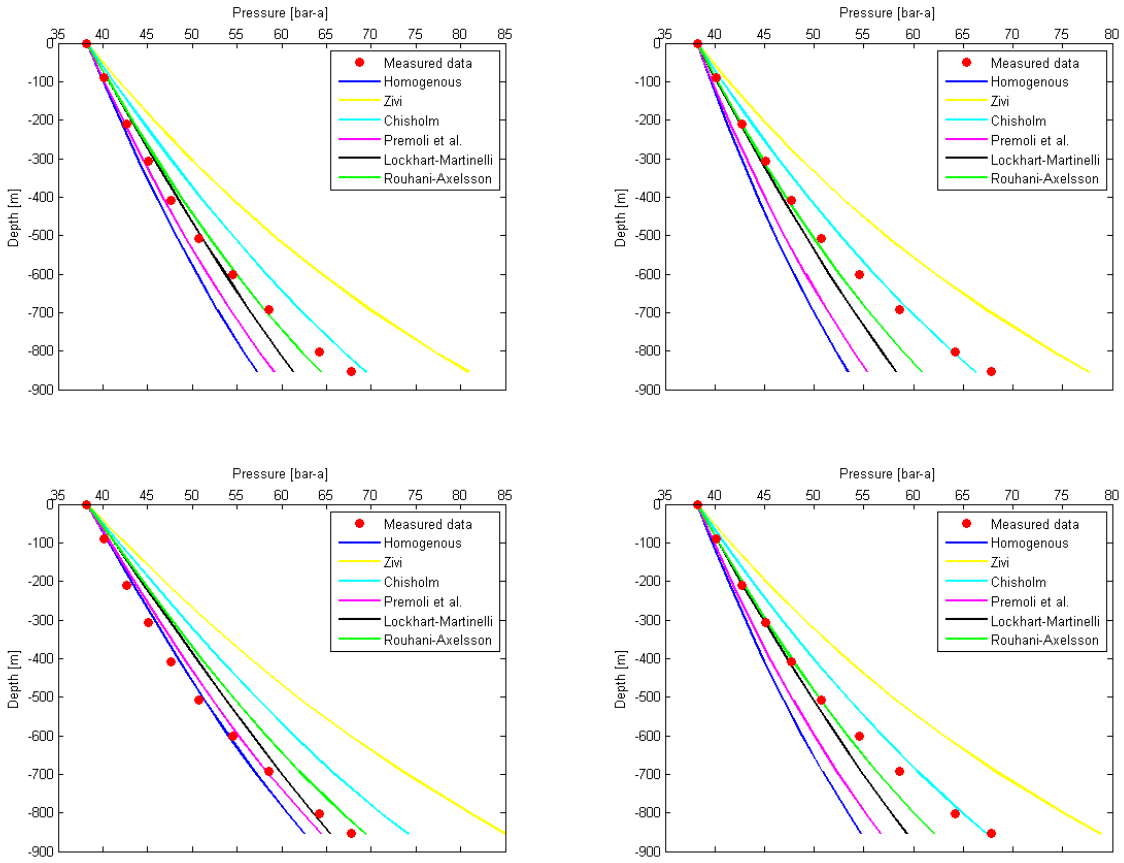

Figure A.3: Simulations for well RN-12 down to the bottom of the production casing; upper left corner: Blasius equation for friction factor and model by Friedel for friction correction factor, upper right corner: Blasius equation for friction factor and model by Beattie for friction correction factor, lower left corner: Swamee-Jain equation for friction factor and model by Friedel for friction correction factor, lower right corner: Swamee-Jain equation for friction factor and model by Beattie for friction correction factor.

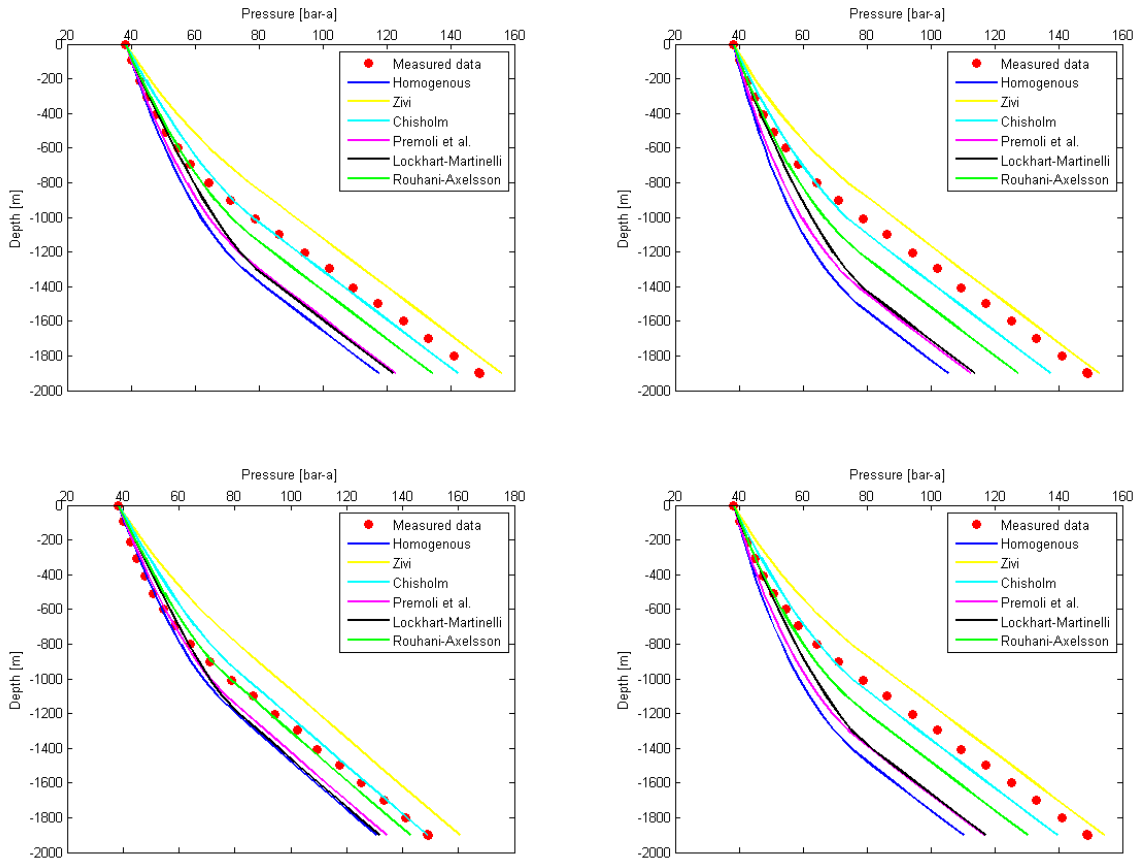

Figure A.4: Simulations for well RN-12 down to the bottom of the well; upper left corner: Blasius equation for friction factor and model by Friedel for friction correction factor, upper right corner: Blasius equation for friction factor and model by Beattie for friction correction factor, lower left corner: Swamee-Jain equation for friction factor and model by Friedel for friction correction factor, lower right corner: Swamee-Jain equation for friction factor and model by Beattie for friction correction factor.

Well RN-13B

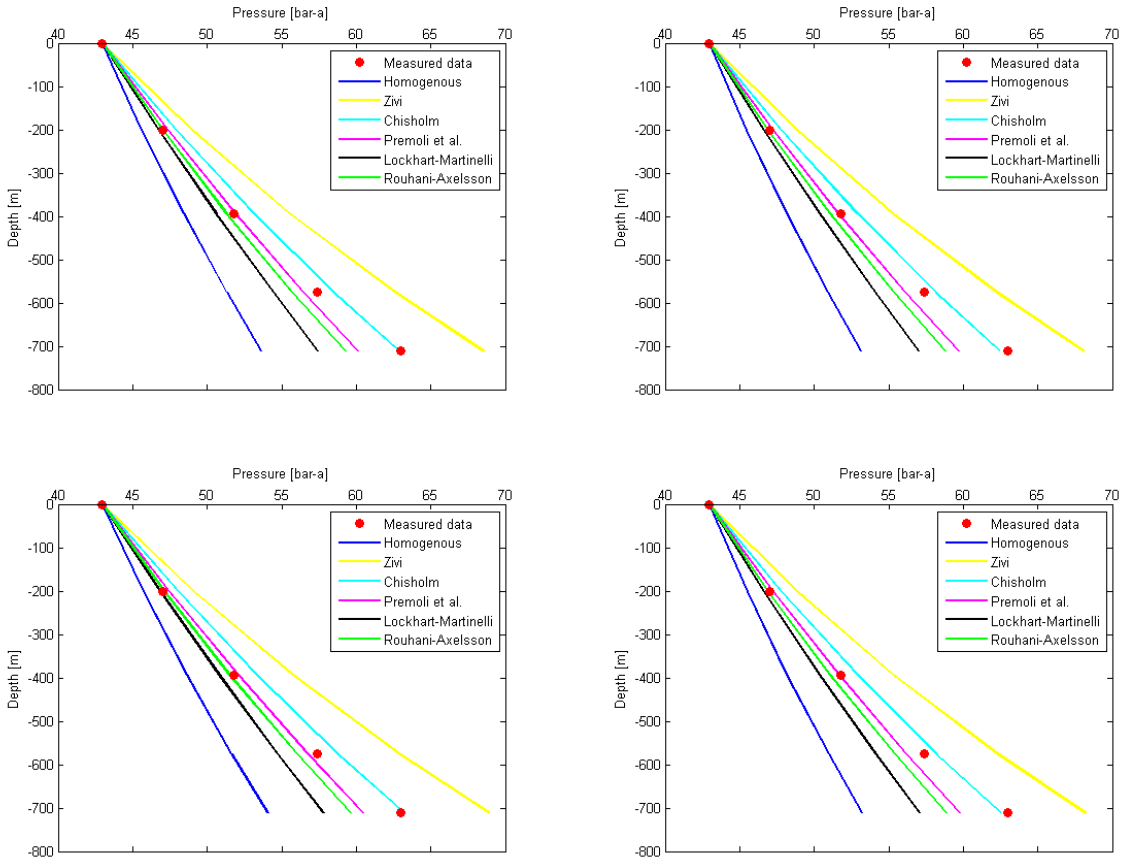

Figure A.5: Simulations for well RN-13B down to the bottom of the production casing along with corrected data; upper left corner: Blasius equation for friction factor and model by Friedel for friction correction factor, upper right corner: Blasius equation for friction factor and model by Beattie for friction correction factor, lower left corner: Swamee-Jain equation for friction factor and model by Friedel for friction correction factor, lower right corner: Swamee-Jain equation for friction factor and model by Beattie for friction correction factor.

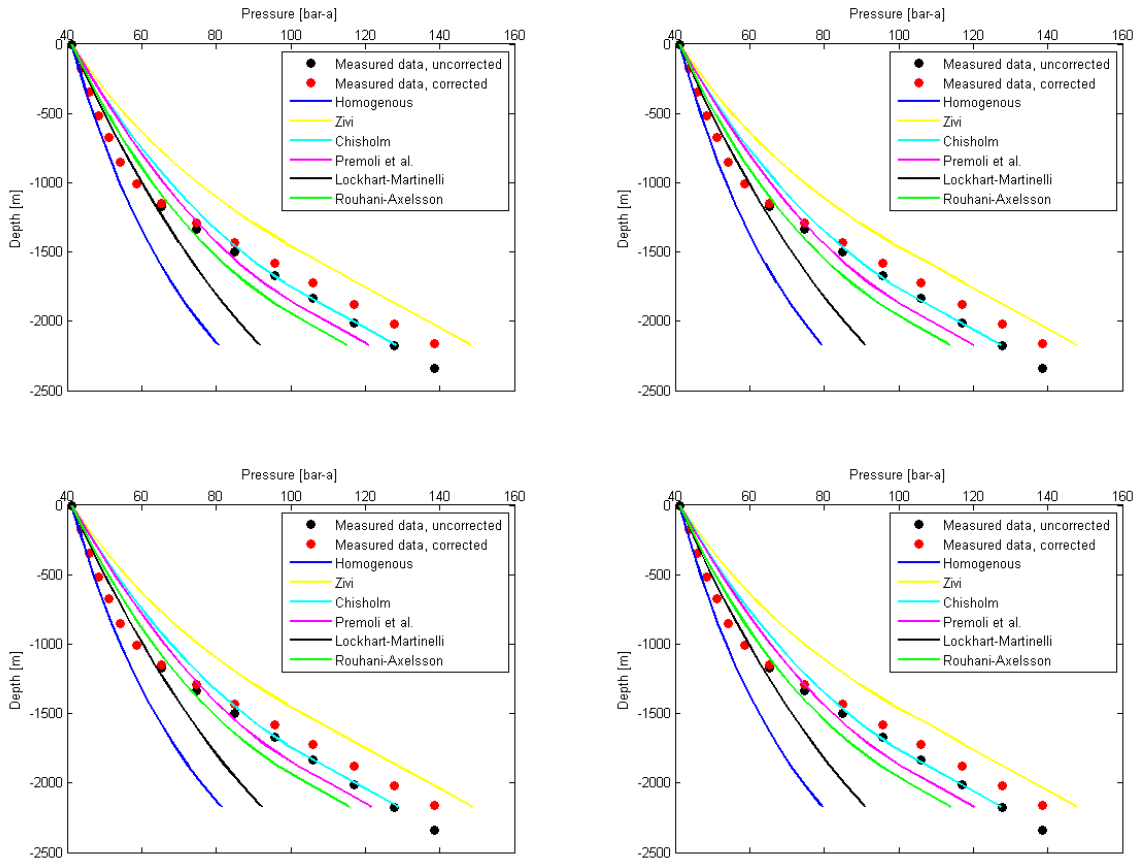

Figure A.6: Simulations for well RN-13B down to the bottom of the well, along with corrected data; upper left corner: Blasius equation for friction factor and model by Friedel for friction correction factor, upper right corner: Blasius equation for friction factor and model by Beattie for friction correction factor, lower left corner: Swamee-Jain equation for friction factor and model by Friedel for friction correction factor, lower right corner: Swamee-Jain equation for friction factor and model by Beattie for friction correction factor.

Well RN-21

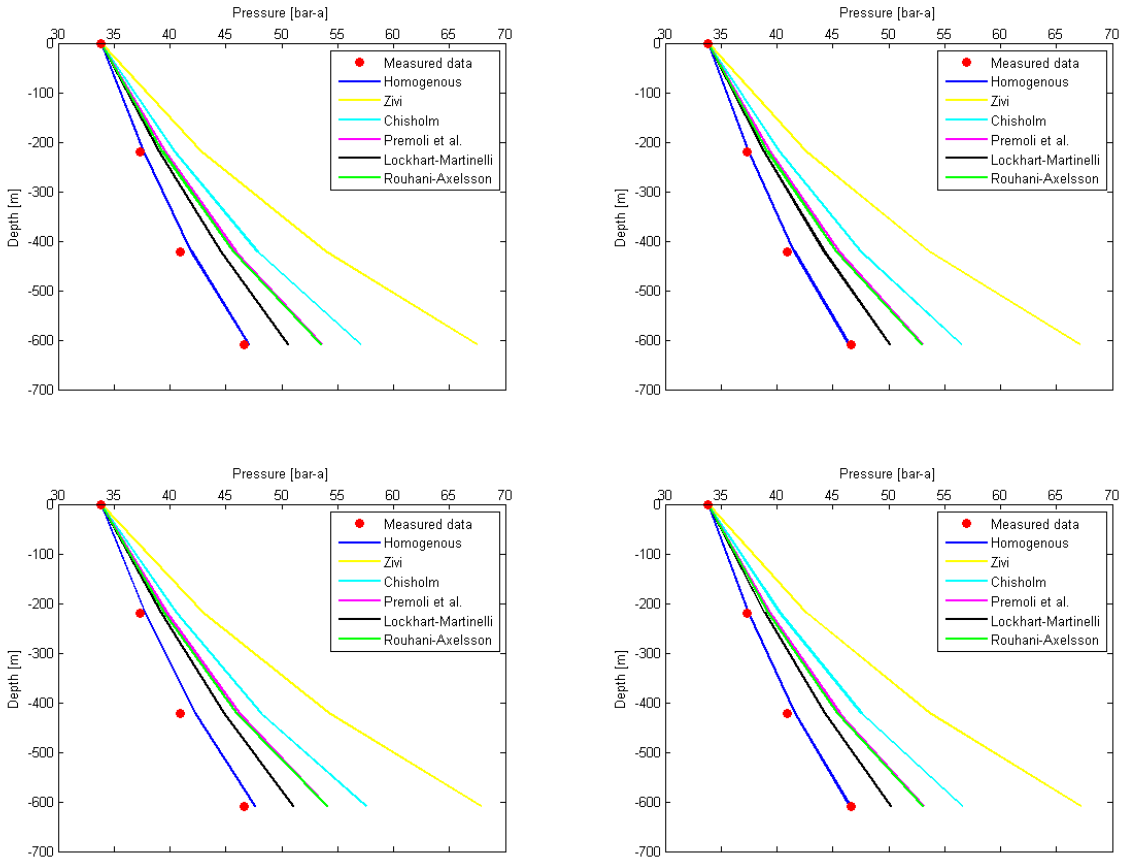

Figure A.7: Simulations for well RN-21 down to the bottom of the production casing; upper left corner: Blasius equation for friction factor and model by Friedel for friction correction factor, upper right corner: Blasius equation for friction factor and model by Beattie for friction correction factor, lower left corner: Swamee-Jain equation for friction factor and model by Friedel for friction correction factor, lower right corner: Swamee-Jain equation for friction factor and model by Beattie for friction correction factor.

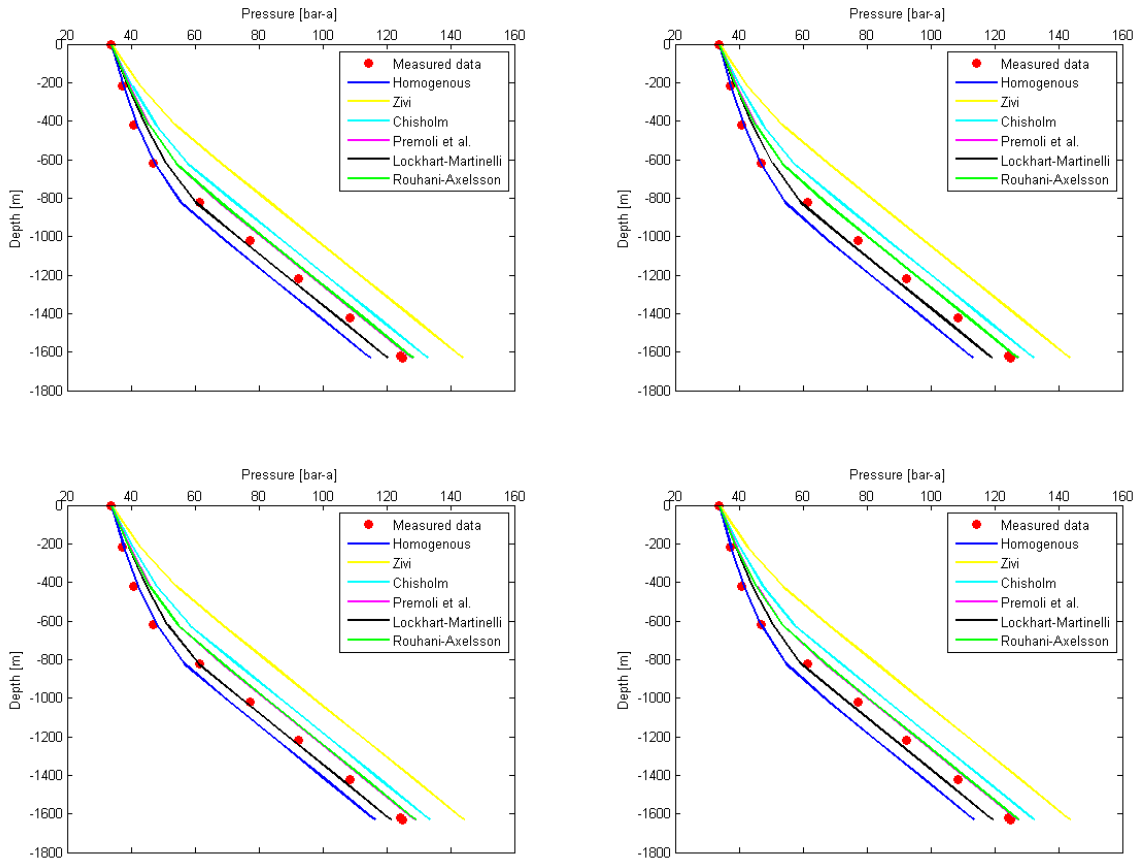

Figure A.8: Simulations for well RN-21 down to the bottom of the well; upper left corner: Blasius equation for friction factor and model by Friedel for friction correction factor, upper right corner: Blasius equation for friction factor and model by Beattie for friction correction factor, lower left corner: Swamee-Jain equation for friction factor and model by Friedel for friction correction factor, lower right corner: Swamee-Jain equation for friction factor and model by Beattie for friction correction factor.

Well RN-22

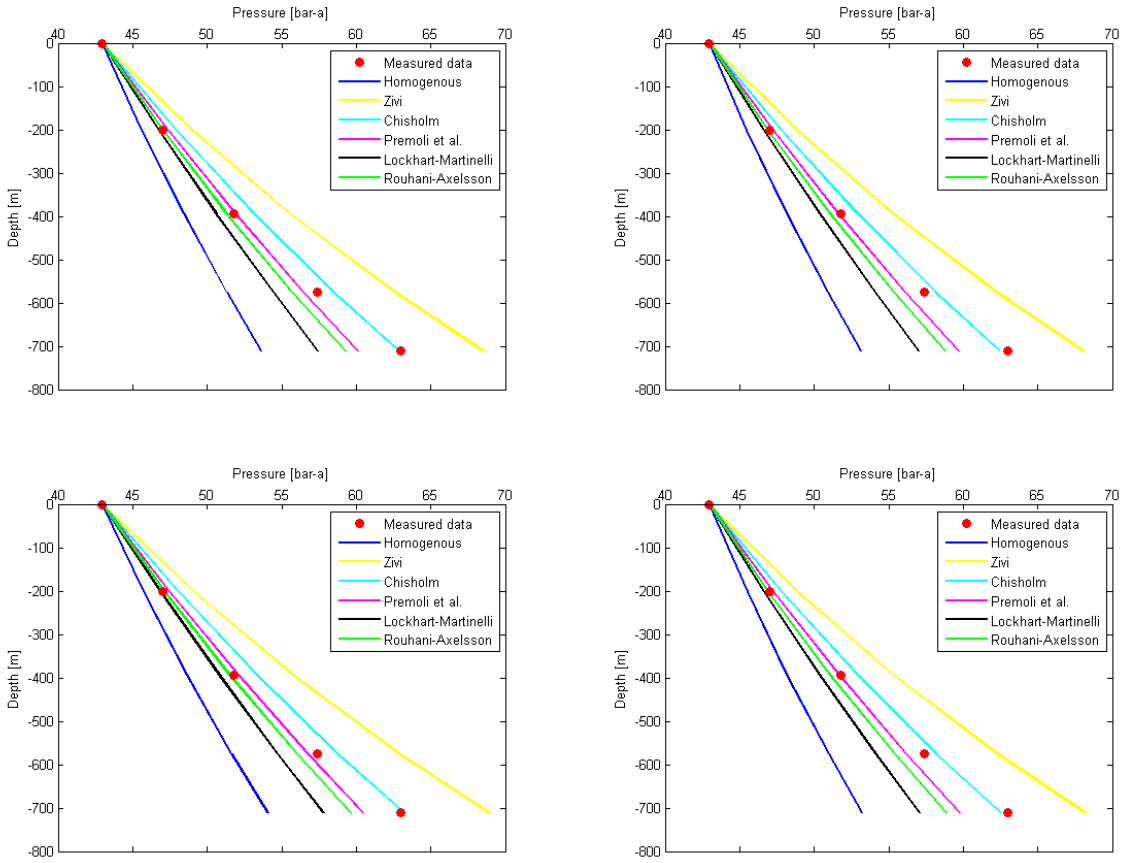

Figure A.9: Simulations for well RN-22 down to the bottom of the production casing along with corrected data; upper left corner: Blasius equation for friction factor and model by Friedel for friction correction factor, upper right corner: Blasius equation for friction factor and model by Beattie for friction correction factor, lower left corner: Swamee-Jain equation for friction factor and model by Friedel for friction correction factor, lower right corner: Swamee-Jain equation for friction factor and model by Beattie for friction correction factor.

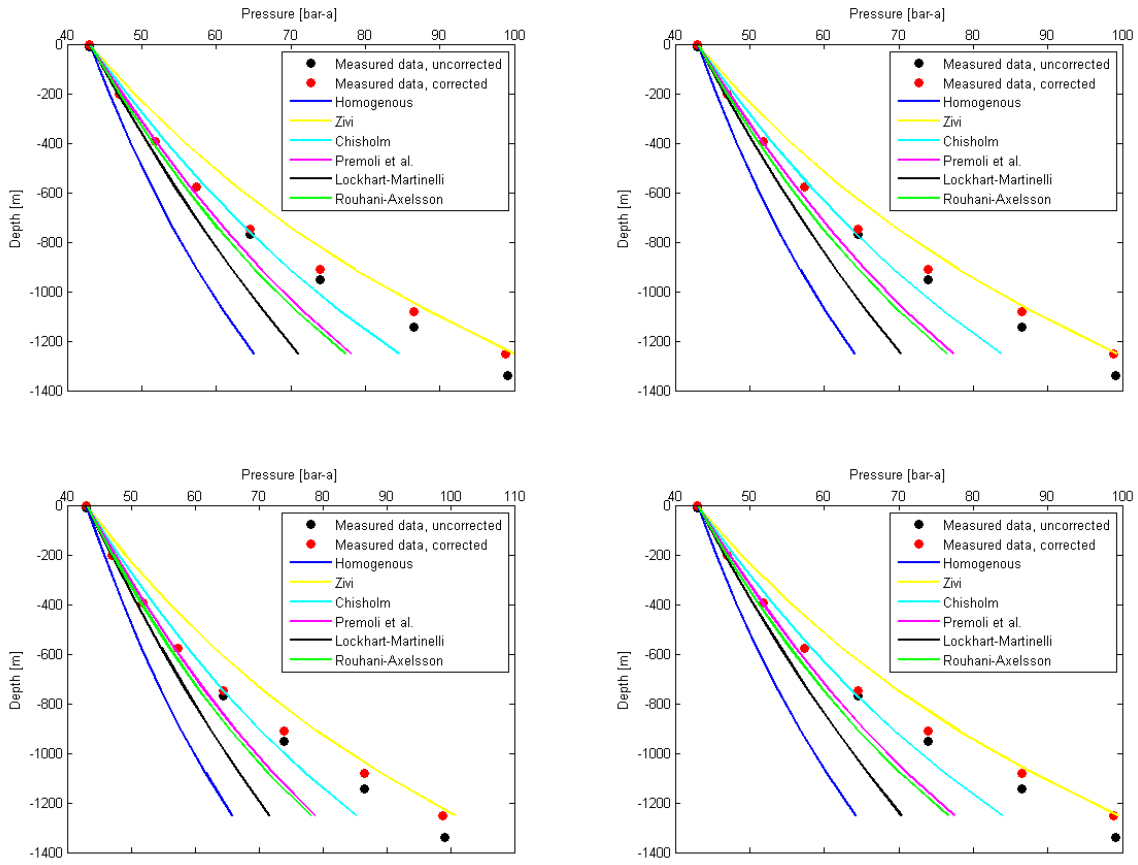

Figure A.10: Simulations for well RN-22 down to the bottom of the well, along with corrected data; upper left corner: Blasius equation for friction factor and model by Friedel for friction correction factor, upper right corner: Blasius equation for friction factor and model by Beattie for friction correction factor, lower left corner: Swamee-Jain equation for friction factor and model by Friedel for friction correction factor, lower right corner: Swamee-Jain equation for friction factor and model by Beattie for friction correction factor.

Well RN-23

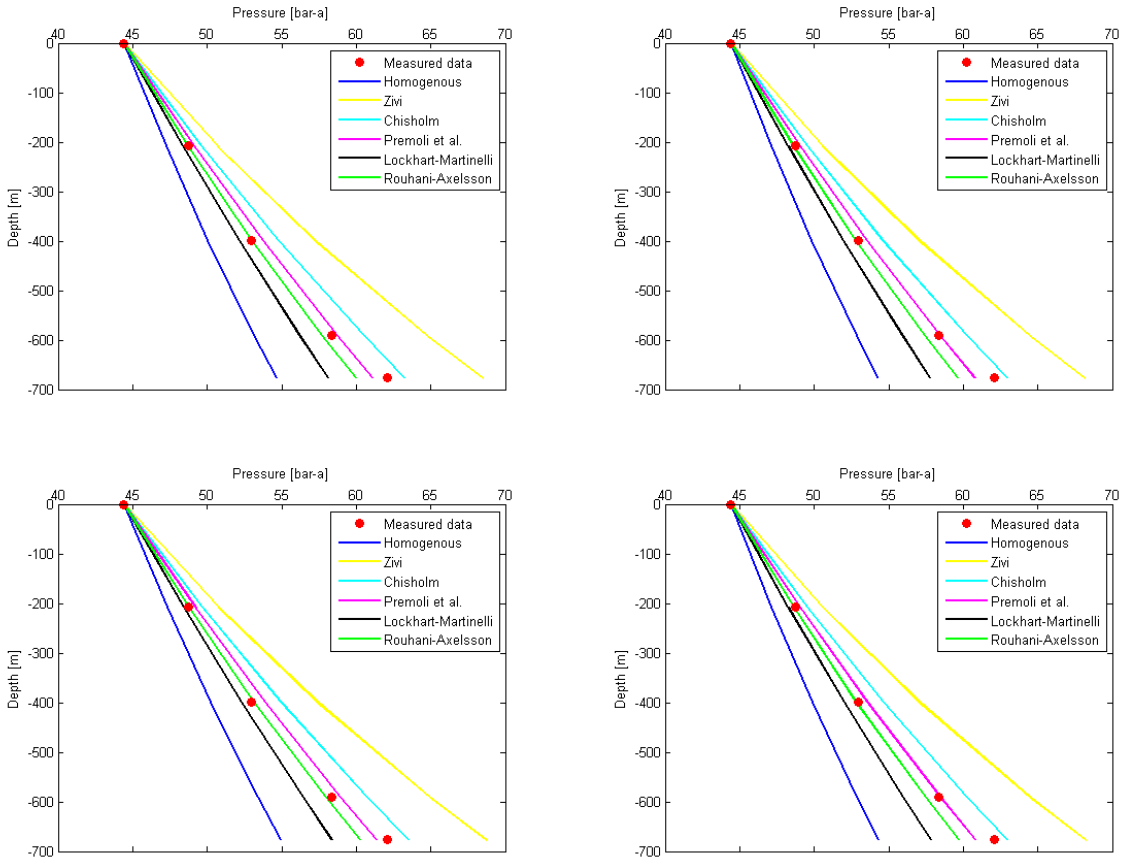

Figure A.11: Simulations for well RN-23 down to the bottom of the production casing along with corrected data; upper left corner: Blasius equation for friction factor and model by Friedel for friction correction factor, upper right corner: Blasius equation for friction factor and model by Beattie for friction correction factor, lower left corner: Swamee-Jain equation for friction factor and model by Friedel for friction correction factor, lower right corner: Swamee-Jain equation for friction factor and model by Beattie for friction correction factor.

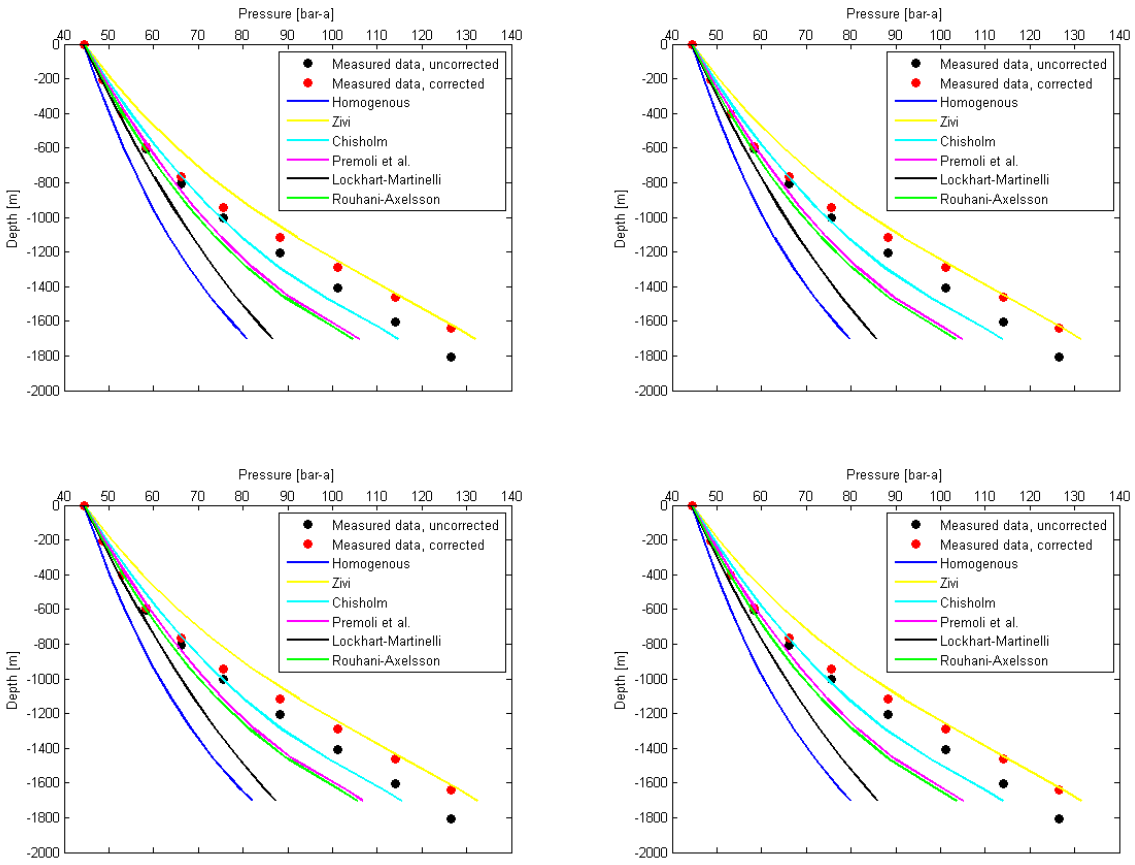

Figure A.12: Simulations for well RN-23 down to the bottom of the well, along with corrected data; upper left corner: Blasius equation for friction factor and model by Friedel for friction correction factor, upper right corner: Blasius equation for friction factor and model by Beattie for friction correction factor, lower left corner: Swamee-Jain equation for friction factor and model by Friedel for friction correction factor, lower right corner: Swamee-Jain equation for friction factor and model by Beattie for friction correction factor.

Well RN-24

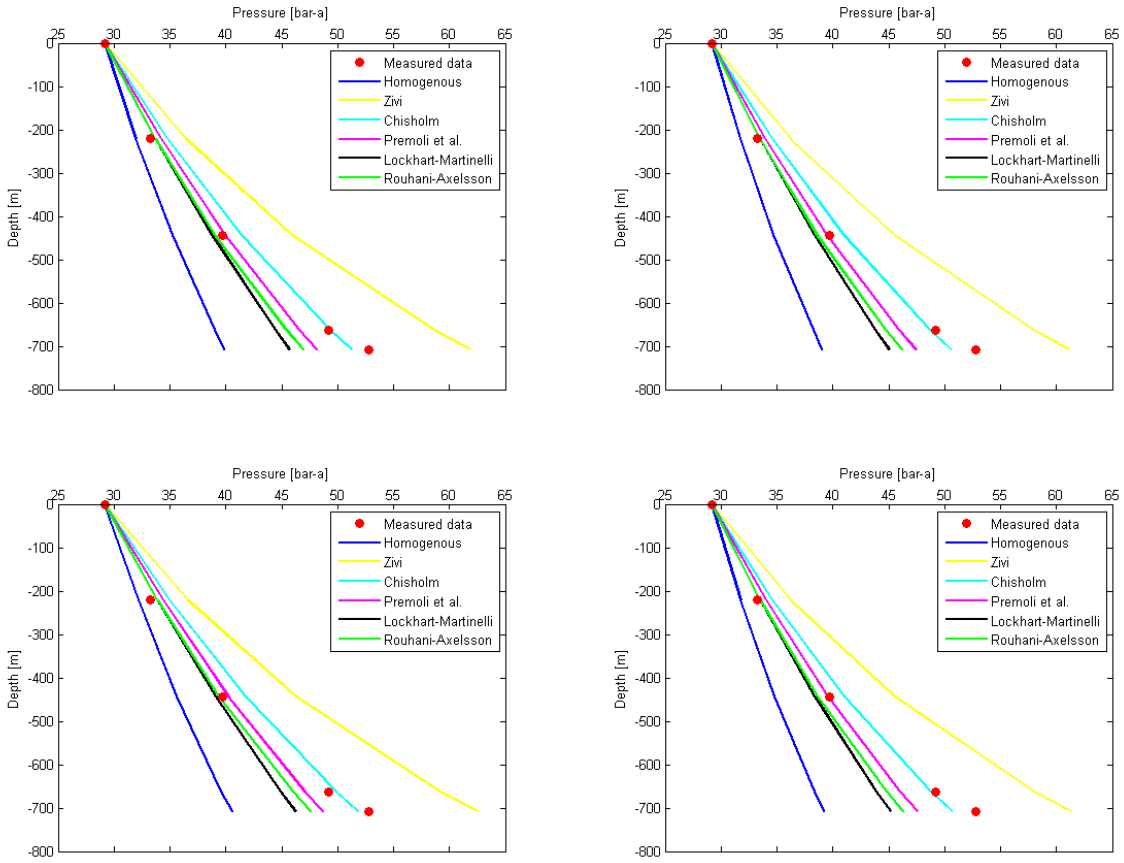

Figure A.13: Simulations for well RN-24 down to the bottom of the production casing; upper left corner: Blasius equation for friction factor and model by Friedel for friction correction factor, upper right corner: Blasius equation for friction factor and model by Beattie for friction correction factor, lower left corner: Swamee-Jain equation for friction factor and model by Friedel for friction correction factor, lower right corner: Swamee-Jain equation for friction factor and model by Beattie for friction correction factor.

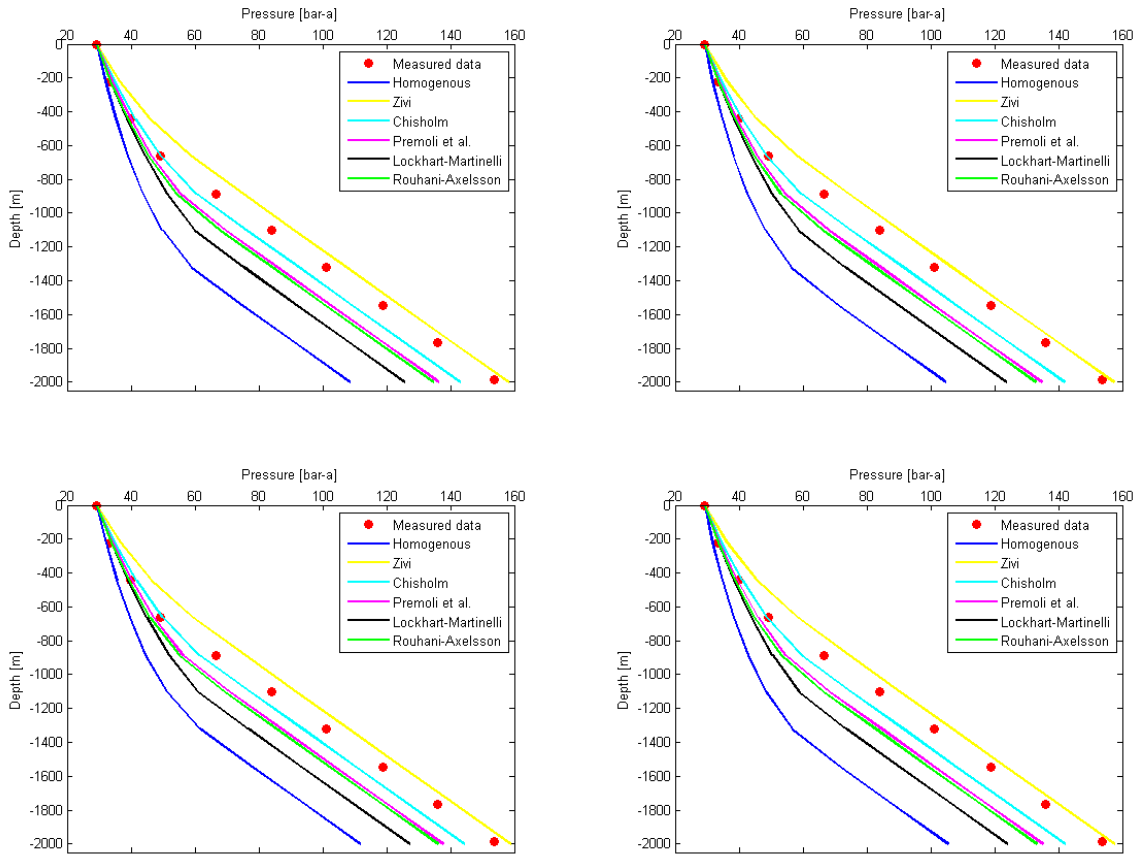

Figure A.14: Simulations for well RN-24 down to the bottom of the well; upper left corner: Blasius equation for friction factor and model by Friedel for friction correction factor, upper right corner: Blasius equation for friction factor and model by Beattie for friction correction factor, lower left corner: Swamee-Jain equation for friction factor and model by Friedel for friction correction factor, lower right corner: Swamee-Jain equation for friction factor and model by Beattie for friction correction factor.

Well RN-27

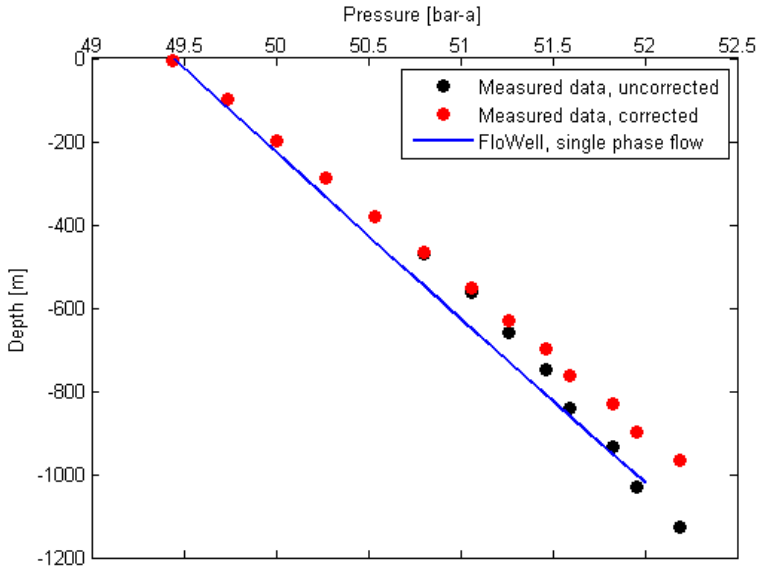

Figure A.15: Simulation for well RN-27 down to the bottom of the well.

Well RN-28

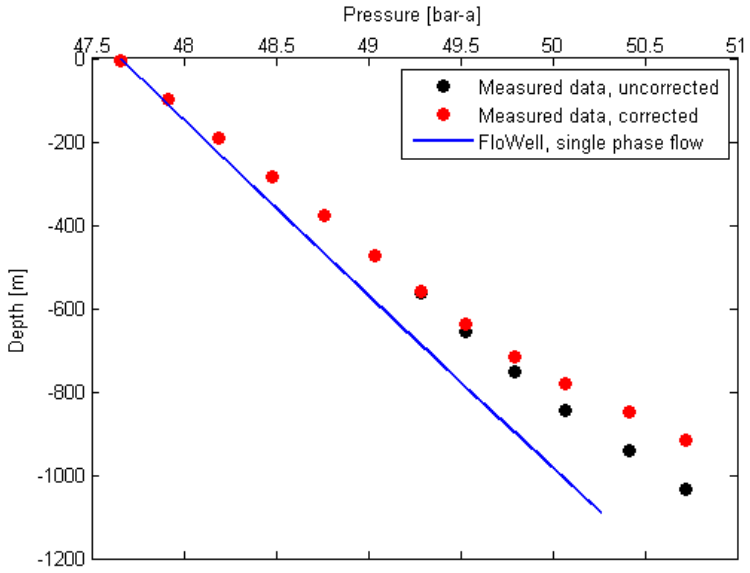

Figure A.16: Simulation for well RN-28 down to the bottom of the well.

Well SV-21

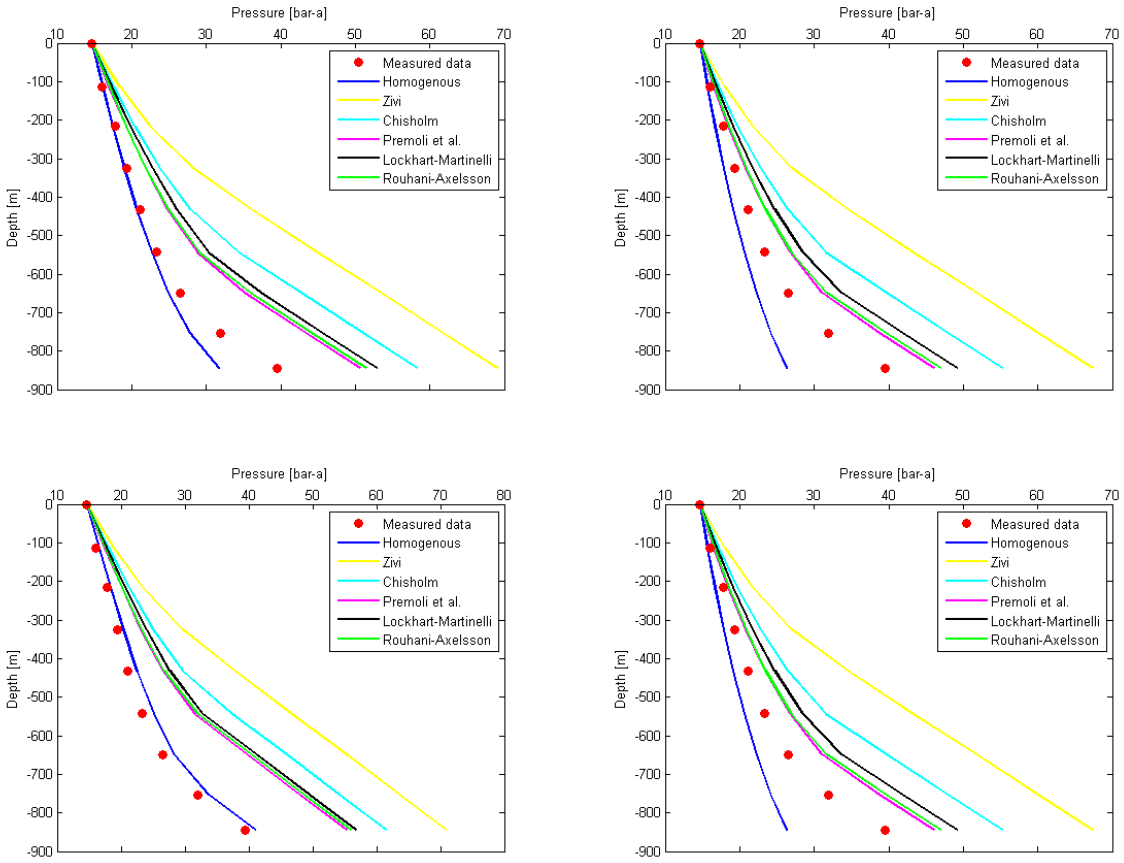

Figure A.17: Simulations for well SV-21 down to the bottom of the production casing; upper left corner: Blasius equation for friction factor and model by Friedel for friction correction factor, upper right corner: Blasius equation for friction factor and model by Beattie for friction correction factor, lower left corner: Swamee-Jain equation for friction factor and model by Friedel for friction correction factor, lower right corner: Swamee-Jain equation for friction factor and model by Beattie for friction correction factor.

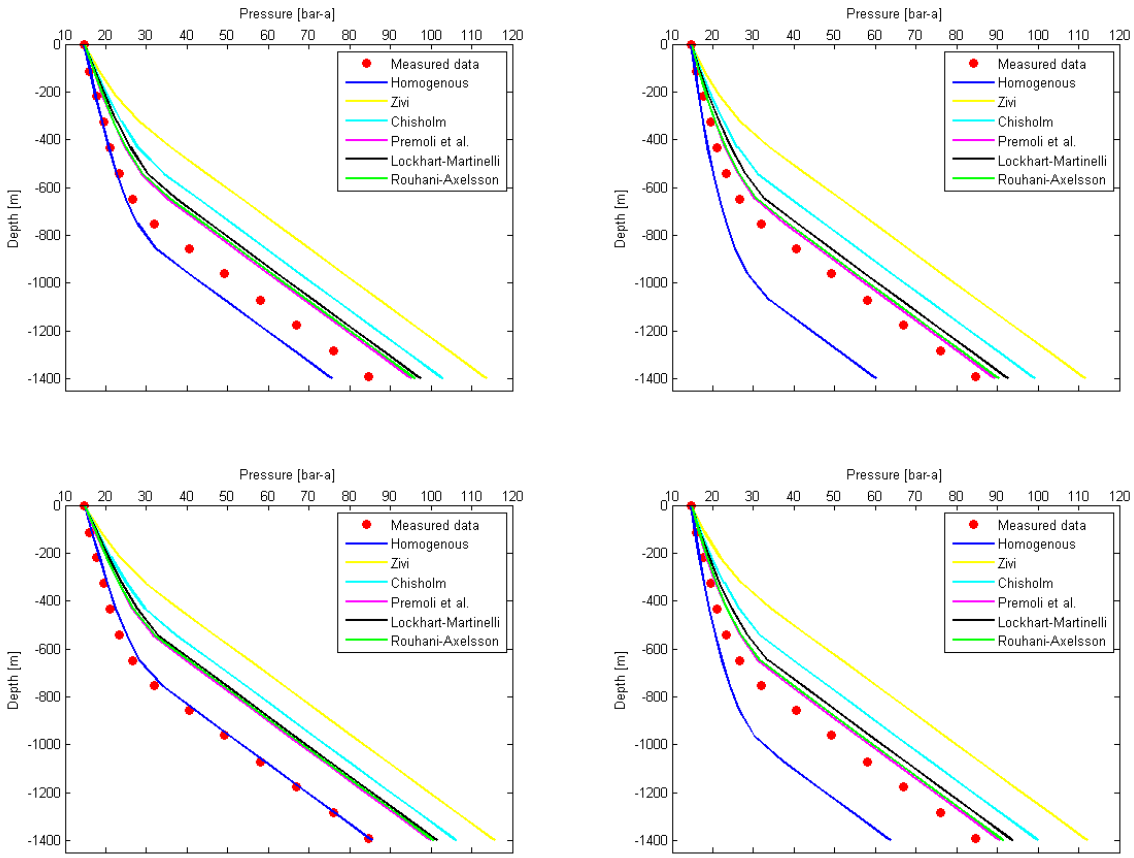

Figure A.18: Simulations for well SV-21 down to the bottom of the well; upper left corner: Blasius equation for friction factor and model by Friedel for friction correction factor, upper right corner: Blasius equation for friction factor and model by Beattie for friction correction factor, lower left corner: Swamee-Jain equation for friction factor and model by Friedel for friction correction factor, lower right corner: Swamee-Jain equation for friction factor and model by Beattie for friction correction factor.

Well SV-22

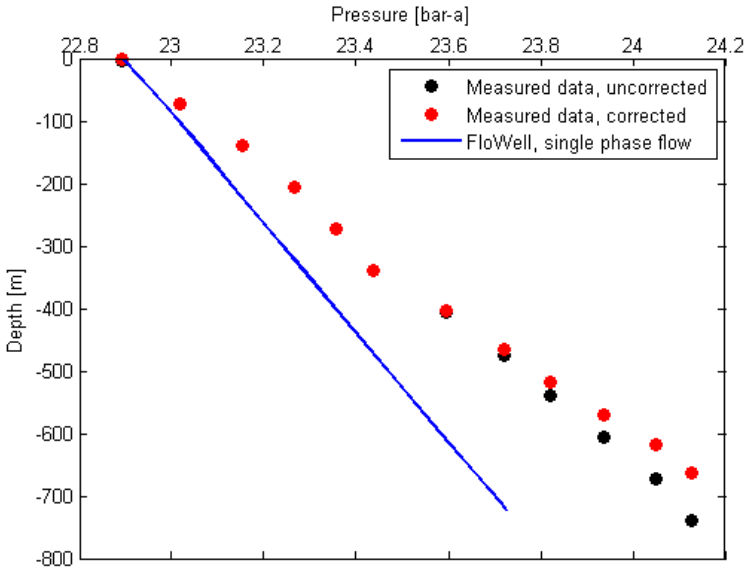

Figure A.19: Simulation for well SV-22 down to the bottom of the well.

Well SV-23

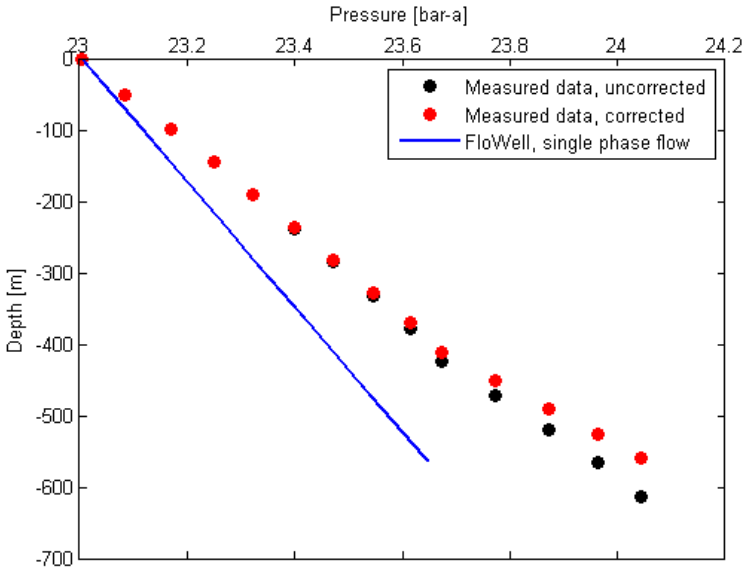

Figure A.20: Simulation for well SV-23 down to the bottom of the well.

B. Temperature Sections for Reykjanes Geothermal Field

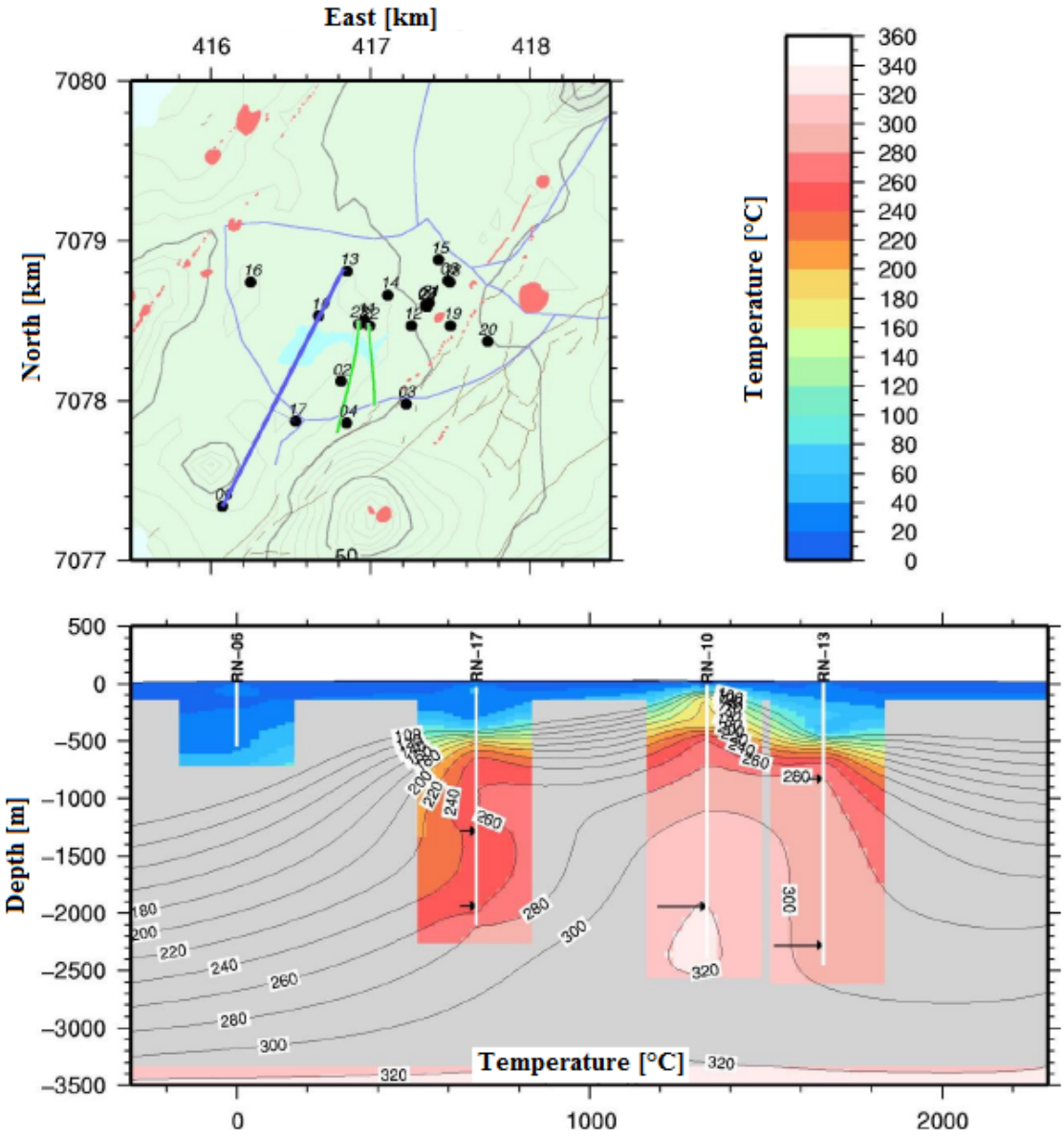

Figure B.1: Temperature section 1, from well RN-06 to RN-13B [50].

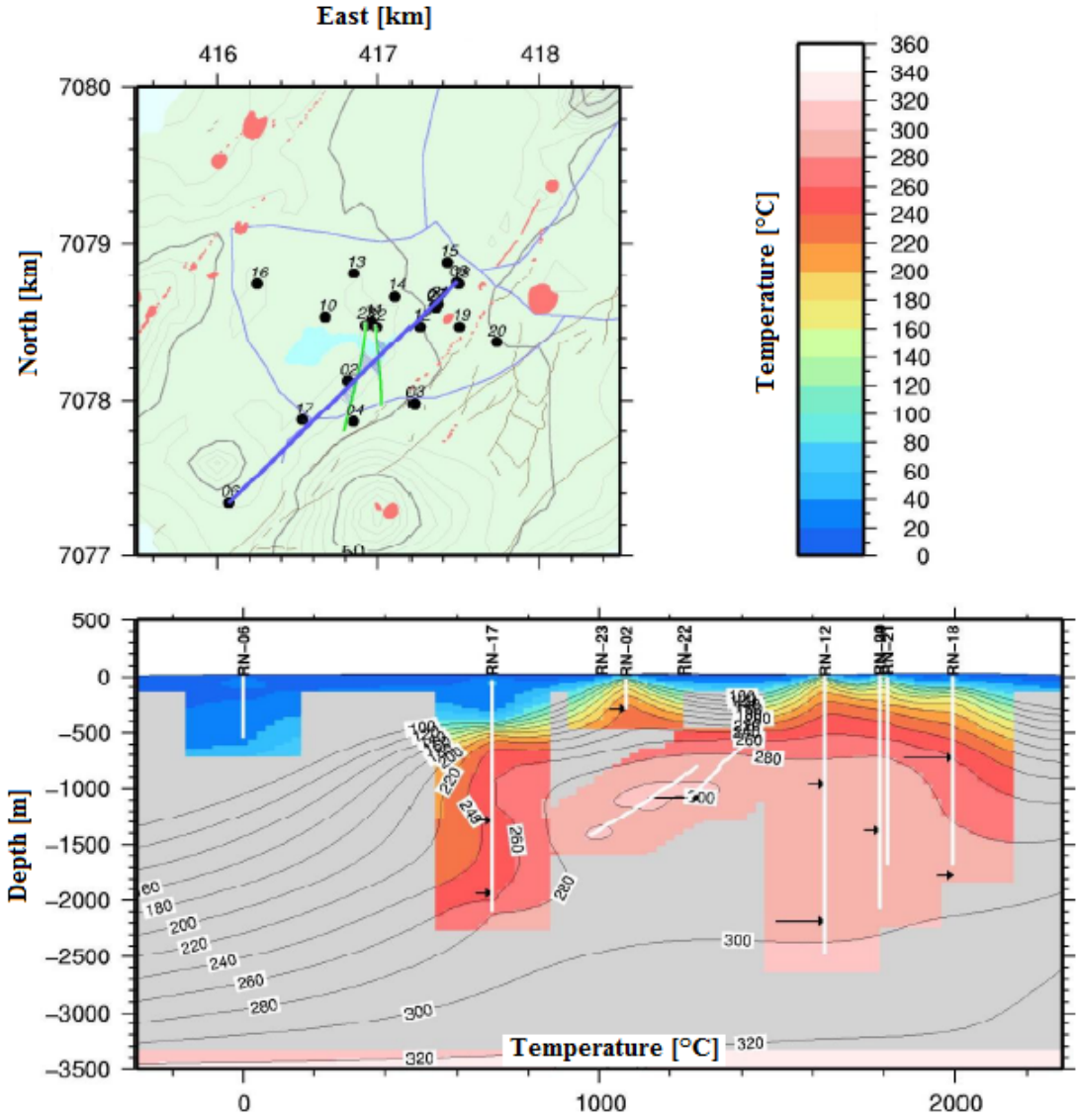

Figure B.2: Temperature section 2, from well RN-06 to RN-18 [50].

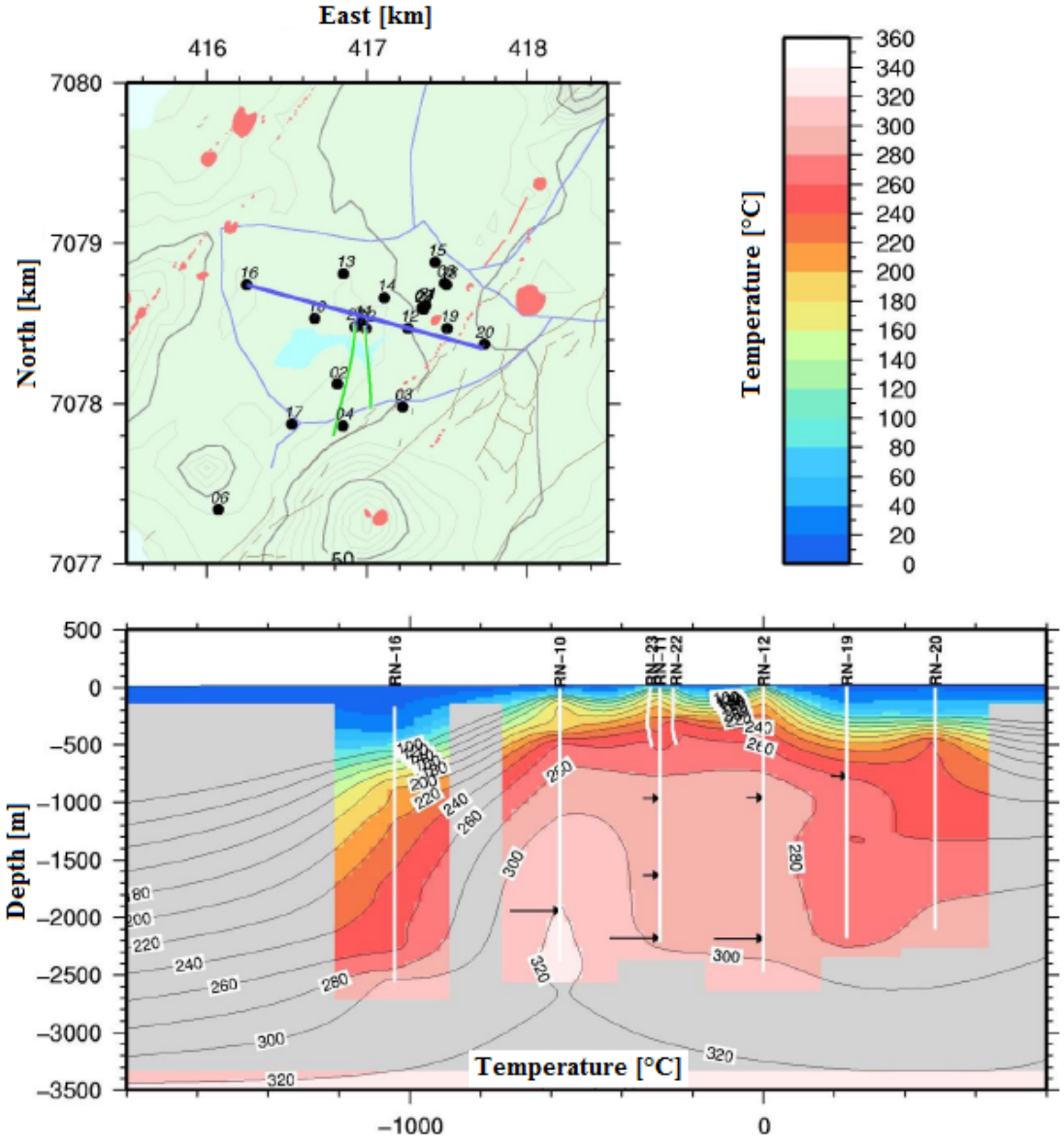

Figure B.3: Temperature section 3, from well RN-16 to RN-20 [50].

C. Natural State Match Results

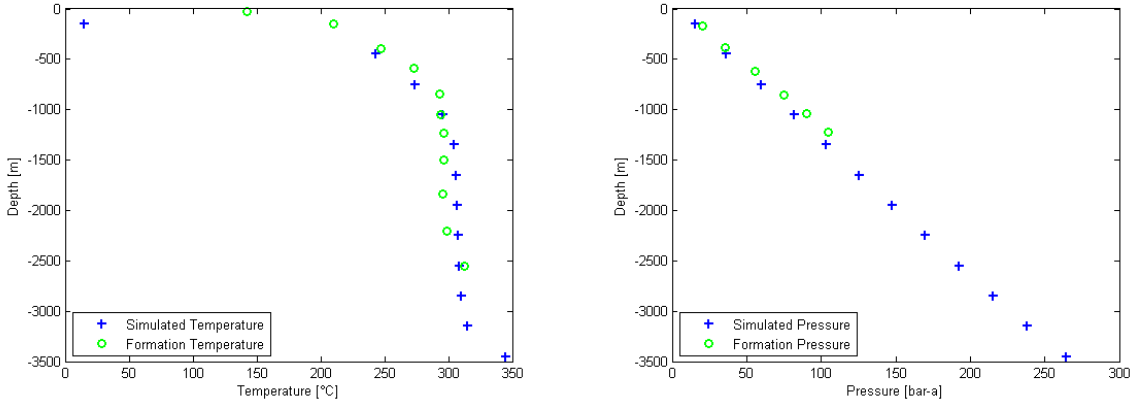

Figure C.1: Formation temperature and pressure versus simulated temperature and pressure for well RN-09.

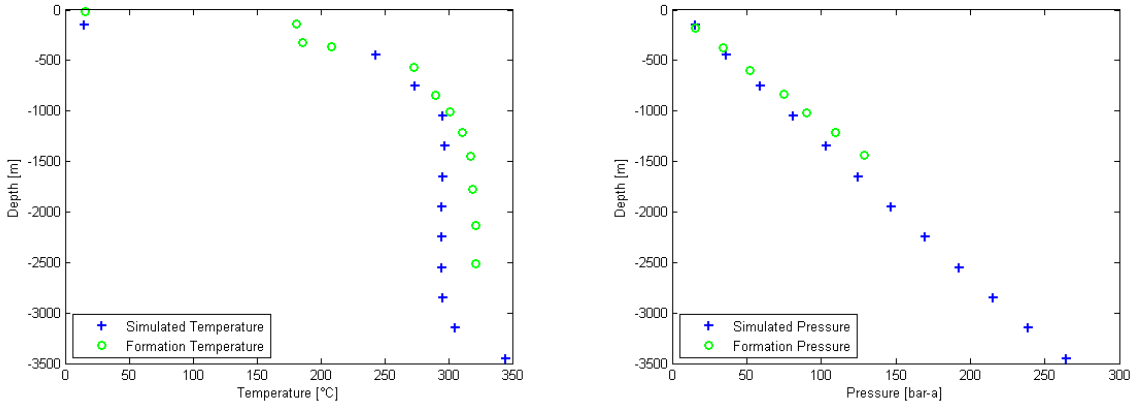

Figure C.2: Formation temperature and pressure versus simulated temperature and pressure for well RN-10.

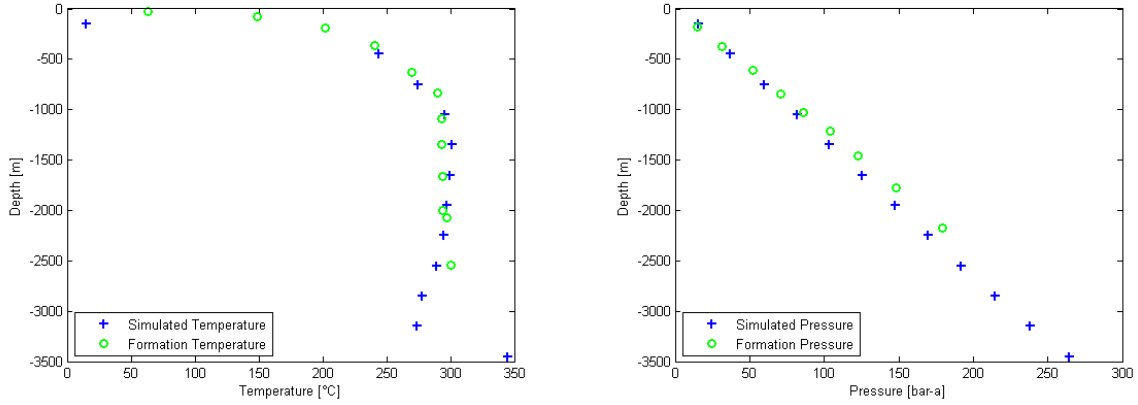

Figure C.3: Formation temperature and pressure versus simulated temperature and pressure for well RN-11.

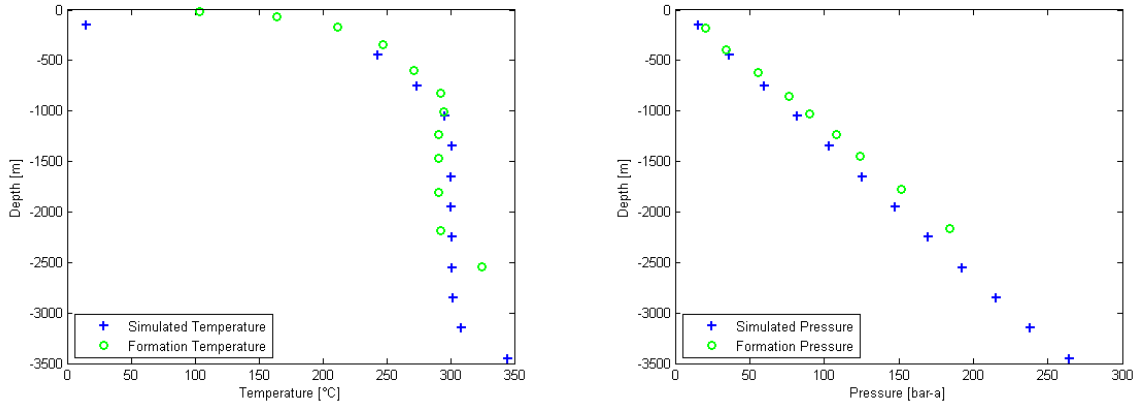

Figure C.4: Formation temperature and pressure versus simulated temperature and pressure for well RN-12.

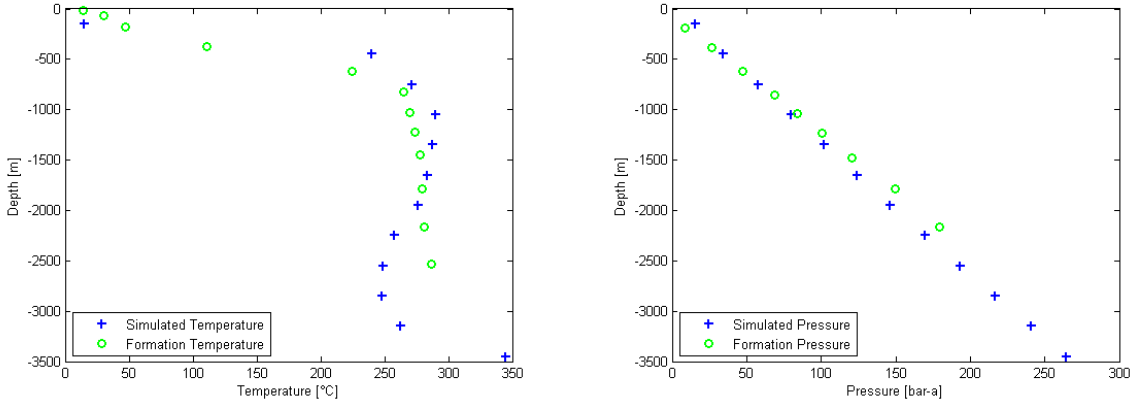

Figure C.5: Formation temperature and pressure versus simulated temperature and pressure for well RN-15.

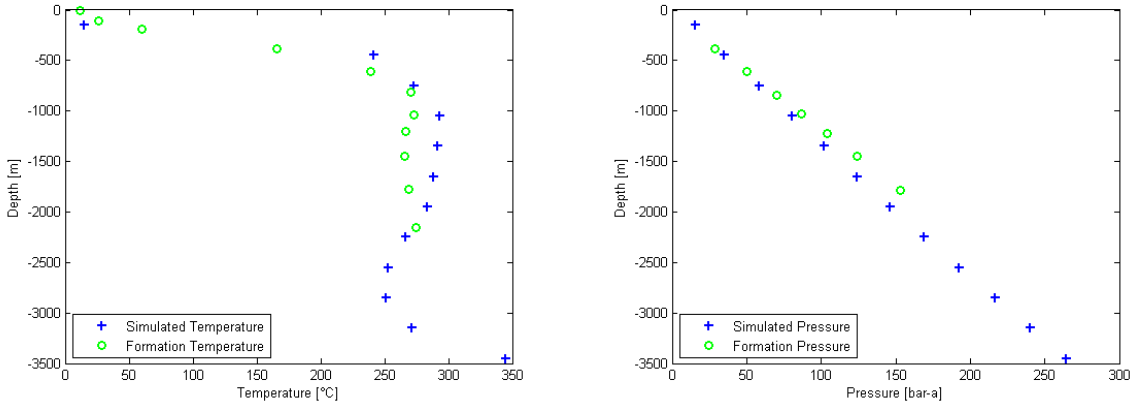

Figure C.6: Formation temperature and pressure versus simulated temperature and pressure for well RN-19.

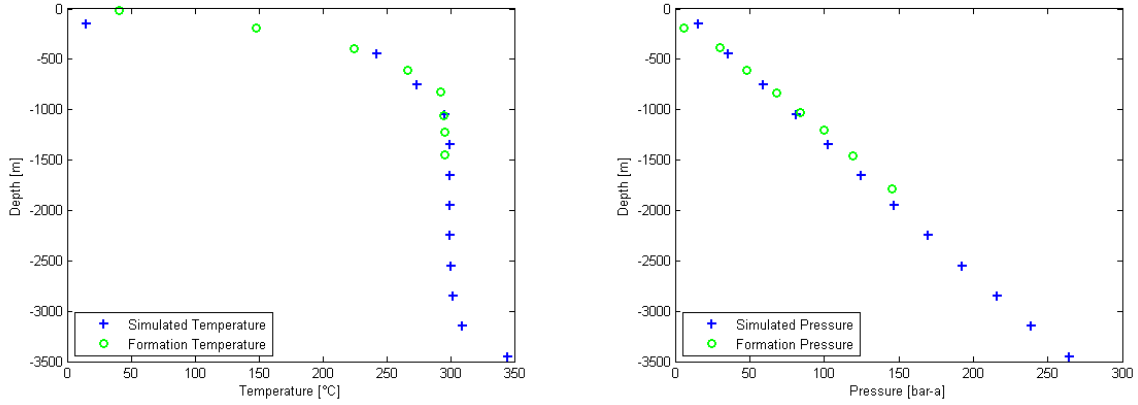

Figure C.7: Formation temperature and pressure versus simulated temperature and pressure for well RN-21.

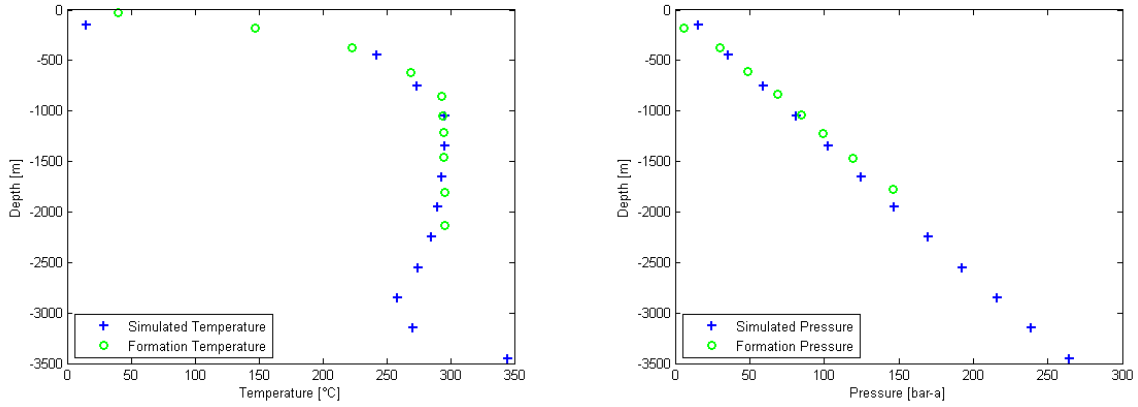

Figure C.8: Formation temperature and pressure versus simulated temperature and pressure for well RN-24.